

CATALYTIC PARTIAL OXIDATION OF PROPYLENE ON METAL SURFACES
BY MEANS OF QUANTUM CHEMICAL METHODS

A THESIS SUBMITTED TO
THE GRADUATE SCHOOL OF NATURAL AND APPLIED SCIENCES
OF
MIDDLE EAST TECHNICAL UNIVERSITY

BY

ALİ CAN KIZILKAYA

IN PARTIAL FULFILLMENT OF THE REQUIREMENTS
FOR
THE DEGREE OF MASTER OF SCIENCE
IN
CHEMICAL ENGINEERING

JANUARY 2010

Approval of the thesis:

**CATALYTIC PARTIAL OXIDATION OF PROPYLENE ON METAL SURFACES
BY MEANS OF QUANTUM CHEMICAL METHODS**

submitted by **ALİ CAN KIZILKAYA** in partial fulfillment of the requirements for the degree of **Master of Science in Chemical Engineering Department, Middle East Technical University** by,

Prof. Dr. Canan Özgen
Dean, Graduate School of **Natural and Applied Sciences**

Prof. Dr. Gürkan Karakaş
Head of Department, **Chemical Engineering**

Prof. Dr. Işık Önal
Supervisor, **Department of Chemical Engineering, METU**

Examining Committee Members:

Prof. Dr. Hayrettin Yücel
Department of Chemical Engineering, METU

Prof. Dr. Işık Önal
Department of Chemical Engineering, METU

Prof. Dr. İnci Eroğlu
Department of Chemical Engineering, METU

Prof. Dr. Şinasi Ellialtıoğlu
Department of Physics, METU

Prof. Dr. Mehmet Çakmak
Department of Physics, Gazi University

Date:

I hereby declare that all information in this document has been obtained and presented in accordance with academic rules and ethical conduct. I also declare that, as required by these rules and conduct, I have fully cited and referenced all material and results that are not original to this work.

Name, Last Name: ALI CAN KIZILKAYA

Signature :

ABSTRACT

CATALYTIC PARTIAL OXIDATION OF PROPYLENE ON METAL SURFACES BY MEANS OF QUANTUM CHEMICAL METHODS

Kızılkaya, Ali Can

M.S., Department of Chemical Engineering

Supervisor : Prof. Dr. Işık Önal

January 2010, 101 pages

Direct, gas phase propylene epoxidation reactions are carried out on model slabs representing Ru-Cu(111) bimetallic and Cu(111) metallic catalyst surfaces with periodic Density Functional Theory (DFT) calculations.

Ru-Cu(111) surface is modelled as a Cu(111) monolayer totally covering the surface of Ru(0001) surface underneath. The catalytic activity is evaluated following the generally accepted oxametallacycle mechanism.

It is shown that the Ru-Cu(111) surface has a lower energy barrier (0.48 eV) for the stripping of the allylic hydrogen of propylene and a higher energy barrier (0.92 eV) towards propylene oxametallacycle (OMMP) formation compared to 0.75 eV barrier for OMMP formation and 0.83 eV barrier for allylic hydrogen stripping on Cu(111), and thus ineffective for propylene oxide production based on the investigated models and mechanism. In order to analyze the observed inability of the Ru-Cu(111) surface to selectively catalyze propylene oxide formation, a Lewis acid probe, SO₂, was adsorbed on the oxygenated Cu(111) and Ru-Cu(111) surfaces and the binding energies, a measure of the basicity of the chemisorbed oxygen on the surfaces, on two systems are compared.

As a conclusion, the reason behind this ineffectiveness of the Ru-Cu(111) surface for selectively catalyzing propylene epoxidation is related to the higher basicity of the atomic oxygen adsorbed on Ru-Cu(111) compared to the oxygen on Cu(111). The results are consistent both with recent publications about propylene epoxidation and previous studies performed about the structure of Ru-Cu catalysts.

Keywords: DFT, Propylene Epoxidation, Ruthenium, Copper, Catalysis

ÖZ

PROPİLENİN METAL YÜZEYLERİ ÜZERİNDE KUANTUM KİMYASAL YÖNTEMLER KULLANILARAK KATALİTİK KİSMİ OKSİDASYONU

Kızılkaya, Ali Can

Yüksek Lisans, Kimya Mühendisliği Bölümü

Tez Yöneticisi : Prof. Dr. Işık Önal

Ocak 2010, 101 sayfa

Propilenin, doğrudan, gaz fazındaki kısmi oksidasyon tepkimeleri periyodik Yoğunluk Fonksiyoneli Teorisi (YFT) ile Ru-Cu(111) bimetalik ve Cu(111) metalik yüzeylerini temsil eden model levhalar üzerinde gerçekleştirilmiştir.

Ru-Cu(111) yüzeyi alttaki Ru(0001) yüzeyini tamamen örten bir Cu(111) tekkatmanı olarak modellenmiştir. Katalitik etkinlik genel olarak kabul görmüş oksimetallikdöngü mekanizmasını izleyerek değerlendirilmiştir.

Ru-Cu(111) yüzeyinin, Cu(111) üzerindeki propilen oksimetallikdöngüsü (OMMP) oluşumu için 0.75 eV ve allilik hidrojen çıkarımı için 0.83 eV etkinleştirme bariyerlerine kıyasla, OMMP oluşumu için daha yüksek (0.92 eV) ve allilik hidrojen çıkarımı için daha düşük (0.48 eV) bariyere sahip olduğu ve bu nedenle incelenmiş olan modeller ve mekanizmaya dayanılarak propilen oksit üretimi için başarısız olduğu gösterilmiştir. Ru-Cu(111) yüzeyinin seçici bir şekilde propilen oksit oluşumunu katalizleme yetersizliği gözlemini analiz etmek için, bir Lewis asidi sondası olan SO₂ oksijenlenmiş Cu(111) ve Ru-Cu(111) yüzeyleri üzerinde adsorbe edilmiş ve iki sistem üzerindeki, yüzey üzerinde kemisorplanmış oksijenin bazikliğinin bir ölçüsü olan, bağlanma enerjileri karşılaştırılmıştır.

Sonu olarak, Ru-Cu(111) yzeyinin propilen oksit oluřumunu seici olarak katalizlemedeki bu yetersizliđinin nedeni Ru-Cu(111) zerinde adsorbe olmuř oksijenin Cu(111) yzeyi zerindeki oksijene kıyasla daha bazik olmasına bađlanmıřtır. Sonular hem propilen epoksidasyonu ile ilgili en son yayınlarla hem de Ru-Cu katalizrlerinin yapısı hakkındaki nceki yayınlarla tutarlıdır.

Anahtar Kelimeler: DFT, Propilen Epoksidasyonu, Rutenyum, Bakır, Kataliz

To My Family,

ACKNOWLEDGMENTS

First of all, I would like to thank Prof. Dr. Işık Önal for his guidance, criticism, and valuable comments throughout this study.

I would like to thank to TÜBİTAK ULAKBİM and the Computer Engineering Department of METU for providing computational time.

I would like to especially thank to Dr. Ferdi Fellah for his guidance, encouragement, responsibility, patience, kindness and always supportive friendship. I also want to thank to Oluş Özbek for his valuable comments about the VASP code.

I am grateful to Berker Fıçıcılar for always giving me an idea in the most complicated situations and for being my friend and mentor since my undergraduate days.

Special thanks to Özlem Soydaş for helping me in the long run of thesis writing. I would like to thank to Ömür Deler for his great friendship, perfect humor and endless love of rock & roll. I would also like to thank to my friends Çağan Sazak, Halim Karataş, Neslihan Güğümcü, Simge Çınar, Korhan Sezgiker, İrem Vural, Gizem Nogay, Buğra Özütemiz and to many others that I could not mention here for sharing the moment with me.

Finally, I would like to send my greatest gratitudes to Cem, Adem and Hatice Kızılkaya for never giving up on me and always being supportive to the greatest extent possible. Without them this thesis would not have been possible.

TABLE OF CONTENTS

ABSTRACT	iv
ÖZ	vi
DEDICATON	viii
ACKNOWLEDGMENTS	ix
TABLE OF CONTENTS	x
LIST OF TABLES	xiii
LIST OF FIGURES	xv
CHAPTERS	
1 INTRODUCTION	1
1.1 Catalysis	1
1.1.1 Fundamentals of Catalysis	1
1.1.2 Heterogeneous Catalysis	3
1.1.2.1 Fundamentals of Heterogeneous Catalysis	3
1.1.2.2 Sabatier Principle	5
1.1.2.3 Transition State Theory	7
1.2 Propylene Epoxidation	9
1.2.1 Basic Properties of Propylene Oxide	9
1.2.2 Industrial Production of Propylene Oxide	10
1.2.2.1 The Chlorohydrin Process	10
1.2.2.2 The Hydroperoxide Process	13
1.2.2.3 Direct Propylene Epoxidation	15
1.3 Computational Quantum Chemistry	15
1.3.1 Basics of Computational Quantum Chemistry	15

1.3.2	Born-Oppenheimer Approximation	17
1.3.3	Variational Principle and Hartree-Fock Theory	18
1.3.4	Post Hartree-Fock Methods	24
1.3.5	Basis Sets	25
1.4	Density Functional Theory (DFT)	26
1.4.1	Principles of DFT	26
1.4.2	Main Approximations for Exchange & Correlation	29
1.4.2.1	Local Density Approximation (LDA)	29
1.4.2.2	Generalized Gradient Approximation (GGA)	30
1.4.2.3	Hybrid Methods	31
1.4.3	Capabilities of DFT	31
1.5	Main Approaches in Quantum Chemical Modelling of Catalytic Systems	33
1.5.1	The Cluster Model Approach	33
1.5.2	The Periodic Approach	35
1.6	Objectives of the Study	38
2	LITERATURE SURVEY	39
2.1	Propylene Epoxidation	39
2.2	Structure of Ruthenium-Copper Catalysts	45
3	COMPUTATIONAL METHODOLOGY	49
3.1	Overview of the Methodology	49
3.2	Preparation and Optimization of the Bulk Structure	51
3.3	Preparation and Optimization of the Slabs	51
3.4	Adsorption of Atomic Oxygen on Slabs	54
3.5	Adsorption of Propylene on Oxygenated Slabs	55
3.6	Formation of Allyl Radical	56
3.7	Formation of Propylene Oxametallacycle (OMMP)	56
3.8	Formation of Propylene Oxide (PO)	56
3.9	Formation of Propionaldehyde (PA)	57
3.10	Allocation of Transition State Structures for Each Reaction	57
3.11	Characterization of Transition State Structures	58

3.12	Adsorption of SO ₂ on Oxygenated Slabs	58
4	RESULTS & DISCUSSION	59
4.1	Adsorption of Atomic Oxygen on Cu(111) and Ru-Cu(111) Surfaces	59
4.2	Adsorption of Propylene on Oxygenated Cu(111) and Ru-Cu(111) Surfaces	61
4.3	Formation of Allyl Radical on Cu(111) and Ru-Cu(111) Surfaces . .	64
4.4	Formation of Propylene Oxametallacycle (OMMP)	65
4.5	Formation of Propylene Oxide (PO) on Cu(111) and Ru-Cu(111) Surfaces	67
4.6	Formation of Propionaldehyde (PA) on Cu(111) and Ru-Cu(111) Surfaces	68
4.7	Allocation of Transition State Structures for Each Reaction	70
4.7.1	Illustration of the Methodology	70
4.7.2	Transition State Structures for Allylic Hydrogen Stripping and OMMP Formation Reactions	72
4.7.3	Transition State Structures for PO and PA formation reactions	75
4.7.4	Vibrational Frequency Analysis	78
4.7.5	Energetics of the Investigated Reactions on Cu(111) and Ru-Cu(111) Surfaces	79
4.8	SO ₂ Adsorption on Oxygen Covered Cu(111) and Ru-Cu(111) Surfaces	81
5	CONCLUSIONS	84
	REFERENCES	87
	APPENDICES	
A	VASP FILES	90
A.1	Sample Input and Output	90

LIST OF TABLES

TABLES

Table 3.1	Crystallographic parameters for Ru and Cu	51
Table 3.2	Cell parameters for Ru and Cu (Å)	51
Table 4.1	Optimized parameters for oxygen chemisorption on Cu(111) and Ru-Cu(111) surfaces	59
Table 4.2	Energetics of propylene adsorption on Cu(111) and Ru-Cu(111) surfaces(in eV)	63
Table 4.3	Structural and energetic parameters for the formation of allyl radical on Cu(111) and Ru-Cu(111) surfaces	65
Table 4.4	Structural and energetic parameters for the formation of OMMP on Cu(111) and Ru-Cu(111) surfaces	67
Table 4.5	Reaction energies of reactions within oxametallacycle mechanism on Cu(111) and Ru-Cu(111) surfaces (in eV)	70
Table 4.6	Relevant bond lengths of TS structures for OMMP formation and allylic hydrogen stripping on Cu(111) and Ru-Cu(111) surfaces (in Å)	75
Table 4.7	Relevant bond lengths of TS structures for PO and PA formations on Cu(111) and Ru-Cu(111) surfaces (in Å)	78
Table 4.8	Single imaginary frequencies of the TS structures obtained for the investigated reactions (cm ⁻¹)	78
Table 4.9	Activation barriers of reactions within oxametallacycle mechanism on Cu(111) and Ru-Cu(111) surfaces (in eV)	79
Table 4.10	Comparison of the energetics obtained on Cu(111) surface with the literature (in eV)	81

Table 4.11 SO ₂ binding energies on oxygenated Cu(111) and Ru-Cu(111) surfaces (in eV)	83
---	----

LIST OF FIGURES

FIGURES

Figure 1.1	Levels of study in heterogeneous catalysis research	5
Figure 1.2	Sabatier's principle illustrated with the volcano plot	6
Figure 1.3	An example of one dimensional potential energy surface	8
Figure 1.4	An example of three dimensional potential energy surface	8
Figure 1.5	Illustration of propylene oxide molecule	9
Figure 1.6	First reaction step of propylene chlorohydrin production	11
Figure 1.7	Second reaction step of propylene chlorohydrin production	11
Figure 1.8	Simplified flowsheet of the chlorohydrin process	12
Figure 1.9	PO production reaction of the chlorohydrin process	12
Figure 1.10	Simplified flowsheet of the PO-SM process	14
Figure 1.11	First reaction step of PO production in PO-SM process	14
Figure 1.12	Second reaction step of PO production in PO-SM process	14
Figure 1.13	Computational burden of different methods in quantum chemistry	27
Figure 1.14	Illustration of bulk Pd and Pd(111) surface in periodic approach	35
Figure 1.15	Representation of the pseudopotential approach	37
Figure 2.1	Optimized structure of the OMME intermediate in ethylene epoxidation reaction	42
Figure 2.2	Mechanism for propylene epoxidation on Ag(111) and Cu(111)	43
Figure 3.1	Top view of the Cu(111) slab	52
Figure 3.2	Side view of the Cu(111) slab	53
Figure 3.3	Top view of the Ru-Cu(111) slab	53

Figure 3.4	Side view of the Ru-Cu(111) slab	54
Figure 4.1	Optimized structure of oxygen chemisorbed on Cu(111) surface	60
Figure 4.2	Optimized structure of oxygen chemisorbed on Ru-Cu(111) surface	60
Figure 4.3	Top view of propylene adsorbed on Cu(111) to undergo AHS	61
Figure 4.4	Top view of propylene adsorbed on Cu(111) to form OMMP	62
Figure 4.5	Top view of propylene adsorbed on Ru-Cu(111) to undergo AHS	62
Figure 4.6	Top view of propylene adsorbed on Ru-Cu(111) to form OMMP	63
Figure 4.7	Top view of allyl and hydroxyl radicals adsorbed on Cu(111)	64
Figure 4.8	Top view of allyl and hydroxyl radicals adsorbed on Ru-Cu(111)	65
Figure 4.9	Top view of OMMP formed on Cu(111)	66
Figure 4.10	Top view of OMMP formed on Ru-Cu(111)	66
Figure 4.11	Top view of PO formed on Cu(111)	67
Figure 4.12	Top view of PO formed on Ru-Cu(111)	68
Figure 4.13	Top view of PA formed on Cu(111)	69
Figure 4.14	Top view of PA formed on Ru-Cu(111)	69
Figure 4.15	Energy profile obtained for OMMP formation reaction on Ru-Cu(111) surface	71
Figure 4.16	Side view of TS structure for allylic hydrogen stripping on Cu(111)	73
Figure 4.17	Side view of TS structure for allylic hydrogen stripping on Ru-Cu(111)	73
Figure 4.18	Side view of TS structure for OMMP formation on Cu(111)	74
Figure 4.19	Side view of TS structure for OMMP formation on Ru-Cu(111)	74
Figure 4.20	Side view of TS structure for PO formation on Cu(111)	76
Figure 4.21	Side view of TS structure for PO formation on Ru-Cu(111)	76
Figure 4.22	Side view of TS structure for PA formation on Cu(111)	77
Figure 4.23	Side view of TS structure for PA formation on Ru-Cu(111)	77
Figure 4.24	Energy profile for propylene epoxidation Reactions on Cu(111) and Ru-Cu(111) surfaces	80
Figure 4.25	Side view of SO ₂ binded to oxygen chemisorbed on on Cu(111)	82
Figure 4.26	Side view of SO ₂ binded to oxygen chemisorbed on on Ru-Cu(111)	82

Figure A.1 A sample INCAR file	91
Figure A.2 A sample KPOINTS file	91
Figure A.3 A sample POSCAR file	92
Figure A.4 A sample POTCAR file (first lines)	93
Figure A.5 A sample POTCAR file (last lines)	94
Figure A.6 A sample “out” file (first lines)	96
Figure A.7 A sample “out” file (last lines)	98
Figure A.8 A sample OUTCAR file (first lines)	99
Figure A.9 A sample OUTCAR file (last lines)	100

CHAPTER 1

INTRODUCTION

1.1 Catalysis

1.1.1 Fundamentals of Catalysis

Catalysis is the key phenomenon that alters almost every event drastically in nature, in industry, in our lives, and even in our bodies. Today, of all the industrially used chemical reactions, ~80% are catalytic and the value of these chemicals add up to about US\$ 2-4 trillion [1].

As a matter of fact, the phenomenon of catalysis has been used since the early ages of mankind. For example, the fermenting of grape juice to produce ethanol is an example of a catalytic process even though people at that ages were not aware of such a fact. Scientifically, the concept of catalysis is put forward by Berzelius after his review in 1835 on a number of reactions which took place in the presence of a substance which remained unaffected. In his famous assertion, Berzelius wrote [2]:

“This is a new power to produce chemical activity belonging to both inorganic and organic nature, which is surely more widespread than we have hitherto believed and the nature of which is still concealed from us. When I call it a new power, I do not mean to imply that it is a capacity independent of the electrochemical properties of the substance. On the contrary, I am unable to suppose that this is anything other than a kind of special manifestation of these, but as long as we are unable to discover their mutual relationship, it will simplify our researches to regard it as a separate power for the time being. It will also make it easier for us to refer to it if it possesses a name of its own. I shall therefore, using a derivation well-known in chemistry, call it the catalytic power of the substances, and the decomposition by

means of this power catalysis, just as we use the word analysis to denote the separation of the component parts of bodies by means of ordinary chemical forces. Catalytic power actually means that substances are able to awaken affinities which are asleep at this temperature by their mere presence and not by their own affinity”

Simply putting, catalysis is the general name given to the occurrence of a chemical reaction in the presence of a catalyst. A catalyst is a substance that increases the rate of approach to equilibrium of a chemical reaction without being (substantially) consumed itself. A catalyst changes the rate but not the equilibrium of the reaction [3]. Catalysts can be imagined as providing new and simpler pathways for the reactants to be converted into products. All catalytic processes are cyclic in nature since the catalyst (ideally) comes out of one reaction and catalyzes another one in the catalytic cycle and finally ends up without being consumed at the end of the reaction.

Catalysis can be classified in various bases according to the point of interest. However, the most general one is the classification upon the phase of the system in which catalysis takes place. According to this classification, the main branches of catalysis are:

- Homogeneous catalysis
- Heterogeneous catalysis

In homogeneous catalysis, the catalyst, reactants and products are all in the same phase, either in gas or liquid phase. The reactions generally evolve through well known organometallic complexes. The examples under this classification are catalysis in homogeneous solutions or catalysis by enzymes. Homogeneous catalysis is though to be very well understood in terms of mechanisms. However, the sensitivity of the catalytic complexes to air, moisture and temperature makes it undesirable. However, the biggest disadvantage is that the valuable catalyst cannot be separated (or separated very hard and unefficiently) from the products since all are in the same phase.

In heterogeneous catalysis, as the name implies, the catalyst and the reactive species are in different phases. To be more specific, solid catalysts are used and the reactants (and products) are generally in gas phase. The main advantage of heterogeneous catalysis over its homogeneous counterpart is that the separation of the catalyst is not a problem at all due to phase

difference [4]. Heterogeneous catalysis far more dominates over homogeneous catalysis in industrial applications and the subject of this work also falls within its framework. Thus, more emphasis will be given to it in the following section.

1.1.2 Heterogeneous Catalysis

1.1.2.1 Fundamentals of Heterogeneous Catalysis

Heterogeneous catalysis is the key to the application of catalysis in an industrial scale. Approximately 90% of all industrial catalytic reactions are heterogeneous [5]. Thus, traditional industries including chemical, food, pharmaceutical, automobile and petrochemical industries rely heavily on heterogeneous catalysis. Furthermore, in order to achieve a sustainable chemical industry that is in harmony with the nature, heterogeneous catalysis is of key importance because of its applications in areas like fuel cells, automotive exhausts and many other subjects related to green chemistry.

Although heterogeneous catalysis is associated with solid catalyst particles, all the reaction is taking place only at the surface of the solid. Thus, an understanding of the surface structure is crucial to understand how the catalyst works. However, there is no industrial catalyst consisting of a single specie. A ‘working’ catalyst generally consists of a combination of several kinds of active metals supported on inert oxide supports [3]. Additionally, they are doped with ‘promoters’ like alkali metals (e.g. potassium) and halogens (e.g. chlorine) with the aim of increasing selectivity. Furthermore, not all of the solid surface acts as a true catalyst in the reactions. Only small specific areas in the surface that are named as ‘active sites’ are involved in catalyzing a specific reaction. Determination of surface intermediates, reaction mechanisms and active sites are some of the hardest and most controversial areas in catalysis society for decades [5].

The steps taking place in a heterogeneous catalytic cycle are summarized as follows:

- Diffusion of the reactants through a boundary layer surrounding the catalyst particle,
- Intraparticle diffusion of the reactants into the catalyst pores and to the active sites,
- Adsorption of the reactants onto active sites,

- Surface reactions involving formation or conversion of various adsorbed intermediates, possibly including surface diffusion steps,
- Desorption of products from catalyst sites,
- Intraparticle diffusion of the products through the catalyst pores,
- Diffusion of the products across the boundary layer surrounding the catalyst particle.

The difficulty of heterogeneous catalysis can be understood if it is considered that all these steps are taking place in very different length and time scales. For example, a typical time scale for the overall catalytic reaction is a second with characteristic length scales that are on the order of 0.1 micron. The time scales for the fundamental adsorption, desorption, diffusion and surface reaction steps that form the overall catalytic cycle however, are often 10^{-3} seconds or shorter [4]. Keeping in mind that the industrial practice of catalysis is done in reactors which are meters long and catalyst optimizations are done considering years long operation including catalyst deactivation periods, we face the microscoping nature of the immense ‘universe of catalysis’ from years to femtoseconds and from meters to angstroms.

Because of these reasons, heterogeneous catalysis is a very broad and interdisciplinary topic that needs the collaboration of experts from different fields. Until now, the experts in the fields of catalyst synthesis, catalyst characterization, surface spectroscopy, physical chemistry, chemical kinetics, chemical reaction engineering and, most recently, with theoretical calculations of catalyst structure and performance using Density Functional Theory (DFT), quantum physics have contributed to the area of heterogeneous catalysis [5].

The studies that are performed by this wide range of experts can be classified as illustrated in Figure 1.1 [5].

Theoretical calculations utilizing DFT falls into the third level of research, ‘The Elucidation Level’. This means that, a DFT expert runs his calculations making use of the data generated by material scientists, engineers, physical chemists, etc. and analyze all this information to arrive to conclusions that increase the insight about the elementary steps of reactions, without making any assumptions about reaction steps beforehand.

In general, DFT calculations assess the structures, stabilities, and reactivity of species adsorbed onto the surface sites. This is very hard and expensive (most often impossible) to do

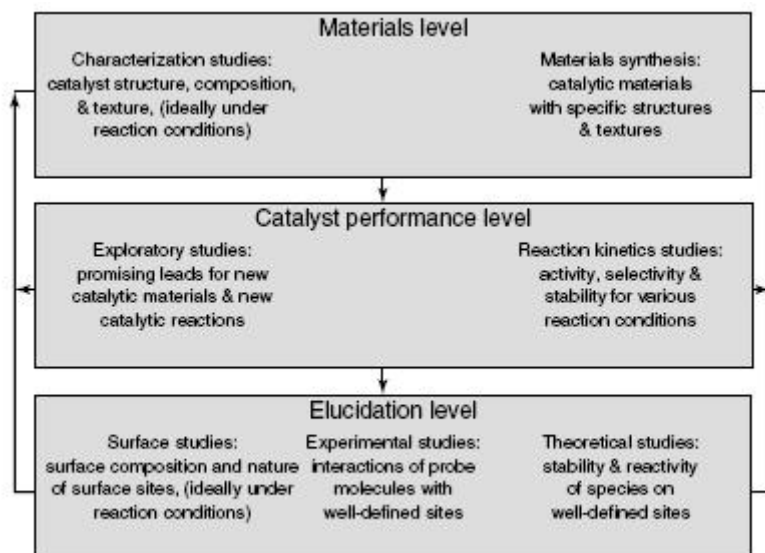


Figure 1.1: Levels of study in heterogeneous catalysis research

by present experimental techniques because of the complicated nature of reactions. However, it should be carefully noted that the aim of DFT calculations is not to determine catalytic parameters without doing experiments. The real objective is first to analyze the available spectroscopic information for a specific surface and reaction and then use DFT to clarify the points that remain in dark due to the inabilities of present spectroscopic techniques. In the ideal case, this results in the development of a model derived from first principles that can explain how to design a specific catalyst for a specific reaction, all based on scientific derivations instead of empirical data.

1.1.2.2 Sabatier Principle

There are several properties that a good catalyst should have. First, the catalyst should exhibit good selectivity for production of the desired products and minimal production of undesirable byproducts. It should achieve adequate rates of reaction at the desired reaction conditions of the process. It should be stable at reaction conditions for long periods of time, or it should be possible to regenerate good catalyst performance by appropriate treatment of the deactivated catalyst after short periods. Finally, a catalyst should have good accessibility of reactants and products to the active sites so that high rates of reactions can be obtained [5].

Beneath these properties, maybe the most important one is the selectivity towards the desired reaction and minimal selectivity towards the undesired reaction(s). This urges for a molecular point of view since selectivity is related to the very fundamental properties of the catalyst surface in atomic detail. Thus, adsorption is in the heart of heterogeneous catalysis. Again, from a molecular view, this is natural since the adsorption characteristics of species on surfaces are determined by structural and electronic structures, which also control the selectivity behavior of a catalyst.

This strong relation between the adsorption characteristics and catalytic ability of surfaces was first demonstrated by Sabatier in 1920. The principle of Sabatier states that a good heterogeneous catalyst is a material that exhibits an intermediate strength of interaction with the reactants, products, and intermediates of the catalytic process [6]. If the reactants and products interact too strongly with the surface, these molecules will block the surface and decrease the amount of surface that is accessible by other molecules, leading to low catalytic activity. On the other hand, if they interact too weak, the surface concentration of the reactant species will be low and the activation energy of the surface reactions will be high. This will also lead to low catalytic activity. Thus, when the adsorption strength of a surface (for a specific molecule) is plotted against the (catalytic) reaction rate, it is seen that the rate goes through a maximum at the optimum adsorption strength. Plots of this type are called ‘volcano plots’ and Sabatier’s principle is illustrated with the volcano plot given in Figure 1.2 [4].

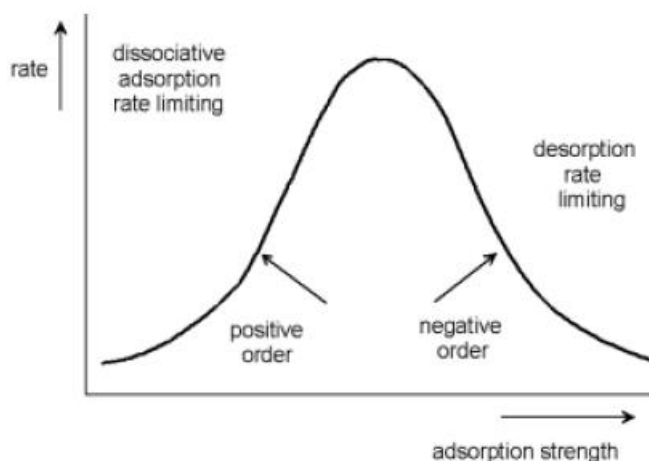


Figure 1.2: Sabatier’s principle illustrated with the volcano plot

1.1.2.3 Transition State Theory

In 1935, Eyring and Polanyi came up with a theory to account for the calculation of rate constants and thus rates of elementary reactions [5]. It is supposed that the elementary reactions go through a path with the lowest energy barrier (i.e. minimum energy path).

They assumed that there is a surface in phase space that divides it into a reactant and a product region. It follows that this dividing surface is located at the transition state. In other words, the maximum energy of the potential energy surface on the minimum energy path is the energy of the transition state and the activation barrier for a reaction can be calculated as the energy difference between the energies of the transition state and the initial state [7].

The properties of the transition state structure, like bond lengths for example, are parameters that directly affect the properties of the catalytic reaction. Thus, in transition state theory, the reaction rate is expressed as in Equation 1.1.

$$r_{TST} = \Gamma \frac{kT}{h} e^{-\Delta G^*/kT} \quad (1.1)$$

where, Γ is the transmission coefficient and ΔG is the free energy difference between the transition state and the initial state.

A potential energy surface represents the variation of the energy of a chemical system as the reacting molecules are located at different points in space. In most cases, the potential energy surface is represented one dimensionally, that is potential energy as a function of the reaction coordinate. A typical potential energy diagram is illustrated in Figure 1.3 [7].

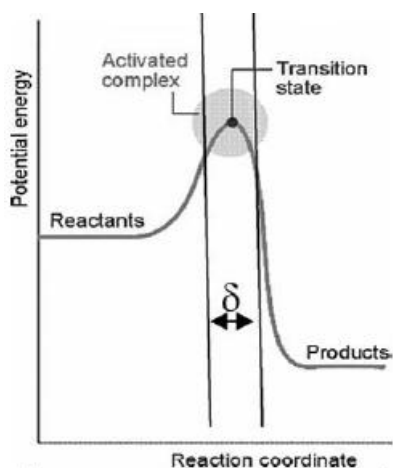


Figure 1.3: An example of one dimensional potential energy surface

However, the energy not only changes along the reaction coordinate but with every spatial coordinate. Thus, the real potential energy surface should be three dimensional covering all three coordinate axes in space. This potential energy surface can only be calculated with quantum chemical calculations. An example of a three dimensional potential energy surface is given in Figure 1.4 [4].

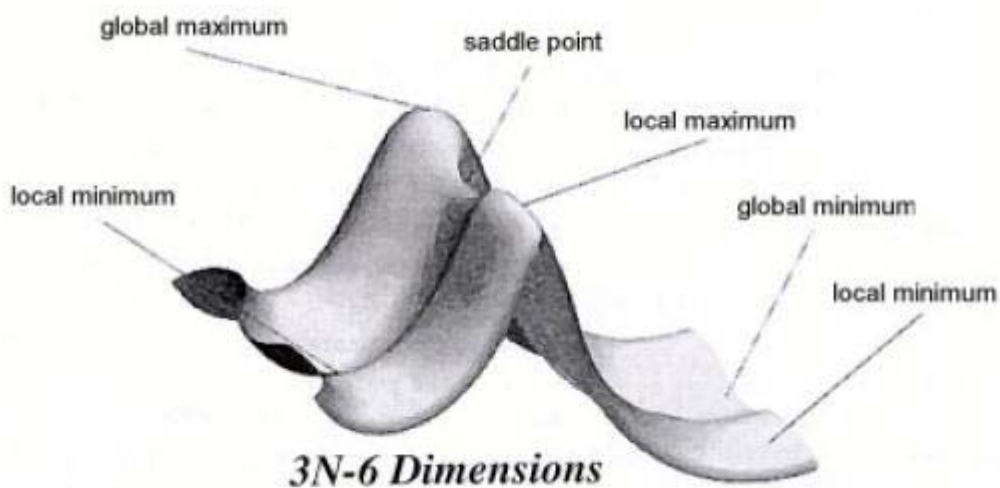


Figure 1.4: An example of three dimensional potential energy surface

The more realistic potential energy surface shown in Figure 1.4 illustrates the presence of local and global minima as well as local and global maxima. The local, and a global minima occur when the derivative of the energy with respect to the structural degree of freedom λ is

zero for all degrees of freedom λ_i (i.e., $dE/d\lambda_i = 0$).

Transition states occur at saddle points along the potential energy surface. The derivative of the energy with respect to the degree of freedom λ_i is zero for all degrees of freedom for transition state structures. In addition, the second derivative of the energy with respect to the degree of freedom λ_i is equal to zero for all degrees of freedom λ_i except for the mode which corresponds to the reaction coordinate.

In practical calculations, this means that the transition state structure calculated for a specific reaction should only show a single imaginary vibrational frequency and that should be along the reaction coordinate.

1.2 Propylene Epoxidation

1.2.1 Basic Properties of Propylene Oxide

Epoxides are cyclic ethers with three ring atoms. Epoxidation, also named as partial oxidation, is the name given to the formation of an epoxide of a selected alkene (unsaturated hydrocarbon containing a double bond). Thus, propylene epoxidation refers to the process where propylene (also referred to as propylene) is reacted with an oxidant and finally converted to propylene oxide (PO). PO molecule is illustrated in Figure 1.5.

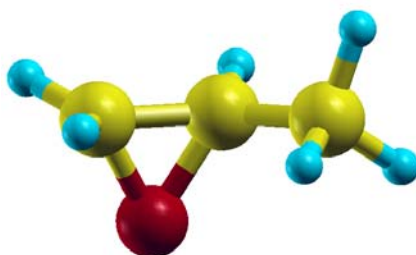


Figure 1.5: Illustration of propylene oxide molecule

PO is a significant organic intermediate for the production of polyether polyols, propylene

glycol and propylene glycol ethers which are all building blocks for polyurethane plastics. PO has a production capacity of about 5.8 million tones per year [8].

PO is a colorless, volatile liquid with a low boiling point of 34.2°C at atmospheric pressure. The three membered ring structure is highly reactive which gives the molecule the ability to undergo many kinds of reactions. Ring opening is the initial step for reactions having the epoxide as a reactant. PO can be converted to primary or secondary alcohols using acid or base catalysts. However, the most abundant use of PO is its use in polymerization to polyether polyols which is performed industrially using a basic catalyst such as KOH.

Further, PO can react with chemicals like water, hydroxyl containing organics, ammonia, amines, carbon dioxide, carbon disulfide, hydrogen sulfide, mercaptans and Grignard reagents. It can also undergo isomerization, hydrogenolysis and Friedel-Crafts reactions [9]. This versatility of the reactions that it can undergo makes PO one of the most important base chemicals in the world.

1.2.2 Industrial Production of Propylene Oxide

PO is produced mainly by two commercial processes, the chlorohydrin process and the hydroperoxide process. Chlorohydrin process is the first discovered one, which was also applied to ethylene epoxidation before the direct epoxidation of ethylene with silver was discovered, and the hydroperoxide process is a relatively new process, designed after the increasing concern over the chlorohydrin process. Nevertheless, both processes are employed in large scale and it is estimated that each process has a share of about 50% in global PO production [9].

1.2.2.1 The Chlorohydrin Process

The chlorohydrin process involves reaction of propylene and chlorine in the presence of water to produce the two isomers of propylene chlorohydrin. This is followed by dehydrochlorination with caustic or lime to PO and salt.

In more detail, the alkene reacts with hypochlorous acid (HOCl) to produce the chlorohydrin. The hypochlorous acid is produced in situ by an equilibrium reaction of the acid with water and chlorine. Afterwards, the chlorohydrin is dehydrochlorinated, using aqueous potassium

hydroxide to produce the epoxide. This route has long been the main process for producing both ethylene oxide and propylene oxide. In the 1940s, the process began to be phased out for ethylene epoxidation, because of the development of a more efficient direct epoxidation process using a silver catalyst. After that discovery, many ethylene epoxidation plants that were using the chlorohydrin process were converted for the epoxidation of propylene. The process is still applied for propylene epoxidation although it is gradually being replaced by the more environmentally friendly hydroperoxide processes.

The two reactions steps that take place in the production of propylene chlorohydrin are illustrated in Figures 1.6 and 1.7 [10].

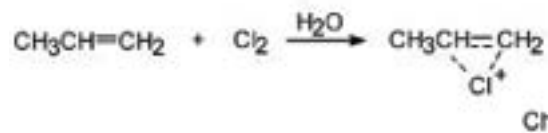


Figure 1.6: First reaction step of propylene chlorohydrin production

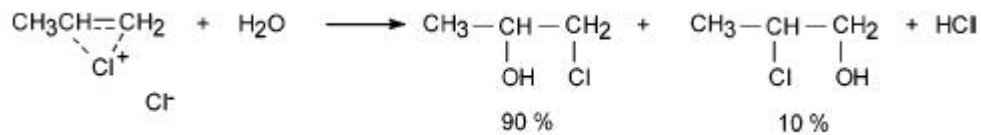


Figure 1.7: Second reaction step of propylene chlorohydrin production

A schematic flowsheet of the process is illustrated in Figure 1.8 [10].

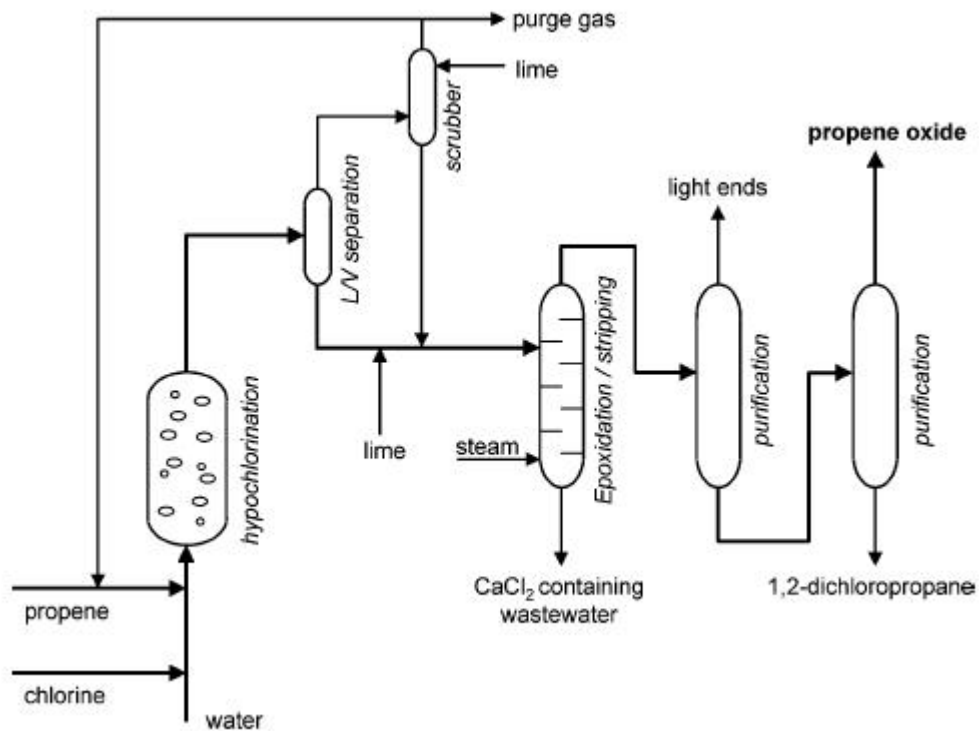


Figure 1.8: Simplified flowsheet of the chlorohydrin process

Dehydrochlorination of propylene chlorohydrin that takes place in the epoxidation reactor results in PO production as illustrated in Figure 1.9 [10].

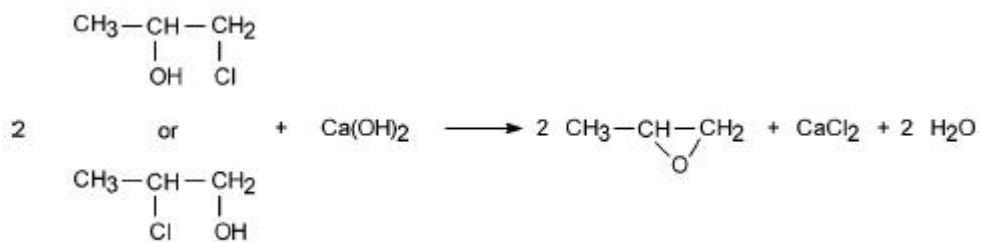


Figure 1.9: PO production reaction of the chlorohydrin process

As can be seen in Figure 1.8, the epoxidation reactor also produces a brine containing poisonous calcium chloride salt. This is one of the major disadvantages of the chlorohydrin process, because the amount of brine (5% CaCl₂) produced is usually about 40 times larger than the amount of PO produced and it is extremely difficult to remove all hydrocarbons from this wastewater stream. The produced calcium chloride salt is not reused since it does not

have an economic value. Thus, the chlorohydrin process causes serious environmental problems. This is the main reason behind the fact that this technology is being phased out by the more 'green' hydroperoxide process.

1.2.2.2 The Hydroperoxide Process

Hydroperoxide processes are based on the peroxidation of an alkane to an alkylhydroperoxide. These alkylhydroperoxides then react with propylene, producing propylene oxide and an alcohol. A characteristic of these processes is that, besides propylene oxide, a coproduct is produced in a fixed ratio, usually 2-4 times the amount of propylene oxide produced. Currently, two variants of this process are applied commercially. The first is the propylene oxide-styrene monomer (PO-SM, also commonly abbreviated as SMPO) process (about 60% of all hydroperoxide plants). In this process, ethylbenzene is oxidized to ethylbenzene hydroperoxide, which reacts with propylene to produce propylene oxide and R-phenyl ethanol. The R-phenyl ethanol is then dehydrated to produce styrene. The second process is the propylene oxide-t-butyl alcohol (PO-TBA) process. In this process, isobutane is oxidized to t-butyl hydroperoxide (TBHP), which reacts with propylene to produce propylene oxide and t-butyl alcohol. This can be dehydrated to isobutene or converted directly with methanol to methyl tertiary butyl ether (MTBE).

The two processes are analogous in principle and the same type of reactions that occur in PO-SM process occur also in PO-TBA process. It is only necessary to replace the ethylbenzene with isobutane as the starting material to pass from PO-SM to PO-TBA process.

A schematic flowsheet of the PO-SM process is illustrated in Figure 1.10 [10].

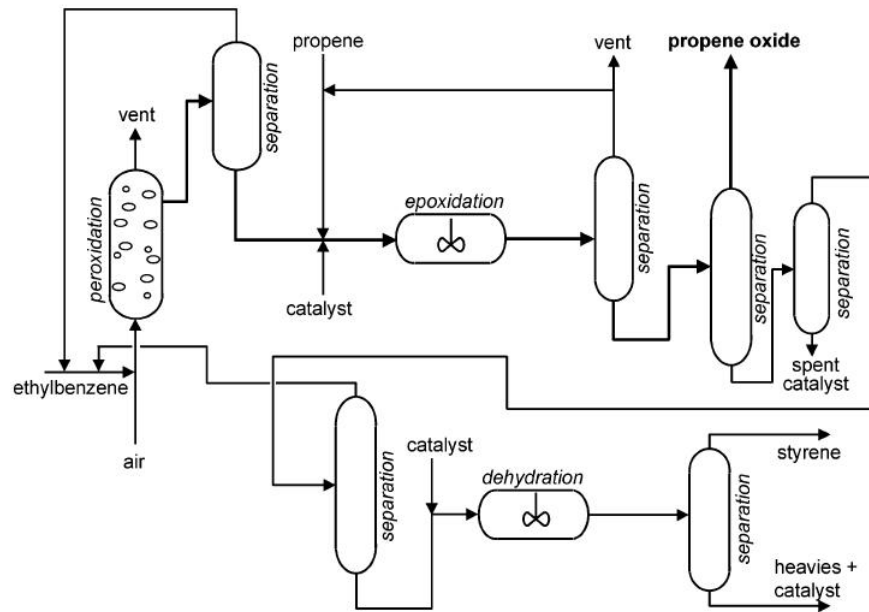


Figure 1.10: Simplified flowsheet of the PO-SM process

The reactions taking place in PO production are illustrated in Figures 1.11 and 1.12 [10].

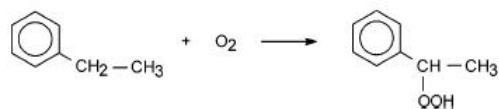


Figure 1.11: First reaction step of PO production in PO-SM process

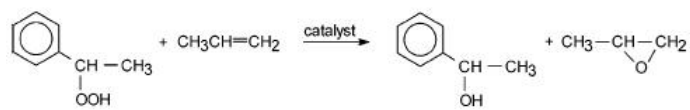


Figure 1.12: Second reaction step of PO production in PO-SM process

1.2.2.3 Direct Propylene Epoxidation

Both of the industrial PO production methods are undesirable because they are either inefficient, indirect, multi-step, expensive or non-environmentally friendly. Thus, serious efforts have been put into discovery of heterogeneous catalysts that can directly epoxidize propylene with air.

Unfortunately, ethylene is the only alkene that can be epoxidized directly with air using a supported silver catalyst and silver is the only selective catalyst serving this purpose. Efforts in directly epoxidizing propylene with silver indicated selectivities about 5% and all products were essentially combustion products [3].

Until now, all attempts to manufacture propylene oxide commercially by the direct oxidation of propylene have been unsuccessful [1].

1.3 Computational Quantum Chemistry

1.3.1 Basics of Computational Quantum Chemistry

Classical mechanics deals with the trajectories of particles which can be calculated theoretically from the knowledge of the initial conditions and the structure of the Hamilton H , or the sum of a kinetic energy contribution T and potential energy function V .

$$H = T + V \quad (1.2)$$

However, the existence of electron and hence electronic motion can not be explained classically, since the electron has also wave characteristics besides its particle nature. For this reason Schrodinger suggested to replace the classical kinetic and potential energy functions of Equation 1.2 with linear operators \hat{T} and \hat{V} and set up a wave equation of the form:

$$\hat{H}\Psi = \hat{T}\Psi + \hat{V}\Psi \quad (1.3)$$

The solutions of Equation 1.3, the so called wavefunctions, would describe the behavior of all

the particles. The quantum mechanical Hamiltonian above is given by:

$$\hat{H} = \hat{T} + \hat{V} \quad (1.4)$$

For one electron system such as the hydrogen atom, with the electron centered on the atomic nucleus, kinetic and potential energy operators are:

$$\hat{T} = -\frac{\hbar^2}{8\pi^2m}\nabla^2 \quad (1.5)$$

$$\hat{V} = -\frac{Ze^2}{r} \quad (1.6)$$

where m is the mass of the electron, r is the distance of the electron from the nucleus, Z is the atomic number, and e is the unit of the electronic charge. The Laplacian (∇^2) is given in Cartesian coordinates.

If we write the quantum mechanical Hamiltonian for a molecule, it will include basically [11]:

1. **Kinetic energy:** The kinetic energy operator for a particle of mass m is given in SI units as,

$$\hat{T} = \frac{1}{m}\nabla^2 \quad (1.7)$$

2. **Electrostatic interactions:** All the particles in a molecule are charged and Coulomb's law applies to the interactions between all of them so that the total energy of interaction between all of them is given by,

$$\hat{I} = \sum_{i=1}^N \sum_{j \neq i, j > 1}^N \frac{q_i q_j}{4\pi\epsilon_0 |\vec{r}_i - \vec{r}_j|} \quad (1.8)$$

where \vec{r}_i is the position vector of a typical particle and q_i is its charge.

1.3.2 Born-Oppenheimer Approximation

With the atomic units used, the molecular Hamiltonian and associated Schrodinger equation is easily written as:

$$\left[\sum_{i=1}^N -\frac{1}{2m_i} \nabla^2(i) + \sum_{i=1}^N \sum_{j=1, j>1}^N \frac{q_i q_j}{4\pi\epsilon_0 |\vec{r}_i - \vec{r}_j|} \right] \Psi(\vec{x}_1, \vec{x}_2, \dots, \vec{x}_n; t) = i \frac{\partial}{\partial t} \Psi(\vec{x}_1, \vec{x}_2, \dots, \vec{x}_n; t) \quad (1.9)$$

However, it is not as easy to solve Equation 1.9 as it is to write it since this equation is a partial differential equation in $3N+1$ variables and because of the appearance of the $\frac{1}{|\vec{r}_i - \vec{r}_j|}$ terms, it is not separable into any equations of smaller dimension. Thus, it is necessary to make some approximations of the electronic structure in order to solve Equation 1.9. The first approximation to be proposed for a solution is the Born-Oppenheimer model. It states that since the nuclei are much more massive than the electrons, the electrons adjust instantaneously to any motion of the nuclei. So it can be considered that the nuclei are fixed at some internuclear separation. This allows to separate the Schrodinger equation into two separate wavefunctions, the nuclear wavefunction Ψ_{nuc} and the electronic wavefunction Ψ_{elec} [12]. Thus the total wavefunction can be written, to a very accurate degree of approximation, as the product of these two separate wavefunctions in the form:

$$\Psi(\vec{x}_1, \vec{x}_2, \dots, \vec{x}_n) = \Psi_{elec}(x_{elec}; r_{elec}) \Psi_{nuc}(r_{nuc}) \quad (1.10)$$

where the first term in Equation 1.10 represents the electronic motion and the second term involves the motion of the nuclei. Furthermore, introducing center of mass and relative coordinates, the nuclear wavefunction reduces to:

$$\Psi_{nuc} \approx \Psi_{trans}(CM) \Psi_{rot} \Psi_{vib} \quad (1.11)$$

where the Center of Mass (CM) translational, rotational and vibrational contributions to the nuclear wavefunction are now explicitly shown. Thus, the problem of determining the structure of a complex molecule reduces to solving each Schrodinger equation for the electronic motion, the translational motion of the center of mass, and the rotational and vibrational

wavefunctions of the nuclei separately. Therefore, for a molecule composed of n electrons, the electronic energy is calculated by the Schrodinger equation in the form:

$$\hat{H}_{elec}(1, 2, \dots, n)\Psi_{elec} = E_{elec}\Psi_{elec}(1, 2, \dots, n) \quad (1.12)$$

The solutions to the electronic Schrodinger equation given by Equation 1.12 are infinite, but for stationary, bound states, only the continuous single value eigenfunctions that disappear at infinity need to be considered, and the electronic energies are the eigenvalues E_i given in:

$$\hat{H}\Psi_i = E_i\Psi_i \quad (1.13)$$

The eigenfunctions are normalized and mutually orthogonal (i.e., orthonormal) which means mathematically that they satisfy the condition:

$$\int \Psi_i\Psi_j d\tau = \langle \Psi_i | \Psi_j \rangle = \delta_{ij} \quad (1.14)$$

In Equation 1.14, the interaction is over the volume element for the electron, and it is given with the matrix or Dirac notation for the integral, where δ_{ij} is the Kronecker delta. The electronic energy of the system, E_i , is the expectation value of the Hamiltonian. The solution for E_i is given as:

$$\int \Psi_i\Psi_j\hat{H}d\tau = \langle \Psi_i | \hat{H} | \Psi_j \rangle = E_i \quad (1.15)$$

1.3.3 Variational Principle and Hartree-Fock Theory

The complete treatment of a quantum mechanical problem involving electronic structure requires the complete solution of the Schrodinger equation given in Equation 1.12. This is only possible for one electron systems, and for many-electron systems, where the electron repulsion term in the Hamilton makes an analytical solution impossible, the variational principle is applied [12]. The variation principle states that if Ψ is a solution to Equation 1.12 then for any small change $\delta\Psi$:

$$\delta E = \delta \langle \Psi_i | \hat{H} | \Psi_j \rangle = 0 \quad (1.16)$$

If this criterion is applied to an electronic wavefunction Ψ , in the required number of dimensions, all the eigenfunctions Ψ_i for the electronic Hamilton will be gathered. If only an approximation to the wavefunction Ψ is used, and then the eigenfunctions Ψ_i and eigenvalues E_i are only approximations to the correct values. The accuracy of the estimates would improve if better approximations for the total wavefunction is used. The orbital approximation suggests that the total electron wavefunction Ψ can be written as the Hartree product of one electron wavefunctions, $\Psi_i \eta(\zeta)$, called spin orbitals [13]. These orbitals include the product of spatial and spin functions, where $\eta(\zeta)$ is the spin function that can take values α or β . Thus, the total wavefunction can be written as:

$$\Psi(1, 2, \dots, n) = O(s)A[\Psi_1(1)\alpha_1\Psi_2(2)\beta_2\dots\Psi_n(n)\beta_n] \quad (1.17)$$

In Equation 1.17, A is the antisymmetrizer, making sure that the wavefunction changes sign on interchange of any two electrons in accordance with the Pauli exclusion principle, and O(S) is a spin projector operator that ensures that the wavefunction remains an eigenfunction of the spin squared operator S^2 . O(S) may become fairly complex but it is equal to unity for a closed shell molecule with all electrons paired in the spin orbitals. Thus, for a closed shell system with $2n$ electrons, and two electrons paired in each spatial orbital, the n electron wavefunction becomes:

$$\Psi(1, 2, \dots, n) = A[\Psi_1(1)\alpha_1\Psi_2(2)\alpha_2\dots\Psi_n(2n-1)\alpha_n\Psi_n(n)\beta_n] \quad (1.18)$$

Equation 1.18 is the well known Slater determinant and it is the correct form for the many electron wavefunction for closed shells as the only determinant of spin orbitals. In order to determine the actual electron spatial orbitals, Ψ_i , for a closed shell system, it is necessary to apply the variational principle for the solution of Equation 1.18. The molecular orbitals, therefore, are obtained by varying all the contributing one electron functions $\Psi_1, \Psi_2, \dots, \Psi_n$ in the Slater determinant until the electronic energy achieves its minimum value. This will give the best approximation to the many electron wavefunction, Ψ and the electronic or molecular orbitals, Ψ_i obtained in that way are referred to as self consistent or Hartree-Fock molecular

orbitals. Mathematically, the problem involves the minimization of the total electron energy with the orthonormality constraint for the electron orbitals [11]. The function to be minimized is given as:

$$G = E - 2 \sum_i \sum_j \varepsilon_{ij} S_{ij} \quad (1.19)$$

where E and S_{ij} (orthonormality) are given as:

$$E = \langle \Psi(1, 2, \dots, n) | \hat{H} | \Psi(1, 2, \dots, n) \rangle, \quad (1.20)$$

$$S_{ij} = \int \Psi_i \Psi_j d\tau \quad (1.21)$$

After the minimization, we get the Hartree-Fock (HF) equation given by:

$$\hat{F}\Psi_i = E_i\Psi_i \quad (1.22)$$

Equation 1.22 states that the most accurate molecular orbitals are eigenfunctions of the Hartree-Fock equation Hamiltonian operator. The one electron HF hamiltonian operator, F , is defined as:

$$\hat{F} = \hat{H}^{core} + \sum_j 2\hat{J}_j - \hat{K}_j \quad (1.23)$$

The first term in Equation 1.23 is the one electron Hamiltonian for an electron moving in the field of bare nuclei and it is defined as:

$$\hat{H}^{core} = \frac{1}{2} \nabla_p^2 - \sum_a Z_a r_{pA}^{-1} \quad (1.24)$$

The second operator represents the average effective potential of all other electrons affecting the electron in the molecular orbital Ψ_i and can be defined by:

$$\hat{J}_j(1) = \int \Psi_j^*(2) \frac{1}{r_{12}} \Psi_j(2) d\tau_2 \quad (1.25)$$

The final operator in Equation 1.23 is the exchange potential and it is due to the effect of the antisymmetry of the total wavefunction on the correlation between electrons of parallel spin and it can be defined as [12]:

$$K_j(1)\Psi_i(1) = \left[\int \Psi_j^*(2) \frac{1}{r_{12}} \Psi_j(2) d\tau_2 \right] \Psi_j(1) \quad (1.26)$$

The eigenvalues of Equation 1.22 are the energies of electrons occupying the orbitals Ψ and thus, are known as orbital energies. In a similar fashion to Equation 1.23, they are defined as:

$$\varepsilon_i = H_{ij}^{core} + \sum_i (2J_{ij} - K_{ij}) \quad (1.27)$$

where H_{ij} , the one electron core energy for an electron moving in the field of bare nuclei, J_j , the coulomb interaction energy and K_{ij} , the exchange energy, are given as:

$$H_{ij}^{core} = \int \Psi_i^*(1) \hat{H}^{core} \Psi_i d\tau_j \quad (1.28)$$

$$J_{ij} = \int \int \Psi_i^*(1) \Psi_j^*(2) \frac{1}{r_{12}} \Psi_i(1) \Psi_j(2) d\tau_1 d\tau_2 \quad (1.29)$$

$$K_{ij} = \int \int \Psi_i^*(1) \Psi_j^*(2) \frac{1}{r_{12}} \Psi_j(1) \Psi_i(2) d\tau_1 d\tau_2 \quad (1.30)$$

The general procedure for the solution of Hartree-Fock equations is iterative. First, a solution for the molecular orbitals Ψ_i is assumed for generating the Hartree-Fock operator F. This estimate generates a set of molecular orbitals and then it is used to repeat the calculations until the orbital no longer changes within a certain tolerance, while further interacting. These orbitals are said to be self consistent with the potential field they generate. In addition to these n occupied orbitals, there will be unoccupied orbitals called virtual orbitals of higher energy. The Hartree-Fock equations are used to reduce the N-electron problem into the solution of n-single-electron systems [4].

A more developed approach to the solution of Hartree-Fock equation is done by the Linear Combination of Atomic Orbitals (LCAO) as given in the formula:

$$\Psi_i = \sum_{\mu} c_{\mu i} \phi_{\mu} \quad (1.31)$$

where the ϕ_{μ} are the atomic orbitals constituting the molecular orbital or basis set.

During the numerical calculations of molecular orbitals, it is necessary to have convenient analytical forms for the atomic orbitals of Equation 1.31 for each type of atom in the molecule. The solutions of the Schrodinger equation for one electron systems (H atom) can be written by separation of variables as:

$$\Phi(r, \theta, \phi) = R_{n,l}(r) Y_{lm}(\theta, \phi) \quad (1.32)$$

where r , θ and ϕ are the spherical coordinates centered on the atom. The angular part of the above equation or $Y_{lm}(\theta, \phi)$ are the spherical harmonics which are defined as:

$$Y_{lm}(\theta, \phi) = \Theta_{lm}(\theta) \phi_m(\varphi) \quad (1.33)$$

where l is the azimuthal quantum number, and m is the magnetic quantum number. For the radial part of the atomic function, the Slater Type Orbitals are used as given in the form:

$$R_{n,l}(r) = (2\zeta)^{\frac{n+1}{2}} [(2n)!]^{-\frac{1}{2}} r^{n-1} \exp(-\zeta r) \quad (1.34)$$

where n is the principle quantum number, and l is the orbital exponent which is a function of the atomic number. Then, the variational principle is applied as previously mentioned except the total electron wavefunction consists of the product of molecular orbitals similar to Equation 1.31. The orthonormality of the electron wavefunction results in:

$$\sum_{\mu\nu} c_{\mu i}^* c_{\nu j} S_{\mu\nu} = \Delta_{ij} \quad (1.35)$$

where $S_{\mu\nu}$, the overlap integral for the atomic orbitals is defined by:

$$S_{\mu\nu} = \int \phi_{\mu}(1)\phi_{\nu}(1)d\tau_1 \quad (1.36)$$

Equations 1.35 and 1.36 result in the Roothan equations given by:

$$\sum_{\nu} (F_{\mu\nu} - \varepsilon_i S_{\mu\nu}) C_{\nu i} = 0 \quad (1.37)$$

The elements of the matrix representation of the Hartree-Fock hamiltonian are given as:

$$F_{\mu\nu} = H_{\mu\nu} + \sum_{\lambda\sigma} P_{\lambda\sigma} [(\mu\nu|\lambda\sigma) - \frac{1}{2}(\mu\lambda|\nu\sigma)] \quad (1.38)$$

$$H_{\mu\nu} = \int \phi_{\mu}(1)\hat{H}^{core}\phi_{\nu}(1)d\tau_i \quad (1.39)$$

$$P_{\mu\nu} = 2 \sum_i^{occ} c_{\mu i}^* c_{\nu i} \quad (1.40)$$

$$(\mu\nu|\lambda\sigma) = \int \int \phi_{\mu}^*(1)\phi_{\nu}^*(1)\frac{1}{r_{12}}\phi_{\lambda}(2)\phi_{\sigma}(2)d\tau_1 d\tau_2 \quad (1.41)$$

$P_{\mu\nu}$ are the elements of the electron density matrix, $H_{\mu\nu}$, the elements of the core Hamiltonian with respect to atomic orbitals, and Equation 1.41 is the general two-electron interaction integral over atomic orbitals [14]. The main improvement of the Roothan equations given in Equation 1.37 is that the Roothan equations are algebraic equations in contrast to the Hartree-Fock equation given in Equation 1.22. The Roothan Equation can be written in matrix form as:

$$FC = SCE \quad (1.42)$$

where E is the diagonal matrix of the ε_i . Hartree-Fock Hamiltonian operator matrix elements are dependent on the orbitals through the elements $P_{\mu\nu}$, and the Roothan equations are solved by first assuming an initial set of linear expansion coefficients $c_{\mu i}$, generating the corresponding density matrix $P_{\mu\nu}$ and computing a first guess to $F_{\mu\nu}$. The diagonalization procedure

depends on standard matrix eigenvalue techniques, and new expansion coefficients are calculated in each guess. This process is repeated until the coefficients stop deviating within a given tolerance [12].

1.3.4 Post Hartree-Fock Methods

The Hartree-Fock solution strategy avoids the direct solution of electron-electron interactions but instead replaces these interactions by a mean field approach. This ignores the fact that the motion of individual electrons may be correlated. By definition, the difference in the energy calculated by Hartree-Fock theory for a specific basis set which treats the systems as a mean field (without correlation) and the exact energy is the correlation energy. There are two primary strategies for treating correlated motion between electrons. Electrons with the same spin behave differently to electrons with opposite spins. The basic Hartree-Fock theory already includes the treatment of electrons with the same spin since the wavefunction is required to be antisymmetric for the theory to be applied. However, HF theory does not treat appropriately the interaction of electrons which have opposite spins. The wavefunction of the system, Ψ , cannot be described by a single determinant. Three general approaches have been developed to treat electron correlation:

- Configurational Interaction (CI),
- Moller-Plesset(MP) Perturbation Theory,
- Coupled Cluster (CC) Theory.

The common part in all of these advanced methodologies is that the electron correlation is treated accurately and to the desired degree with the selection of the method according to the compromise between computational time and accuracy. Thus, chemical and physical parameters can be determined very accurately. However, there is a big disadvantage that the computational requirement for these procedures are too high to model catalytic systems that have different kind of atoms in numbers as high as tens or hundreds. The comparison of the computational scaling of some selected post HF methods with respect to the number of atoms (N) are given below:

$$HF(N^4) < MP2(N^5) < CISD, MP3, CCSD(N^6) < MP4, CCSD(T)(N^7) \quad (1.43)$$

Thus, the applicability of these methods are limited to single molecules or geometrically fixed systems [4].

1.3.5 Basis Sets

Essentially in all ab initio (first principles) methods, the structural positions of the atoms and their basis functions are the only required parameters to calculate the electronic ground state, which puts them into the class of first principle methods that do not require empirical information. In order to expand the molecular orbital, an unknown function, in a set of known functions we need an infinite number of basis functions. An unknown molecular orbital (MO) can be thought of as a function in the infinite coordinate system covered by the complete basis set. When a finite basis is used, only the components of the MO along those coordinate axes corresponding to the selected basis can be represented. So, in order to increase the accuracy as much as possible, a necessary volume of basis set has to be used consisting of the correct type of basis function in order to represent the MO more accurately. If a single basis function is able to produce the unknown molecular orbital better than another, the number of basis functions needed to represent the MO will be smaller, which will decrease the number of iterations to be made. Thus, a variety of different basis sets currently exist and depend on the solution method used, the type of problem considered and the degree of accuracy required for solution. These functions can take on one of several mathematical forms, including Slater type functions, Gaussian functions and plane waves [4].

Gaussian (GTO) or Slater (STO) type basis functions are often used because they have a smaller computational cost required in the solution process. Solid state systems, consisting of infinite solid surfaces described by periodic methods, on the other hand, are more naturally represented by using periodic plane wave basis functions. The comparison of basis functions, guidelines for the selection of basis sets according to the chemical system investigated and both advantages and disadvantages of the basis sets will be discussed in more detail in the following section.

1.4 Density Functional Theory (DFT)

1.4.1 Principles of DFT

Density Functional Theory (DFT) is one of the most celebrated and powerful quantum chemical methods for calculating the ground state total energy of many body systems. Some of the opportunities that this theory offers to a surface chemist are summarized as follows:

- Unique opportunity of investigating the catalytic surfaces at atomic level,
- Atomic level perspective of the catalyst surface leading to the identification of the surface intermediates which can not be (exactly) detected by current experimental techniques,
- Determination of the energetics of various reactions and prediction of reliable reaction models which are in accordance with experiments favorably [15].

In DFT the total energy of a system is expressed as a functional of the total electron density. It was not until the 1960's that an exact theoretical framework called Density Functional Theory (DFT) was formulated by Kohn and Sham in 1965 [16], which later (in 1998) brought Walter Kohn the Nobel Prize in Chemistry. Earlier, motivated by the search for practical electronic structure calculations, Slater [17] had developed an approach, later to become the $X\alpha$ method, which was originally intended as an approximation to Hartree-Fock theory. Today, the $X\alpha$ method is generally viewed as a simplified form or precursor of density functional theory.

In principle, DFT neither does offer the calculation of new physical or chemical parameters, nor it offers a completely new physical concept in electronic structure calculations. Basically, although the fundamental quantity is the wavefunction, Hartree-Fock theory is also a density matrix theory [11]. What makes DFT so special for quantum chemists is that the CPU requirement of DFT scales with N^3 as opposed to the other wavefunction methods which scale at least with N^4 or higher. This allows the modelling of complex chemical systems (hundreds of atoms) consisting of various molecules, surfaces together with the adsorbed atoms, reactants, products and transition state structures on it which cannot be modelled with wavefunction methods because of their high computational cost. This phenomenon is illustrated in

Figure 1.13 [4].

Method	Number of basis functions	Estimates for the maximum number of atoms that can currently be handled
DFT	N^3-N^4	50-100
HF	N^4	
MP2	N^5	25-50
MP4	$<N^5$	
CISD	N^7	10-15
QCISD	N^7	

Figure 1.13: Computational burden of different methods in quantum chemistry

The practical application of DFT is attributed to work of Hohenberg and Kohn, who stated that the ground-state energy for a system is a unique functional of its electron density [18]. Afterwards, Kohn and Sham founded DFT by showing how the energy could be separated into kinetic energy for the motion of the electrons, potential energy for the nuclear electron attraction, the Coulombic electron-electron repulsion and finally exchange&correlation which covers all other electron-electron interactions [16]. Thus, the energy of an N-particle system can then be written as:

$$E[\rho] = T[\rho] + V[\rho] + E_c[\rho] + E_{xc}[\rho] \quad (1.44)$$

where,

$$T[\rho] = 2\sigma_i \Psi_i \left[-\frac{\hbar^2}{2m} \right] \nabla^2 \Psi d^3 r \quad (1.45)$$

$$V[\rho] = \int V_{ion}(r) \rho(r) d^3 r \quad (1.46)$$

$$E_c[\rho] = \frac{e^2}{2} \int \frac{\rho(r)\rho(r')}{|r-r'|} d^3 r d^3 r' \quad (1.47)$$

This formulation is derived keeping in mind that N-particle system could be rewritten as a set of n-electron problems (similar to the molecular orbitals in wavefunction methods) which

could be solved self consistently. In mathematical terms,

$$\hat{H}\Psi_i = \varepsilon_i\Psi_i \quad (1.48)$$

where,

$$\hat{H} = -\frac{\hbar^2}{2m}\nabla^2 + V_{ion}(r) + \frac{e^2}{2} \int \frac{\rho(r)\rho(r')}{|r-r'|} d^3r + V_{xc}(r) \quad (1.49)$$

In Equation 1.49, the terms represent the kinetic energy of the electron, the potential for nuclear-electron attractive interactions and the coulombic repulsive interactions between electrons, respectively. $V_{xc}(r)$ corresponds to the exchange correlation potential which is the derivative of the exchange correlation energy given in Equation 1.44. $V_{xc}(r)$ is also defined as the electron chemical potential. In that sense, it can be written as:

$$\mu_{xc}(r) = \frac{\delta E_{xc}[\rho(r)]}{\rho(r)} \quad (1.50)$$

Equation 1.44 could be solved exactly provided that all the terms in it were known. That is true except for the exchange & correlation energy term. The existence of correlations between the electrons, the main formal difficulty encountered in treating a materials problem in quantum mechanics, is a familiar one in many contexts. The positions and motions of the particles that make up a molecule or material are correlated because the particles interact with each other and exert forces upon each other as they move. In quantum mechanics, the situation is further compounded by forces that evolve from the Pauli Exclusion Principle governing electrons. This causes correlations to appear even between noninteracting particles that have no direct interaction with each other. Such forces are referred to as exchange forces. Whether due to interactions (e.g., the Coulomb force) or exchange, correlations can be characterized as either long or short range. The former can be dealt with by averaging techniques and a mean field or a self consistent field (meaning that the field experienced by an atom depends on the global distribution of atoms). Short range correlations involve the local environment around a particular atom, i.e., deviations of the local environment from average behavior, and are much more difficult to treat. In large part, the central problem of quantum methods in chemistry and condensed matter physics has been the search for more and more accurate

ways of incorporating exchange & correlation energy into mean field theory. Thus, it can be said that Density Functional Theory calculations are accurate as the approximation for E_{xc} . Fortunately, there are a number of very useful approximations for the calculations of E_{xc} in DFT.

1.4.2 Main Approximations for Exchange & Correlation

1.4.2.1 Local Density Approximation (LDA)

The most basic solution to calculate E_{xc} is the local density approximation which assumes that exchange-correlation per electron is equivalent to the exchange correlation per electron in a homogeneous electron gas which has the same electron density at a specific point r [4]. This is typically written as:

$$E_{xc}(r) = \rho(r)\varepsilon_{xc}[\rho(r)] \quad (1.51)$$

The local density approximation (LDA) is valid only in the region of slowly varying electron density. LDA also does not take into account the spin paired case. ‘Different densities for different spins’ are used in that case and this method is named as Local Spin Density Approximation (LSD) [11]. The exchange-correlation energy for the homogeneous electron gas can be written in LDA as the sum of separate exchange and correlation energies defined as:

$$E_{xc} = E_x + E_c \quad (1.52)$$

where,

$$E_x = \frac{-9}{4}\alpha_{ex}\frac{3}{4\pi} \sum_{\gamma} \int [\rho_1^{\gamma}(r_1)]^{4/3} dr_1 \quad (1.53)$$

$$E_c = \int \rho_1(r_1)\varepsilon_c[\rho_1^{\alpha}(r_1)\rho_1^{\beta}(r_1)]dr_1 \quad (1.54)$$

where $\varepsilon_c[\rho_1^{\alpha}(r_1)\rho_1^{\beta}(r_1)]$ represents the correlation energy per electron in a gas with the spin densities α and β . Simplified versions of LDA were known long before the formal develop-

ment of DFT. Of particular importance is Hartree-Fock-Slater, or $X\alpha$. This method retains only the exchange part and does not take into account the correlations between electrons. The LDA approximation is obviously an oversimplification of the actual density distribution and is well known to lead to calculated bond and binding energies that are over predicted by $\sim 10\%$ [19]. However, despite the simplicity of the fundamental assumptions, LDA method is often found to provide results with similar accuracy similar to those obtained by wavefunction based Hartree-Fock Theory.

1.4.2.2 Generalized Gradient Approximation (GGA)

Improvements over the LDA approach have to consider a non-uniform electron gas. A step in this direction is to make the exchange and correlation energies dependent not on the electron density, but also on derivatives of the density. Such methods are known as Generalized Gradient Approximation (GGA). GGA methods are also sometimes referred to as non local methods, although this is a bit misleading since the functionals depend only on the density (and derivatives) at a given point, not on a space volume like in the Hartree-Fock exchange energy. There are many forms of GGA and each of them is known with the name of its developer. Some of the most important include BP86 (Becke and Perdew corrections), PW91 (Perdew-Wang exchange functional), PBE (Perdew-Burke-Ernzerhof) or RPBE (Revised PBE functional). For of example, the widely used Becke (B88) correction to LSD for the exchange is given by :

$$E_x^g = b \sum_{\sigma} \frac{\rho_{\sigma} x_{\sigma}^2}{|1 + 6bx_{\sigma} \sinh^{-1} x_{\sigma}|} \quad (1.55)$$

where,

$$x_{\sigma} = \frac{\nabla \rho}{\rho_{\sigma}^{4/3}} \quad (1.56)$$

In Equation 1.56 x_{σ} is the dimensionless density gradient and ρ_{σ} is the density. The term b is a fitting parameter for the energy that is regressed against atomic data [4].

Perdew and Wang proposed a gradient correction to the LSD formulation. It appeared in 1986 and is known as by the acronym PW86. Then the formalism was modified by Perdew

and Wang in 1991, this modified form of the formalism is known as PW91 or P91. The gradient corrected exchange functionals of PW86 and PW91 are given in Equations 1.57 and 1.58 with a and b terms as constants.

$$\varepsilon_x^{PW86} = \varepsilon_x^{LDA}(1 + ax^2 + bx^4 + cx^6)^{1/15} \quad (1.57)$$

$$\varepsilon_x^{PW86} = \varepsilon_x^{LDA} \left[\frac{1 + xa_1 \sinh^{-1}(xa_2) + (a_3 + a_4e - bx^2)(x^2)}{1 + xa_1 \sinh^{-1}(xa_2) + a_5x^2} \right] \quad (1.58)$$

where x is defined the same as in Equation 1.56

1.4.2.3 Hybrid Methods

Recent developments in functionals attempt to couple an exchange component derived from Hartree-Fock theory which provides for a more exact match of the exchange energy for single determinant systems along with the correlation (and exchange) calculated from LDA theory in ‘hybrid’ functionals. One of the most famous is the B3LYP functional, which is a combination of the Lee, Yang and Parr functional and the three-parameter model by Becke [20]. The functional is given in Equation 1.59.

$$E_x^{B3LYP} = a_0 H_x^{HF} + a_x E_x^{B88} + (1 - a_c) E_c^{VWN} + a_c E_c^{LYP} \quad (1.59)$$

The parameters like a_0 are determined by fitting the results of the calculations to experimental data. Thus, the hybrid methods are not fully ‘ab initio’ in the sense that they require experimental data.

1.4.3 Capabilities of DFT

DFT is applicable to all atoms of the periodic table, provided relativistic effects are taken into account for heavier elements such as third row transition metals, rare earths, and actinides. The approach can be used for metallic, covalent, and ionic bonds. The application field ranges from metallic condensed systems to organic molecules. With the inclusion of gradient corrections for the exchange & correlation term, even weaker interactions such as hydrogen bonds

can be reasonably well described. DFT calculations utilizing Local Density Approximation (LDA) may encounter problems for narrow gap insulators and certain oxides. LDA tends to overemphasize the metallic character and care has to be taken in the interpretation of the density functional one electron energies. Furthermore, weaker bonds like hydrogen bonds are significantly overestimated in the LDA. The primary results of density functional calculations are the electron density, the spin density, the total energy and wave functions. From these quantities, one can derive important electronic, optic and magnetic properties including dipole moments and polarizabilities. DFT calculations for systems in their electronic ground state can be used to estimate electronic excitation energies including work functions, optical and UV spectra, and core level spectra for solids, surfaces, and molecules [21].

Quite consistently, for bonds in solids, molecules, and surfaces, interatomic equilibrium distances are predicted by precise density functional calculations to within about 0.02 Å of experiment while bond angles and dihedral angles are found within a few degrees of their experimental values. Within the local density approximation, binding energies are typically overestimated, sometimes by as much as a factor of two. Inclusion of non local gradient corrections improves the values of binding energies and brings them to within about 10 kJ/mol of experiment. The results obtained at this level of theory are comparable with sophisticated correlated quantum mechanical methods such as coupled cluster theory. Vibration frequencies are predicted to within 10-50 cm^{-1} . Unfortunately, at present there is no clear theoretical path that would allow the systematic improvement of the accuracy of density functional methods [4].

Density functional calculations are possible for systems of the order of 100 atoms. By exploring point group symmetry, calculations for clusters of over 1000 atoms have been demonstrated for fixed geometries. While the self-consistent-field procedure converges typically in 10-20 iterations for organic materials and semiconductors, metallic systems and especially magnetic transition metals such as Fe and Ni are very difficult to converge. In practice, this limits the size of systems that can be treated to approximately less than 60 atoms per unit cell or cluster.

Depending on the system under investigation, for example a metallic alloy or a molecular crystal, density functional theory can be implemented in quite different ways thus leading to efficient methods for particular materials. On the other hand, practical Hartree-Fock methods

require the use of Gaussian basis functions, which can be fairly inefficient for some systems. Thus, in general, density functional theory tends to be computationally more efficient than Hartree-Fock calculations. Without doubt, compared with correlated post Hartree-Fock methods, density functional calculations are by far more efficient computationally, scaling at worst with a third power in the number of basis functions as illustrated in Figure 1.13. In fact, significant effort is dedicated to the development of so called order-N methods, i.e. methods for which the computational effort increases linearly with system size. Such methods have been successfully demonstrated, yet the pre-factor is rather large so that these methods are competitive with conventional density functional implementations only for systems with several hundred atoms [22].

All together, these properties of DFT gives it an immense power in modelling of catalytic systems which makes it provide answers to many questions long debated in heterogeneous catalysis [23].

1.5 Main Approaches in Quantum Chemical Modelling of Catalytic Systems

1.5.1 The Cluster Model Approach

Computational quantum chemistry was first used for finite molecular systems which involve molecules and cluster models that describe the catalytic systems. Cluster models use the same basis used in many ab initio wavefunction methods, i.e. Gaussian or Slater basis sets. This is due to the fact that cluster models are used for the description of local chemical phenomena. Matter of fact, much of chemical phenomena is local since chemical forces are short range [24]. However 'local' is used here in the sense that the properties of the chemical system is effected by only a few neighbouring atoms. This would be a accurate way of modelling isolated molecules, gas phase reactions, as well as specific portions of ordered zeolites, oxides or very small nanoclusters in magnitudes of tens of atoms. In all of the mentioned systems, the reacting systems are basicly in gas or liquid phase even if interacting with a small portion of metal atoms. In cluster methods, this 'small portion' is at most 15-20 atoms, depending on the system modelled [25].

With such an approach, the biggest advantage would be the detailed picture one obtains of the shape of the individual orbitals of surface atoms(or every atom, if the system is a molecule)

and the modification brought to them by the presence of other atoms [26]. There is also a technical advantage of using cluster methods. Since quantum chemistry was ‘founded’ with the aim of computing the properties of atoms and their interactions, all high level ab-initio wavefunction techniques can be embedded to cluster methods which allows the selection of the the level of theory on the basis of accuracy beforehand. The key features related to heterogeneous catalysis that can be calculated with cluster methods include [27]:

- Geometry of adsorbed species,
- XPS and IR spectra of adsorbed species,
- d-d transitions,
- Spectroscopic transitions of defects (F centers),
- Magnetic coupling,
- Effective model hamiltonian parameters,

However, cluster method has well known disadvantages especially in the treatment of metallic systems. First of all, in order to model long range effects, clusters too large to be properly handled may be needed. Second, it is shown that the calculated parameters vary as functions of cluster size, thus care must be taken in order to interpret the obtained results. Furthermore, unwanted surface effects may arise. This is because the cluster has surfaces on all sides, not just the side the adsorbate reacts with and furthermore the limited surface of interest on the cluster leads to the undesired ‘edge effects’ where the parameters are effected unrealistically due to the edges of the cluster. However, the biggest disadvantage of the cluster method can be summarized with a debatable question: How many atoms are needed in the cluster to ‘describe the metal’? As the question implies, the representation of a metal substrate with, e.g., 20 atoms at most is definitely not realistic since this model cannot reproduce the band structure of the metal [25]. Thus, although in some lucky cases, catalytic properties over a metal surface can be described up to some extent with cluster methods, this model is not the choice of ‘modern’ quantum chemical methodology.

Because of the mentioned deficiencies of the cluster model in treating metals, solid state physics community later developed another type of model which allows the accurate modelling of solid surfaces, the so called ‘periodic approach’.

1.5.2 The Periodic Approach

The periodic approach, also known as the ‘semi-infinite crystal approach’ assumes non localized wavefunctions corresponding to the electrons in the periodic solid. In this approach, the band structure associated with the solid is calculated and the adsorbate is treated as a perturbation on this potential [25]. In order to model the periodicity of the solid, a supercell approach is needed to represent the repeated pattern of the solid, in contrast to the local nature in cluster methods. The supercell is defined by three lattice vectors as well as the length along these vectors, thus providing a three dimensional unit cell. The supercell is used to replicate the system infinitely along all three vectors using periodic boundary conditions, thus simulating the solid state. For three dimensional bulk systems this is straightforward. The simulation of surfaces, however, requires the metal atoms to be truncated along the vector perpendicular to the surface and replaced with a vacuum region. The unit cell is still repeated periodically along all three vectors. In this case, however, the result is a set of periodic slabs of some metal thickness sandwiched between two vacuum regions as shown in Figure 1.14 [4].

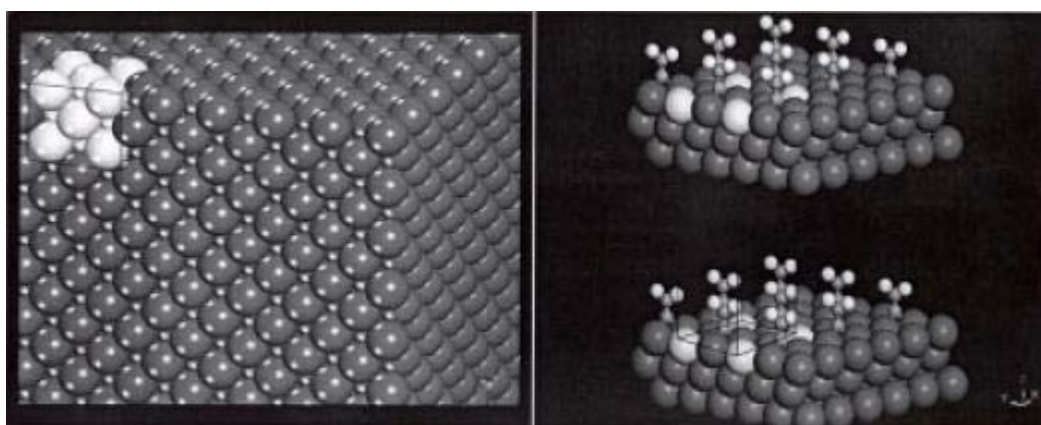


Figure 1.14: Illustration of bulk Pd and Pd(111) surface in periodic approach

The wavefunction, according to Bloch’s theorem, is one which contains a wave like portion, an exponential term and a periodic cell portion, $f_i(r)$ [28]. The wavefunction is expanded to take on the same periodicity of the lattice. The wavefunction is described by the summation of plane waves expanded out to a chosen cut-off energy. In mathematical terms, this can be written with Equations 1.60 and 1.61.

$$\Psi_i(r) = \sum_G c_{i,k} + \text{Exp}[i(k + G)r]f_i(r) \quad (1.60)$$

$$f_i(r) = \sum_G c_{i,G} + \text{exp}[iGr] \quad (1.61)$$

where,

G is the reciprocal lattice vector represented by $\vec{GR} = 2\pi m$, m is an integer and k is the symmetry label in the first Brillouin zone.

The choice of the cutoff energy dictates the expansion of the wavefunction. Increasing the cutoff energy is, therefore, similar to increasing the number of orbitals in a molecular calculation in that it increases the accuracy by allowing for more expansive wavefunction [28].

The numerical integration for periodic solid state systems is typically carried out in reciprocal space, in contrast to real space in cluster method, where the first Brillouin zone is divided and described by a finite number of k -points. The k -points describe the sampling of the electronic wavefunction. Observables such as the energy and the density are integrated over all k -points within the first Brillouin zone. Chadi-Cohen [29] and Monkhorst-Pack [30] are two particular approaches that have been developed to provide an optimal division of special k -points to provide a reasonably accurate description of the electronic potential. The total energy of the system should converge with increasing number of k -points since the increase in the number provides a denser k -point mesh and finer sampling of the Brillouin zone.

The single particle wavefunctions are then described by plane wave basis sets that obey Bloch's theorem [28]. Although plane waves are the natural choice for periodic systems, they pose difficulties in accurately solving for the wavefunction near the core of the nuclei. The orbitals near the nuclei core are tightly bound and have significant oscillations, both of which make it difficult to model using expanded plane waves. They require an extensive number of plane waves, which is CPU intensive. Since most of the chemistry occurs via the valence electrons, the detailed electronic structure of the core can be avoided by using pseudopotentials. The pseudopotential approach substitutes the strong ionic potential and valence wavefunction with a weaker (and mathematically speaking, smoother) pseudopotential along with pseudo wavefunctions. The pseudopotential removes the radial nodes in the core region

and matches the valence electron wavefunction outside of the core region. This is shown in Figure 1.15.

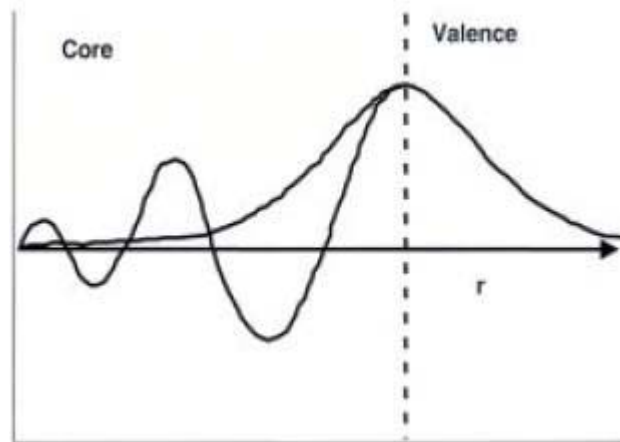


Figure 1.15: Representation of the pseudopotential approach

The parameters that can be computed accurately with the periodic approach are given as follows:

- Elastic constants,
- Chemisorption energies,
- Coverage effects,
- Long range interactions,
- Collective effects,
- k-space properties,
- Diffraction patterns,
- Valence band spectroscopy.

So far, beneath computational quantum chemistry methods only DFT is embedded into the periodic approach and it is shown that the magnetic effects for some semiconductors are not treated properly with this approach [27]. Nevertheless, the periodic approach gives the researcher extreme control over the model since the material is properly represented and it is

computationally efficient. Thus, the periodic approach outlines the cluster method by far in modelling the catalytic reactions over metallic substrates.

1.6 Objectives of the Study

The objectives of this study are summarized as follows:

- To theoretically evaluate the catalytic activity of Cu(111) metallic and Ru-Cu(111) bimetallic surfaces for propylene epoxidation by means of DFT,
- To investigate the reason(s) behind the catalytic activity of the systems.

On one side, Cu(111) metallic surface is important to model theoretically since there are both experimental and theoretical indications that this surface provides the best selectivities obtained among the pure metallic catalysts used. On the other side, the Ru-Cu(111) bimetallic system represents a good model system to investigate how the electronic structure changes relate to catalytic activity because of its precisely controllable surface structure. Thus, it would be valuable to compare the information about propylene epoxidation obtained from the investigations of these systems and relate them to fundamental concepts such as surface and electronic structure. This methodology is a key to obtain basic principles in design of new bimetallic propylene epoxidation catalysts. Furthermore, to our knowledge, there are neither theoretical nor experimental studies on Ru-Cu catalysts as propylene epoxidation catalysts.

In order to achieve these objectives, design of stable and realistic surface models for both Cu(111) and Ru-Cu(111) surfaces based on literature data is accomplished first. Afterwards, the necessary and sufficient conditions for the reactions to be investigated are modelled with DFT calculations. Finally, starting from these conditions, both the desired and undesired reactions taking place in the governing epoxidation mechanism are modelled with DFT calculations which makes it possible to obtain energy profiles and selectivity information based on the energetics. The reason behind the difference in propylene oxide selectivity of the two systems will also be investigated by modelling specific chemical reactions that shed light on the electronic structure of the studied surfaces.

CHAPTER 2

LITERATURE SURVEY

2.1 Propylene Epoxidation

Despite extensive research in laboratories and companies worldwide over the previous decades, direct partial oxidation (epoxidation) of propylene with molecular oxygen still continues to be the “Holy Grail” of heterogeneous catalysis [31]. This is mainly due to the fact that while the industrial production of the two carbon analogue of PO, ethylene oxide (EO), can be achieved with direct oxidation, using a supported silver catalyst, this is not true for PO [32].

In fact, the goal of utilizing an appropriate catalyst that could be used in direct heterogeneous PO production could not be achieved with any metal today. Furthermore, there has been even less improvement in gaining insight and understanding for analyzing the reasons behind the inability of the catalysts for the selective and high conversion PO production.

Because of these reasons, direct epoxidation of propylene is one of the biggest challenges for the catalysis society, as it was decades ago.

As already mentioned, the industrial production of propylene oxide (PO) is essentially governed by two processes today, namely the chlorohydrin and the hydroperoxide processes. Both of these processes are unfavored because of environmental and economic reasons [9]. The chlorohydrin process produces a brine containing calcium chloride waste ~40 times larger than the amount of PO produced and thus causes serious environmental problems. On the other hand, the hydroperoxide process produces a fixed amount of styrene or t-butyl alcohol co-products in a volume that is ~3 times larger than that of PO, which causes a lot of separation related problems and makes the process economy dominated by the the co-product

market [10]. Thus, it is more than desirable to achieve a direct and selective process for the partial oxidation of propylene using oxygen.

There have been numerous experimental studies regarding the issue with different catalysts, supports and oxidants. Among the most promising of these is the use of gold nanoparticles supported on titania, discovered by Haruta et al. [33]. Gold has long been thought to be chemically inert, however, the studies of Haruta has shown that its catalytic performance is to a great extent tunable by control of the particle size and by controlled selection of the support metal oxide. In this study, the selective oxidation of propylene was performed in a gas containing oxygen and hydrogen. It was stated that when gold is deposited on TiO_2 by a deposition-precipitation technique as hemispherical particles with diameters smaller than 4.0 nm it produces propylene oxide with selectivities higher than 90% and conversions of 1-2% at temperatures of 303-393 K. It was also postulated that oxidation of hydrogen to form water is depressed by propylene, whereas propylene oxidation is not only enhanced but also restricted to partial oxidation by hydrogen. Due to this observation and due to gold deposition in Temperature Programmed Desorption (TPD) spectra, it was proposed that propylene is adsorbed on the surfaces of both gold particles and the TiO_2 support.

The reaction rate was found to be nearly independent on the concentration of propylene and increasing linearly with increasing concentrations of oxygen and hydrogen. With these results, they suggested that propylene adsorbed on a gold surface may react with oxygen species formed at the perimeter interface between the gold particles and the TiO_2 support through the reaction of oxygen with hydrogen. Surprisingly, through careful Transmission Electron Microscope (TEM) observation it was shown that gold particles larger than 2.0 nm in diameter produce propylene oxide, whereas smaller gold particles produce propane.

Although, the process discovered by Haruta is remarkable, it has some major disadvantages as also put together by Haruta in a later publication. The drawbacks can be summarized as low conversion of propene, rapid catalyst deactivation and regeneration problems [34]. Further, including the high cost of hydrogen in the drawbacks, it is obvious that this process is far from being the desired case. Besides, the mechanism of the reaction and the reason of the promoting effect of hydrogen is not clear.

One other major discovery by Cowell et al. was that the $\text{Cu}(111)$ single crystal surface was selective for the epoxidation of higher level alkenes, namely butadiene, without the need of

any doping or hydrogen addition [35] under Ultra High Vacuum (UHV) conditions. They carried out Temperature Programmed Reaction (TPR) and X-ray Photoelectron Spectroscopy (XPS) measurements and concluded that the Cu(111) surface was effective with producing epoxybutene with ~100% selectivity.

They also stated that the minimum necessary and sufficient conditions for butadiene epoxidation on Cu(111) are butadiene molecules adsorbed on Cu metal sites in the vicinity of oxygen adatoms. With the addition of Cs to the system, the conversion of butadiene to epoxybutene remarkably increased from ~50 to ~90%. Combining this result with the XPS measurements of the surface for different Cs loadings, it was understood that the primary function of Cs was to reduce oxidic Cu₂O structures and to create metallic Cu atoms which were the active sites for epoxidation.

It was also presented by the same group that silica supported copper catalysts showed propylene oxide selectivities comparable to the system of Haruta et. al [33] without the need of hydrogen co-feeding or alkali addition. Their catalysts were stable under reaction conditions of atmospheric pressure and temperatures up to 350°C. The maximum selectivity of 53% was obtained at 225°C and 0.25% propylene conversion. The increasing of temperature decreased the selectivity towards epoxide formation. They linked this to the fact that metallic copper turns to copper oxide structure at high temperatures, which is inactive for epoxidation. Further, Using XPS, Auger Electron Spectroscopy (AES) and High Resolution Electron Microscopy (HREM), they concluded that the active form of copper was Cu⁰ species in highly dispersed, “atomic like” form [36]. Thus, they extended their discussion that metallic form of copper was a highly selective epoxidation catalyst even operating under atmospheric conditions.

Following these discoveries, there have been other studies using copper based catalysts with different dopants and oxidants [37, 38, 39]. There are also examples of FeO [40], Ag-Cu alloy [41] catalysts and also gas phase oxidation schemes [42]. However, besides being helpful towards the solution of the problem, these studies are far from giving the desired performance in PO production. Moreover, there is not a real consensus on the active phase and little emphasis on the reaction mechanism.

Compared to the efforts in developing a better catalyst for PO production, there has been very little effort on understanding why the studied catalysts perform poor for the desired

reaction [8, 43]. However, in our opinion, in an issue such as propylene epoxidation where experimental means alone have been proven ineffective to solve the issue, the importance of theoretical studies on model catalysts would be invaluable, even if they could serve purpose of gaining the very basics of fundamental insight about the reaction.

The difficulty in propene epoxidation is generally accepted to be associated with the existence of allylic hydrogens in the propylene molecule [44]. In their study, Cant and Hall observed that they could obtain selectivities to propylene oxide as high as 14% for propylene in which the allylic hydrogens have been replaced with deuterium while for the ‘normal’ propylene, this value would range between 0 to 5% using a silver catalyst. One of the important experimental surface science studies with the aim of gaining mechanistic insight about the subject is the work conducted by Barteau and Madix [45]. With TPD and surface titration experiments, they came up with a mechanism in which propylene reacts irreversibly to form hydroxyl groups plus adsorbed carbon on the surface. They also stated that the formation of OH species equal in number to the initial oxygen coverage clearly indicates that the combustion of propylene involves a hydrogen abstraction process and not an attack of the oxygen upon the carbon framework.

Later, through various experimental and theoretical studies, an oxametallacycle intermediate (referring to the Oxygen-Metal-Metal-Ethylene backbone, named as OMME) in the ethylene epoxidation reaction is proposed to be the common intermediate for the formation of both EO and acetaldehyde, the latter being the precursor for combustion [46, 47, 48, 49]. The OMME intermediate proposed is given in Figure 2.1 [46].

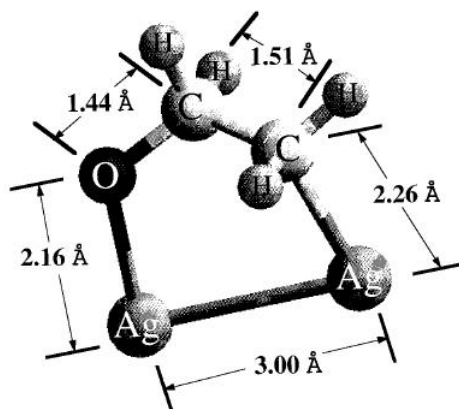


Figure 2.1: Optimized structure of the OMME intermediate in ethylene epoxidation reaction

The oxametallacycle mechanism is commonly accepted today in heterogeneous catalysis society as the governing mechanism in alkene epoxidation [8].

In a recent theoretical publication, Torres et al. proposed that also for PO formation a common intermediate, OMMP (propylene oxametallacycle, the analog of OMME) exists and the selectivity of the reaction towards PO formation is associated with the relative energy barriers of OMMP formation and allylic hydrogen stripping reactions [8]. The oxametallacycle reaction mechanism for the propylene epoxidation is given in Figure 2.2 [8].

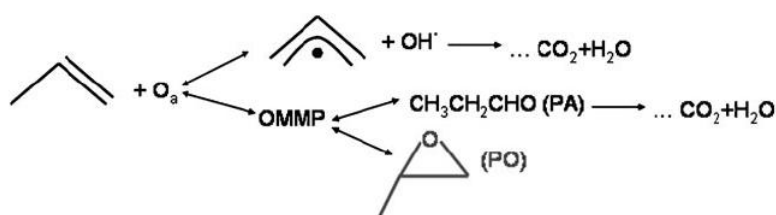


Figure 2.2: Mechanism for propylene epoxidation on Ag(111) and Cu(111)

The energy profiles were obtained through obtaining transition state structures for each reaction in the mechanism. The investigation of the mechanism starts with the co-adsorption of oxygen and propylene on the surfaces. Different arrangements of co-adsorbed propylene and oxygen were investigated in order to give the desired reactions.

Optimization of two different types of OMMP intermediates were performed in the study. The first type is the one that has the terminal unsaturated carbon attached to the surface oxygen and the second type is the middle carbon attached to the surface oxygen. For both Ag(111) and Cu(111) surfaces, the second type of OMMP were found to have significantly higher activation barriers than the first type and this path was neglected. It was also proposed in another publication that the second type of OMMP would form only upon PO adsorption and not as a product of the reaction of propylene and oxygen.

For Ag(111) surface the competing pathways of allylic hydrogen stripping and OMMP formation were shown to have activation barriers of 0.30 eV and 0.60 eV, respectively. Surprisingly, for Cu(111), the results were strikingly different, activation barrier of 0.60 eV for allylic hydrogen stripping and 0.54 eV for OMMP formation. The activation barriers for the formation of propylene oxide (PO) and propionaldehyde (PA) on Cu(111) were calculated as 0.96 eV and 1.10 eV, respectively .

With these results, it was concluded that the key difference between silver and copper resides in the primary chemistry. As can be seen from the comparison of relative activation barriers of allylic hydrogen stripping and OMMP formations, silver favors allylic hydrogen stripping while copper favors OMMP formation.

They also investigated the reason behind the difference between the two metals. It was proposed that lower basicity of oxygen adsorbed on Cu(111) compared to Ag(111) was the key factor that was responsible for the change in the order of magnitudes of the competing reactions and thus the selectivity for PO formation. This conclusion was arrived after the adsorption of Lewis acid probe, SO₂, on the oxygenated surfaces. It was calculated that the binding energy of SO₂ to the oxygen on Ag(111) surface was 1.03 eV higher than on the Cu(111) surface and thus, the oxygen on Cu(111) surface was lower in basicity [8].

Very recently, the same group studied Au(111) surface for propylene epoxidation [43], in a similar manner to the work in [8]. This time, only the primary chemistry, i.e. the allylic hydrogen stripping and OMMP formation reactions were investigated and it was emphasized that the selectivity to PO production was dependant only on the primary chemistry. For OMMP formation, the formation of second type of OMMP was found to be inhibited by a high activation barrier as was the case for Ag(111) and Cu(111) surfaces.

As already known, Au(111) surface was found ineffective for propylene epoxidation, since the barriers towards allylic hydrogen stripping and OMMP formation were calculated as 0.20 eV and 0.52 eV respectively. In order to account for this inefficiency of the Au(111) surface, the acid and base constants, PK_a and PK_b , were calculated for Au(111), Ag(111) and Cu(111) surfaces and the values were plotted against activation barrier of allylic hydrogen stripping reaction.

It was observed that the lowest activation barrier and the highest base constant were calculated for Au(111) surface. Because of that observation, they concluded that the oxygen basicity was the crucial parameter in determining the selectivity for PO formation on metal surfaces [43].

2.2 Structure of Ruthenium-Copper Catalysts

An interesting model system, after the famous discovery of Sinfelt et al., is the Ru-Cu bimetallic system [50]. This system deserves special interest because, at least, it is one of the first studies that resulted in the concept of ‘bimetallic cluster’ catalysts. Sinfelt used the phrase ‘bimetallic catalysts’ instead of using the word ‘alloy’. In his own words, this is explained as:

“In a highly dispersed state, systems of interest include a variety of metallic combinations that do not correspond to known bulk alloys. For this reason, we have chosen the term ‘bimetallic clusters’ rather than alloys in referring to highly dispersed supported bimetallic systems where the catalytic behaviour indicates significant interaction between the metallic components”

In fact, the Ru-Cu system corresponds to an extreme case where the components are completely immiscible in the bulk, i.e. no alloy formation, even at very high temperatures and after annealing [51]. In his pioneer study, Sinfelt synthesized the silica supported Ru-Cu catalyst via a simple co-impregnation procedure and reduced the catalyst in hydrogen environment in order to get the metallic form. Afterwards, catalytic data were taken in the hydrogenolysis of ethane to methane reaction.

Hydrogenolysis is a type of reaction where a carbon-carbon bond undergoes lysis (cleavage) by reacting with hydrogen [52]. Sinfelt observed that rate of hydrogenolysis decreases significantly with increasing copper concentration. It is also known that copper is a poor catalyst for hydrogenolysis reaction since it cannot adsorb and dissociate hydrogen. However, if the copper would exist as a separate entity, it would not affect the activity of ruthenium. Thus, it was concluded that the metals exist as bimetallic clusters and both structural and electronic effects would contribute to that change in catalytic activity. Further, it was postulated that number of ruthenium atoms at the surface would decrease substantially with the addition of copper, based on the hydrogen chemisorption data [50].

After this discovery, the structure of the Ru-Cu system was investigated in more detail by Sinfelt. In a successive study, based on hydrogen chemisorption and X-Ray Diffraction (XRD) measurements, a model of the bimetallic Ru-Cu system was postulated as a thin layer of copper at the surface of a crystallite composed of pure ruthenium [53]. In detail, it was postulated that copper was bonded chemically to ruthenium at the surface and the interaction

was analogous to copper chemisorbed on ruthenium.

The conclusions arrived on the structure of Ru-Cu system is solid and convincing but indirect since it is based on catalytic activity and chemisorption data. Thus, a direct investigation was made by Sinfelt to solidify his postulates on the system. This direct evidence came from an Extended X-ray Absorption Fine Spectroscopy (EXAFS) study of the silica supported Ru-Cu catalyst system [54]. This study is also significant since it is one of the first studies to show the diagnostic power of EXAFS on catalyst characterization.

From EXAFS data, one can obtain information on the number and type of neighboring atoms about a given absorber atom and on interatomic distances. Thus, it is possible to obtain information on the environment of each type of atom present in a complex material.

It was shown that EXAFS measurements done at the K-absorption edge of copper revealed significantly different functions which revealed that Cu atoms had Ru atoms as nearest neighbors as well as other Cu atoms. The measurements done at the K-absorption edge of Ru revealed minor differences with the Ru reference signal, which meant that Ru atoms were coordinated to Cu atoms to a very small extent. Combining these results with the data obtained from chemisorption and catalytic activity tests, the model of Cu atoms chemisorbed on pure Ru substrate was proven.

Further, the diameter of the investigated bimetallic clusters were found as 32 Å (average). With that magnitude of the cluster, surface atoms would constitute about half of the total atoms and thus the surface consists entirely of copper in the form of a monolayer covering the internal ruthenium core [54].

These results were verified at the same time by the group of Nobel prize winner Gerrard Ertl by his studies on Ru(0001) single crystal surfaces [55]. They investigated the growth of Cu layers on Ru(0001) substrate with a detailed look at the electronic and structural relationships between the two metals. In order to accomplish these goals, they used various instrumentation tools including Low Energy Electron Diffraction (LEED), AES, TPD and work function measurements. After a very thorough and detailed investigation, they underlined the growth characteristics of Cu layers over Ru(0001) surface.

It was concluded that high Cu deposition temperatures like 500°C supported the formation of a 2 dimensional homogeneous monolayer of Cu(111) formation and clearly reduce the

tendency to form three dimensional (3D) hills. In fact, even at lower depositing temperatures, the surface grew epitaxially to the Ru(0001) substrate beneath and after a ‘transition period’, characteristic of the Cu(111) surface were obtained. About the electronic structure, through work function measurements, it was concluded that a charge transfer occurs from the Ru substrate to the Cu monolayer.

In the successive study of the same group, hydrogen chemisorption was investigated on Ru-Cu model catalysts [56]. Again, in agreement with the prior studies of the group and of Sinfelt’s, they concluded that the small deposits of Cu drastically suppressed the hydrogen chemisorption capacity of the system. After these two studies, they came up with the final conclusion that the model Ru-Cu catalysts prepared by depositing varying amounts of Cu on Ru(0001) substrate is a realistic model that can resemble the properties of ‘real’ catalyst used by Sinfelt.

Later, the results about the growth characteristics of Cu layers on Ru(0001) substrates were extended in more detail with Scanning Tunneling Microscopy (STM) measurements [57]. These STM studies revealed that the first Cu layer expands 5.5% from the bulk Cu(111) lateral spacing to grow pseudomorphically, with the Cu atoms occupying the threefold hollow sites of the Ru(0001) surface. These studies also showed that, at 300 K, the growth is layer-by-layer up to at least 2 ML.

Furthermore, there were other studies conducted in order to measure the spacing between the successive layers of Cu on Ru(0001), which cannot be measured by STM [58]. These studies were conducted on Cu layers grown on Ru(0001) and oxygen-precovered Ru(0001) by X-ray Photoelectron Diffraction (XPD) measurements and theoretical single scattering cluster (SSC) and multiple scattering cluster (MSC) diffraction calculations. The publications confirmed results of STM measurements that first Cu layer on Ru(0001) substrate is fully completed before the second layer begins to grow.

The distance between the Cu monolayer and the Ru substrate was consistently measured experimentally and calculated theoretically as 2.15 Å. Furthermore, the measurements done on oxygen oxygen-precovered Ru-Cu system indicated that all of the oxygen floats on the Cu overlayer, and that none of the oxygen is subsurface or remains at the Cu/Ru interface. This result is further verified by XPS measurements [58].

Overall, these experimental and theoretical studies form the basis of our surface model for the Ru-Cu bimetallic system where a Cu(111) monolayer is located over a Ru(0001) substrate. It should be noted that there are neither theoretical nor experimental studies on propylene epoxidation using Ru-Cu catalysts, which is one of our motivations to investigate this important bimetallic systems.

CHAPTER 3

COMPUTATIONAL METHODOLOGY

3.1 Overview of the Methodology

Density Functional Theory (DFT) calculations throughout the study are performed using Vienna Ab initio Simulation Package (VASP), a code that utilizes the periodic modelling of systems with the use of supercell approach and plane wave basis sets [59]. The reciprocal space of the supercells are described with a $4 \times 4 \times 1$ k-point Monkhorst-Pack mesh [30]. The exchange-correlation energy has been calculated within the generalized gradient approximation (GGA) using the PW91 functional [60, 61]. The core electrons are described with the Projector Augmented Wave (PAW) method [62].

PAW method mainly takes advantage of a ‘transformation’ where the numerically convenient, smooth, auxiliary wavefunctions are obtained and then transformed into the all-electron (full) wavefunctions. In that sense, the method resembles augmented wave methods because it benefits from the full wavefunction but it also makes a clear distinction between core and valence electrons and thus resembles pseudopotential method. The total energy functional is evaluated from the full wavefunction and is divided into three parts. The first part is the planewave part and involves only smooth functions, used to describe electrons far from nucleus. The remaining two parts are evaluated on radial grids in a spherical harmonics expansion, suitable for core electrons. The main approximation of the method is the frozen core approximation which treats atomic data inside a radial grid as frozen quantities during calculations.

The energy cut-off is taken as 500 eV to ensure high precision. Total energies are calculated using a first-order Methfessel-Paxton smearing function with a width of 0.2 eV. Optimizations have been carried out until the net force acting on atoms are smaller than 0.01 eV/Å. The

dipole moment due to the usage of an asymmetric slab was removed with standard dipole correction [63].

Saddle points in the minimum energy path are found with Climbing Image-Nudged Elastic Band (CI-NEB) [64] method for each elementary step in the reaction mechanism after the initial and final states of the reaction have been optimized. All transition states have been characterized by vibrational frequency analysis within the harmonic oscillator approximation. During the vibrational analysis, the relaxed atoms are displaced from their equilibrium positions twice (0.02 Å)

All calculations are performed analogously for the Cu(111) and Ru-Cu(111) structures throughout the study. The investigated reaction mechanism for propylene epoxidation is the generally accepted oxametallacycle mechanism illustrated in Figure 2.2. The general procedure of the calculations can be summarized as follows:

1. Preparation and optimization of the bulk structure
2. Preparation and optimization of the slabs
3. Adsorption of atomic oxygen on slabs
4. Adsorption of propylene on oxygenated slabs
5. Formation of allyl radical
6. Formation of propylene oxametallacycle (OMMP)
7. Formation of propylene oxide (PO)
8. Formation of propionaldehyde (PA)
9. Allocation of transition states (TS) for each reaction
10. Characterization of transition state structures
11. Adsorption of SO₂ on oxygenated slabs

3.2 Preparation and Optimization of the Bulk Structure

For the preparation of the bulk structures of Ru and Cu metals, standard crystallographic information was used [65]. The crystal structures of Ru and Cu metals are given in Table 3.1.

Table 3.1: Crystallographic parameters for Ru and Cu

	Cu	Ru
Lattice	Face Centered Cubic (FCC)	Hexagonal Close Packed (HCP)
Space Group	Fm-3m	P63/mmc
Space Number	225	194
Cell Parameters	a=b=c=3.610 Å	a=b=2.710 Å, c=4.280 Å

Since the DFT calculations are not exact and the forces acting on atoms will be different than the ‘real’ forces acting on it, it is necessary to optimize cell parameters and use the calculated values in the construction of slabs. The parameters given in Table 3.1 were used as input parameters and the cell parameters were optimized.

The optimized cell parameters (truncated to 4 significant figures) are given in Table 3.2.

Table 3.2: Cell parameters for Ru and Cu (Å)

	Cu	Ru-Cu
Input Parameter	a=3.610	a=2.710, c=4.280
Optimized Parameter	a=3.636	a=2.730, c=4.303

3.3 Preparation and Optimization of the Slabs

Slabs are constructed using the optimized cell parameters. Cu(111) surface is modeled with slabs containing 4 atomic layers. Generally, 4 or 5 layers are used in literature to model reactions on metal surfaces [8, 27, 43, 49]. Furthermore, Cu(111) surface was previously investigated for propylene epoxidation reaction using a 4 layer model, giving results consistent with experiments [8], which justifies our model of a 4 layer Cu(111) slab. Ru-Cu(111) bimetallic surface is modeled as one monolayer of copper atoms preferentially located over the 3 fold fcc sites of the Ru(0001) surface (corresponding to $\theta = 1.0$), consistent with the

experimental and theoretical literature [50, 55, 58]. In the construction of the Ru-Cu(111) surface, first, a Ru(0001) slab consisting of 4 atomic layers was optimized. Afterwards, the copper monolayer is optimized over the optimized Ru(0001) slab.

Throughout the calculations, the bottom two layers of the slabs have been kept fixed to represent bulk structure while all other atoms in the systems have been relaxed in all degrees of freedom. A vacuum height of ~ 10 Å is used over the slabs and the reactive species are optimized on only one side of the slab. A $p(3 \times 3)$ supercell is used for both systems corresponding to a coverage of $\theta = 0.11$ for all reactive species. After the optimization of the Cu monolayer on Ru(0001) substrate, the distance between the Cu monolayer and Ru substrate is calculated as 2.13 Å, in agreement with the 2.15 Å value of prior theoretical and experimental studies [58]. The top and side views for the Cu(111) and Ru-Cu(111) surfaces are given in Figures 3.1, 3.2, 3.3, 3.4.

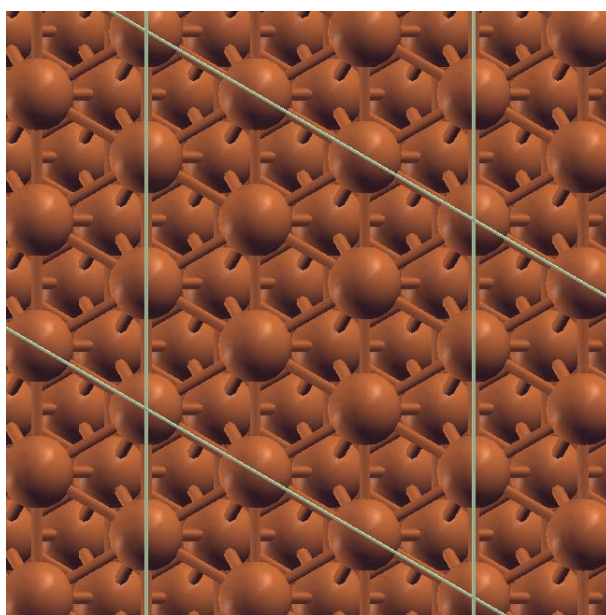


Figure 3.1: Top view of the Cu(111) slab

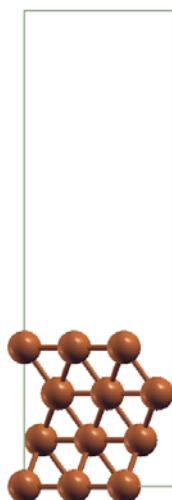


Figure 3.2: Side view of the Cu(111) slab

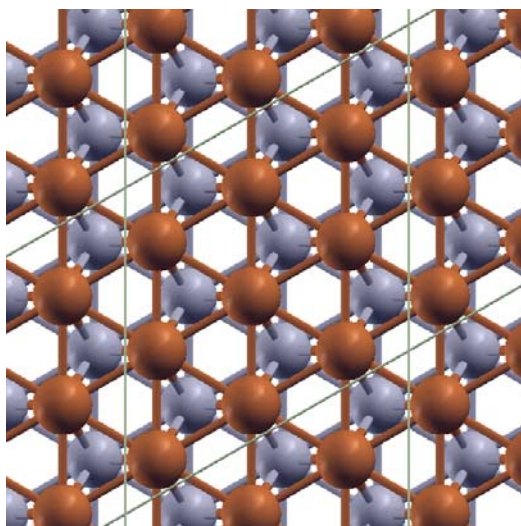


Figure 3.3: Top view of the Ru-Cu(111) slab

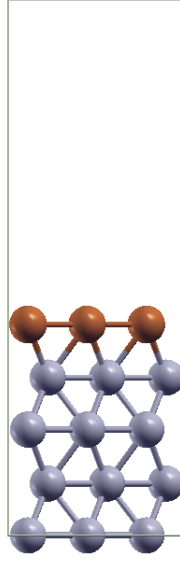


Figure 3.4: Side view of the Ru-Cu(111) slab

3.4 Adsorption of Atomic Oxygen on Slabs

After the Cu(111) and Ru-Cu(111) surfaces are optimized, atomic oxygen was adsorbed on the most favorable adsorption site, i.e. hcp site of the surfaces as stated in the literature [66]. In order to calculate the oxygen adsorption energy of the slabs, an isolated oxygen atom in a 15 Å cube was optimized and its energy was used in the calculation of oxygen adsorption energy. Oxygen adsorption energy was calculated according to Equation 3.1.

$$E_{ads}^O = E_{system} - E_{slab} - E_{Oatom} \quad (3.1)$$

where E_{ads}^O is the oxygen adsorption energy, E_{system} is the energy of the system of adsorbed oxygen on the metallic surface, E_{slab} is the energy of the clean slab and E_{Oatom} is the energy of an isolated oxygen atom.

3.5 Adsorption of Propylene on Oxygenated Slabs

In order to give the desired reactions, propylene must be adsorbed on the surface together with oxygen as emphasized heavily in the literature [67]. The strategy followed in order to find the most favorable adsorption sites for propylene is as follows:

In all geometry optimizations in VASP, one of the most important parameters is the initial guess given to the code. Thus, in order to find the favorable adsorption site for propylene adsorption, various configurations were considered depending on the relative positions of the active site of the propylene molecule and the oxygen. For example, for the allylic hydrogen stripping reaction, propylene should be adsorbed on the surface in a configuration so that the allylic hydrogen of the propylene should be close to the oxygen and pointing downwards. If the initial guess is given to the code in that sense, a global minima is obtained. If, say, the initial guess is given such as the propylene is farther away from the oxygen atom or propylene is at a geometry with the unsaturated carbon close to surface oxygen, either the calculation will not converge, or the geometry obtained will not result in the desired reaction.

The mentioned concept of ‘appropriate initial guess’ is used in obtaining the reactants, intermediates and products throughout the study. The most correct way of ‘guessing’ the suitable configuration of the molecules is, of course, theoretical and (more reliably) experimental literature information on the structure of the studied systems. The initial guesses and thus the optimized structures for all the species in this study have solid proofs based on various studies in the literature as previously mentioned in the Literature Survey.

Analogous to oxygen adsorption, the energy of an isolated propylene molecule is calculated to be used in the calculation of adsorption energies. Adsorption energy of propylene is calculated according to Equation 3.2.

$$E_{ads}^{prop} = E_{system}^{prop} - E_{oxslab} - E_{prop} \quad (3.2)$$

where E_{ads}^{prop} is the propylene adsorption energy, E_{system}^{prop} is the energy of the system of co-adsorbed oxygen and propylene on the surface, E_{oxslab} is the energy of the oxygenated slab and E_{prop} is the energy of an isolated propylene molecule.

3.6 Formation of Allyl Radical

Given close enough to the oxygenated slab in the appropriate geometry, the propylene will undergo allylic hydrogen stripping and will yield two radical species adsorbed on the surface, the allyl and the hydroxyl radicals. The reaction energy of the allylic hydrogen stripping reaction is calculated according to Equation 3.3.

$$E_{formation}^{allyl} = E_{system}^{allyl} - E_{system}^{prop} \quad (3.3)$$

where $E_{formation}^{allyl}$ is the reaction energy of allylic hydrogen stripping reaction, E_{system}^{allyl} is the energy of the system of adsorbed allyl and hydroxyl radicals on the surface and E_{system}^{prop} is as defined in Equation 3.2.

3.7 Formation of Propylene Oxametallacycle (OMMP)

Given close enough to the oxygenated slab in the appropriate geometry, the propylene will make two bonds with the surface, the first between the double bonded terminal carbon of propylene and oxygen, the second between the bridge carbon of propylene and a metal atom of the surface. This structure is named as propylene oxametallacycle (OMMP), the description of which is given in the Literature Survey. The reaction energy of the OMMP formation reaction is calculated according to Equation 3.4.

$$E_{formation}^{OMMP} = E_{system}^{OMMP} - E_{system}^{prop} \quad (3.4)$$

where $E_{formation}^{OMMP}$ is the reaction energy of the OMMP formation reaction, E_{system}^{OMMP} is the energy of OMMP structure and E_{system}^{prop} is as defined in Equation 3.2.

3.8 Formation of Propylene Oxide (PO)

For PO formation, PO molecule is given close to the surface as the initial guess and optimized. The optimized structure of PO molecule is found as PO adsorbed over the surface. The reaction energy of the PO formation reaction is calculated according to Equation 3.5.

$$E_{formation}^{PO} = E_{system}^{PO} - E_{system}^{OMMP} \quad (3.5)$$

where $E_{formation}^{PO}$ is the reaction energy of the PO formation reaction, E_{system}^{PO} is the energy of PO adsorbed on the surface and E_{system}^{OMMP} is as defined in Equation 3.4.

3.9 Formation of Propionaldehyde (PA)

For PA formation, PA molecule is given close to the surface as the initial guess and optimized. The optimized structure of PA molecule is found as PA adsorbed over the surface. The reaction energy of the PA formation reaction is calculated according to Equation 3.6.

$$E_{formation}^{PA} = E_{system}^{PA} - E_{system}^{OMMP} \quad (3.6)$$

where $E_{formation}^{PA}$ is the reaction energy of the PA formation reaction, E_{system}^{PA} is the energy of PA adsorbed on the surface and E_{system}^{OMMP} is as defined in Equation 3.6.

3.10 Allocation of Transition State Structures for Each Reaction

The transition state structures for the investigated reactions are calculated with Climbing Image-Nudged Elastic Band (CI-NEB) method. This method is used to identify minimum energy paths and activation energy barriers for chemical reactions or diffusion processes in solid surfaces. CI-NEB makes use of two point boundary conditions, the initial and the final configurations. A set of images of the system, where the number of images is selected by the user, is generated between the initial and final configurations. All intermediate images are optimized with a force based optimization algorithm simultaneously with the chain of states method [27].

In the study, propylene adsorbed on the oxygenated system is the initial configuration for both allylic hydrogen stripping and the OMMP formation reactions. After the OMMP is formed, the structure is the initial configuration for both PO and PA formation reactions. Thus, after the optimized geometries for adsorbed propylene, OMMP, allyl radical, PO and PA structures are determined, the appropriate CI-NEB calculations between the initial and

final configurations of the desired reactions results in energy profiles. Consecutively, saddle points of the energy profiles are identified as transition state structures.

3.11 Characterization of Transition State Structures

All transition states have been characterized by vibrational frequency analysis within the harmonic oscillator approximation. During the vibrational analysis, the relaxed atoms are displaced from their equilibrium positions twice (0.02 Å) and the second derivative (i.e. the Hessian) matrix of the total energy was calculated. The structures were ensured to be transition state structures since they have a single mode of imaginary frequency which is along the reaction coordinate.

3.12 Adsorption of SO₂ on Oxygenated Slabs

It is crucial to come up with a reason behind the energy profiles obtained with the two different structures modelled. Recently, it is proposed in the literature that the reason for the difference in propylene epoxidation selectivities between the two metallic surfaces is mainly due to the different basicity of atomic oxygen adsorbed on the surfaces [8, 43]. Thus, in this study, a Lewis acid chemical probe, SO₂, was adsorbed on the oxygenated surface (making a bond with oxygen) and the adsorption energy of SO₂ was calculated in order to evaluate the basicity. As in analogy with previous cases, the energy of an isolated SO₂ molecule was calculated to be used in the calculation of the adsorption energy of SO₂. Equation 3.7 gives the formulation of SO₂ adsorption energy.

$$E_{ads}^{SO_2} = E_{system} - E_{oxslab} - E_{SO_2} \quad (3.7)$$

where $E_{ads}^{SO_2}$ is the SO₂ adsorption energy, E_{system} is the energy of of the system of SO₂ adsorbed on the oxygenated slab, E_{SO_2} is the energy of the isolated SO₂ molecule and E_{oxslab} is used as defined in Equation 3.2.

CHAPTER 4

RESULTS & DISCUSSION

4.1 Adsorption of Atomic Oxygen on Cu(111) and Ru-Cu(111) Surfaces

Atomic oxygen was adsorbed on the most favorable hexagonal close packed (hcp) adsorption site of the pre-optimized Cu(111) and Ru-Cu(111) surfaces, in agreement with prior studies of atomic oxygen adsorption on metal surfaces [66]. The calculated adsorption energies and structural parameters for oxygen chemisorption on the investigated systems are given in Table 4.1.

Table 4.1: Optimized parameters for oxygen chemisorption on Cu(111) and Ru-Cu(111) surfaces

	Cu(111)	Ru-Cu(111)
Adsorption Energy (eV)	4.65	4.88
Cu-O distance (Å)	1.90	1.92

Optimized geometries of the oxygenated surfaces are given in Figures 4.1 and 4.2.

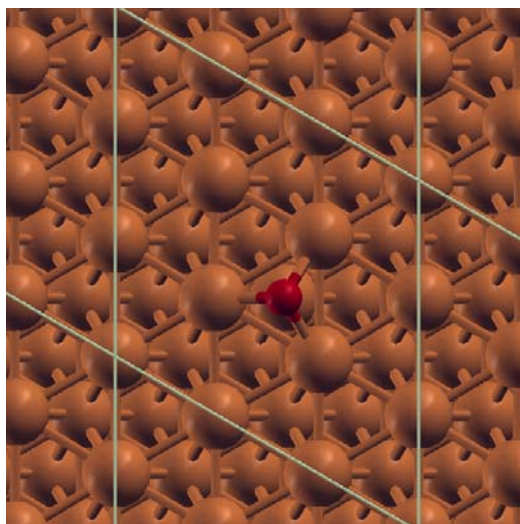


Figure 4.1: Optimized structure of oxygen chemisorbed on Cu(111) surface

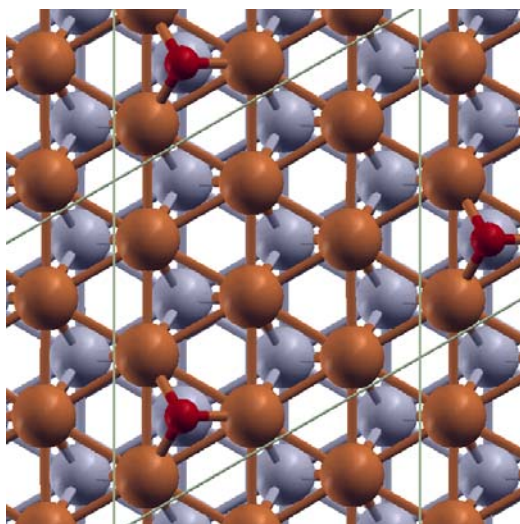


Figure 4.2: Optimized structure of oxygen chemisorbed on Ru-Cu(111) surface

From the calculated parameters given in Table 4.1, it is easily seen that the Ru substrate has an electronic effect on the Cu monolayer since the surface structure is essentially similar in both systems. Oxygen is adsorbed more strongly on Ru-Cu(111) system by 0.23 eV, which means that the Ru-Cu(111) surface has more tendency to bond atomic oxygen on the surface, which may be associated with an increase in the electron density around the Cu atoms on the surface of the Ru-Cu(111) system, compared to the Cu(111). The difference in bonding energy also manifests itself in terms of bond length.

4.2 Adsorption of Propylene on Oxygenated Cu(111) and Ru-Cu(111) Surfaces

After atomic oxygen is adsorbed on the surface, the necessary step is propylene adsorption. The carbon atom of propylene having an allylic hydrogen is named as C3, the neighboring carbon atom as C2 and the farthest one as C1. From the various adsorption configurations on Cu(111) and Ru-Cu(111) surfaces, where propylene is located close enough to atomic oxygen, the stable configurations that can lead to OMMP formation (oxygen linked to C1) or allylic hydrogen stripping (AHS) are illustrated in Figures 4.3, 4.6, 4.5 and 4.6 and the energetics are summarized in Table 4.2. The formation of another type of OMMP (C2 bonded to oxygen and C1 bonded to a metal atom) was reported to be energetically unfeasible on various fcc metals including Cu(111) surface [8, 43] and thus will not be the subject of this work.

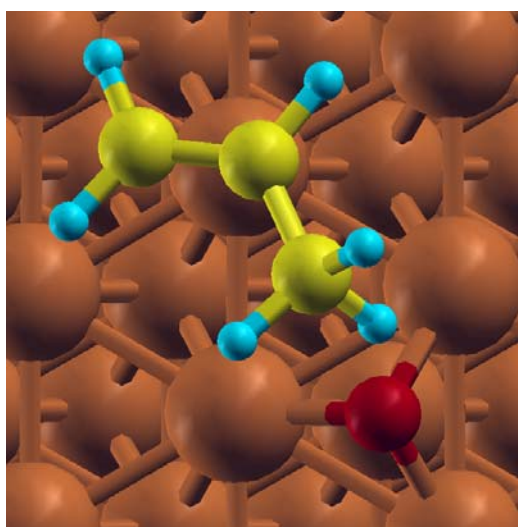


Figure 4.3: Top view of propylene adsorbed on Cu(111) to undergo AHS

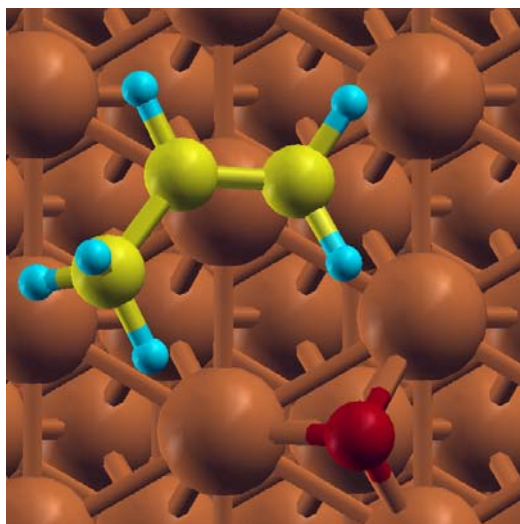


Figure 4.4: Top view of propylene adsorbed on Cu(111) to form OMMP

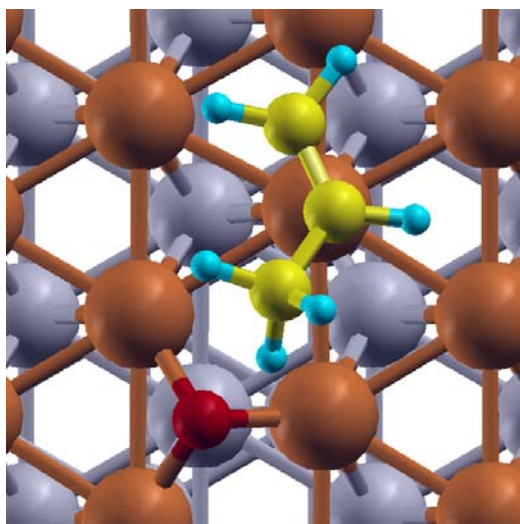


Figure 4.5: Top view of propylene adsorbed on Ru-Cu(111) to undergo AHS

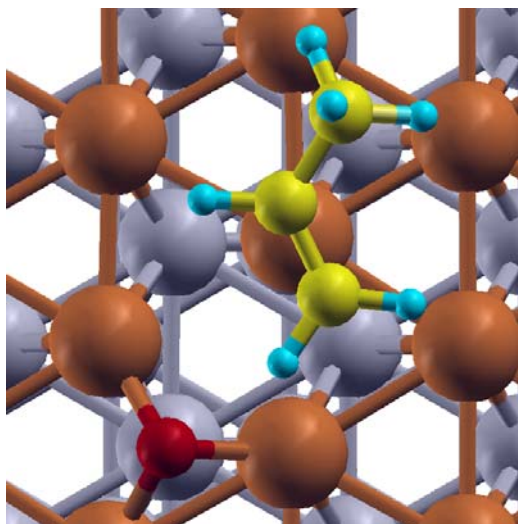


Figure 4.6: Top view of propylene adsorbed on Ru-Cu(111) to form OMMP

Table 4.2: Energetics of propylene adsorption on Cu(111) and Ru-Cu(111) surfaces(in eV)

	Cu(111)	Ru-Cu(111)
OMMP	0.146	0.482
AHS	0.161	0.276

From the results given in Table 4.2, it can be concluded that propylene adsorbs more exothermically on Ru-Cu(111) compared to Cu(111) for both OMMP formation and allylic hydrogen stripping reactions. However, while for the Cu(111) surface propylene is adsorbed a little more strongly in the precursor state for allylic hydrogen stripping, it is seen that for the Ru-Cu(111) surface the exothermicity is much higher for the adsorption of propylene in the OMMP precursor state.

Together with the increased exothermicity of the oxygen chemisorption, these results point out that the Ru-Cu(111) surface may have an increased electron density compared to the pure Cu(111) surface.

4.3 Formation of Allyl Radical on Cu(111) and Ru-Cu(111) Surfaces

After the adsorption of propylene, close enough to the chemisorbed oxygen with a geometry where propylene is located with the allylic hydrogen over the oxygen, the propylene will undergo allylic hydrogen stripping and will yield two radical species chemisorbed on the surface, the allyl and the hydroxyl radicals. The minimum energy path for this reaction is a proton transfer from propylene to oxygen. The optimized geometries of adsorbed allyl and hydroxyl radicals on Cu(111) and Ru-Cu(111) surfaces are given in Figures 4.7 and 4.8.

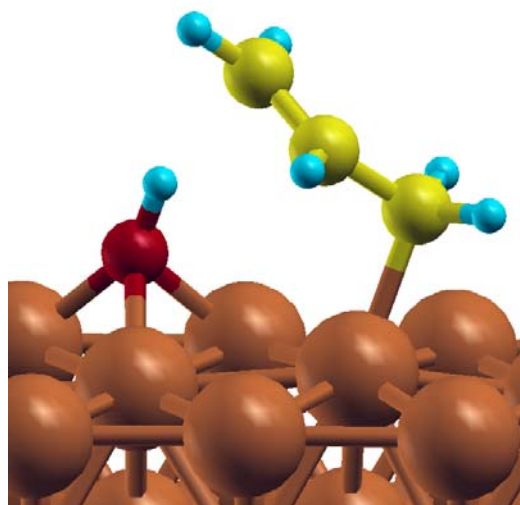


Figure 4.7: Top view of allyl and hydroxyl radicals adsorbed on Cu(111)

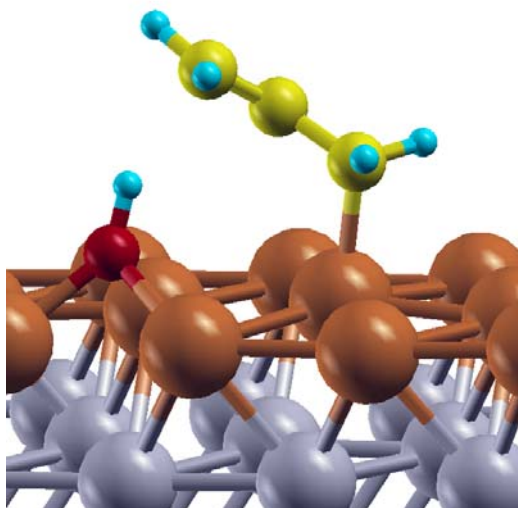


Figure 4.8: Top view of allyl and hydroxyl radicals adsorbed on Ru-Cu(111)

The important parameters calculated for the formation of allyl and hydroxyl radicals are given in Table 4.3.

Table 4.3: Structural and energetic parameters for the formation of allyl radical on Cu(111) and Ru-Cu(111) surfaces

	Cu	Ru-Cu
O-H distance (Å)	1.00	0.99
Cu-C3 distance (Å)	2.09	2.08
Reaction Energy (eV)	0.242	0.068

4.4 Formation of Propylene Oxametallacycle (OMMP)

After the adsorption of propylene, close enough to the chemisorbed oxygen with a geometry where propylene is located with the allylic hydrogen over the oxygen, the propylene will make two bonds with the surface, the first between the double bonded terminal carbon of propylene and oxygen, the second between the bridge carbon of propylene and a metal atom of the surface. This structure is named as propylene oxametallacycle (OMMP) and it is formed by the rotation of the double bond through an axis perpendicular to the surface placed on the C2 atom. The optimized OMMP structures formed on Cu(111) and Ru-Cu(111) surfaces are given in Figures 4.9 and 4.10.

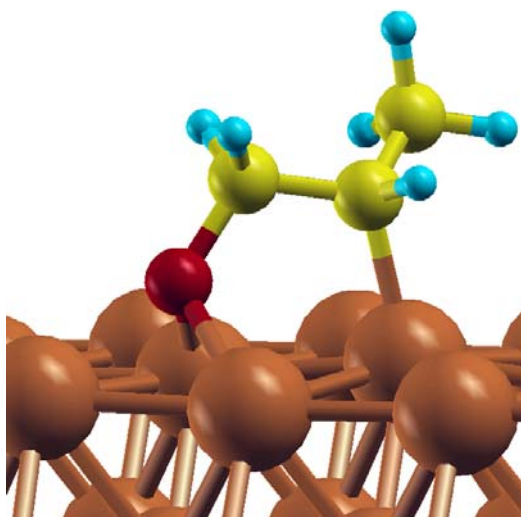


Figure 4.9: Top view of OMMP formed on Cu(111)

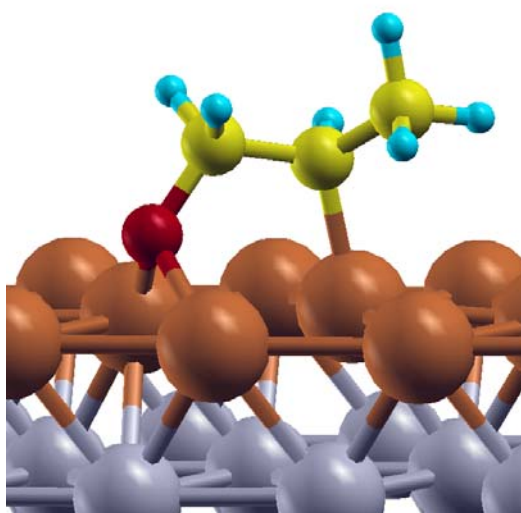


Figure 4.10: Top view of OMMP formed on Ru-Cu(111)

The important parameters calculated for the formation of OMMP are given in Table 4.4.

Table 4.4: Structural and energetic parameters for the formation of OMMP on Cu(111) and Ru-Cu(111) surfaces

	Cu	Ru-Cu
O-C1 distance (Å)	1.46	1.45
Cu-C2 distance (Å)	2.08	2.05
Reaction Energy (eV)	0.199	0.301

4.5 Formation of Propylene Oxide (PO) on Cu(111) and Ru-Cu(111) Surfaces

The OMMP intermediate formed can evolve to either PO or PA. The closure of the C-O bond and the ring formation results in PO formation. The optimized geometries of PO formed on the systems are given in Figures 4.11 and 4.12. The reaction energies for PO formation are calculated as 0.471 eV for Cu(111) surface and 0.894 eV for Ru-Cu(111) surface.

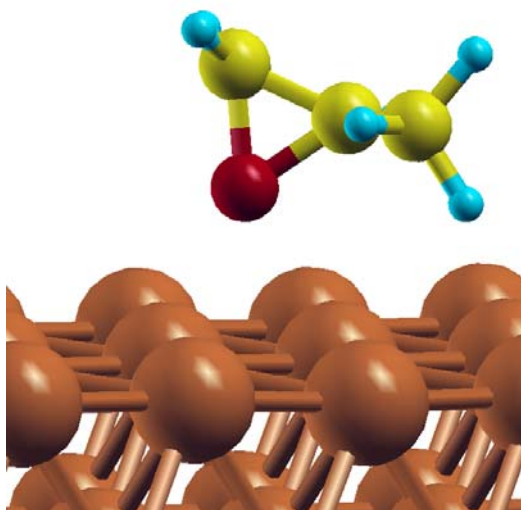


Figure 4.11: Top view of PO formed on Cu(111)

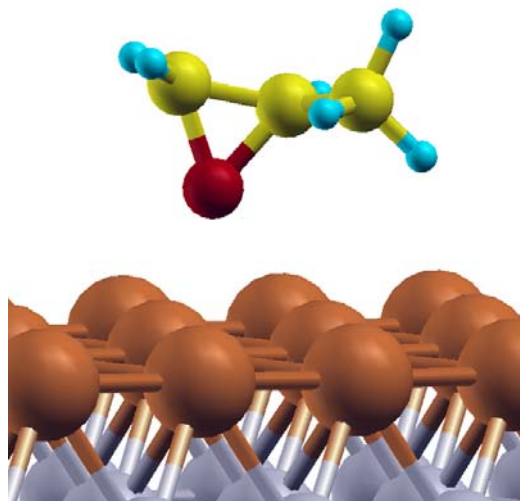


Figure 4.12: Top view of PO formed on Ru-Cu(111)

4.6 Formation of Propionaldehyde (PA) on Cu(111) and Ru-Cu(111) Surfaces

A proton transfer from the carbon bound to the oxygen atom to the unbound carbon in OMMP structure results in aldehyde formation, which is thought as a precursor to combustion. The calculated geometries of PA on systems are given in Figures 4.13 and 4.14. The reaction energies for PA formation are calculated as -0.399 eV for Cu(111) surface and 0.471 eV for Ru-Cu(111) surface.

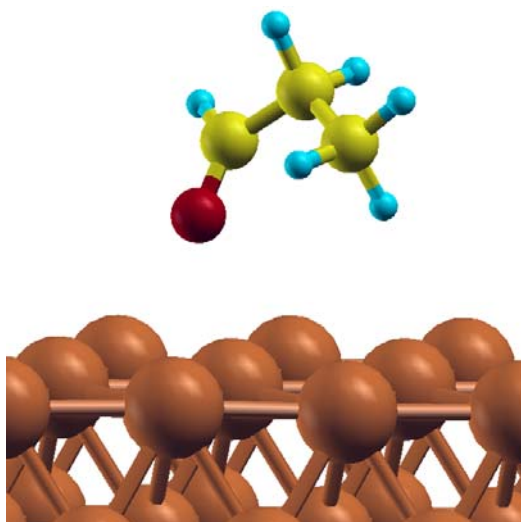


Figure 4.13: Top view of PA formed on Cu(111)

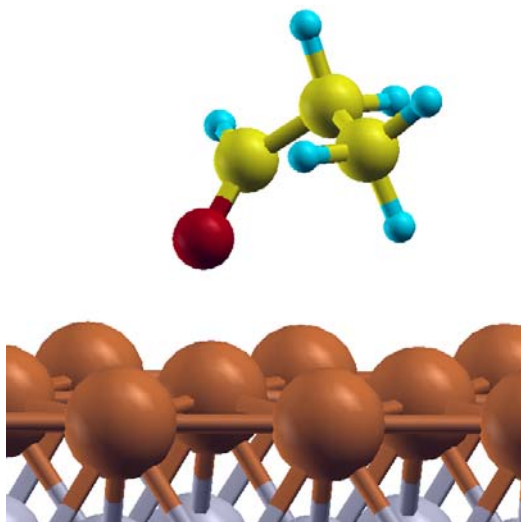


Figure 4.14: Top view of PA formed on Ru-Cu(111)

The reaction energies obtained for each investigated reaction in the mechanism are given in Table 4.5.

Table 4.5: Reaction energies of reactions within oxametallacycle mechanism on Cu(111) and Ru-Cu(111) surfaces (in eV)

Formations	Cu(111)	Ru-Cu(111)
Allyl	0.242	0.068
OMMP	0.199	0.301
PO	0.471	0.894
PA	-0.399	0.025

4.7 Allocation of Transition State Structures for Each Reaction

4.7.1 Illustration of the Methodology

Transition state structures for the investigated reactions are calculated with Climbing Image-Nudged Elastic Band (CI-NEB) method. Propylene adsorbed on the oxygenated system is the initial configuration for both allylic hydrogen stripping and the OMMP formation reactions. After the OMMP is formed, the structure is the initial configuration for both PO and PA formation reactions. Thus, after the optimized geometries for adsorbed propylene, OMMP, allyl radical, PO and PA structures are determined, the appropriate CI-NEB calculations between the initial and final configurations of the desired reactions results in the transition state (TS) structures and energy profiles.

For example, for the calculation of the TS for OMMP formation, first the adsorbed propylene is optimized on the surface. Then, OMMP structure is also optimized. Afterwards, CI-NEB calculations are performed between the adsorbed propylene (initial state) and OMMP structure (final state). This results in the generation of a reaction coordinate and an energy profile for the investigated reaction through the simultaneous optimization of a selected number of images along the minimum energy path. The energy profile obtained for OMMP formation on Ru-Cu(111) surface is shown in Figure 4.15 to illustrate the methodology.

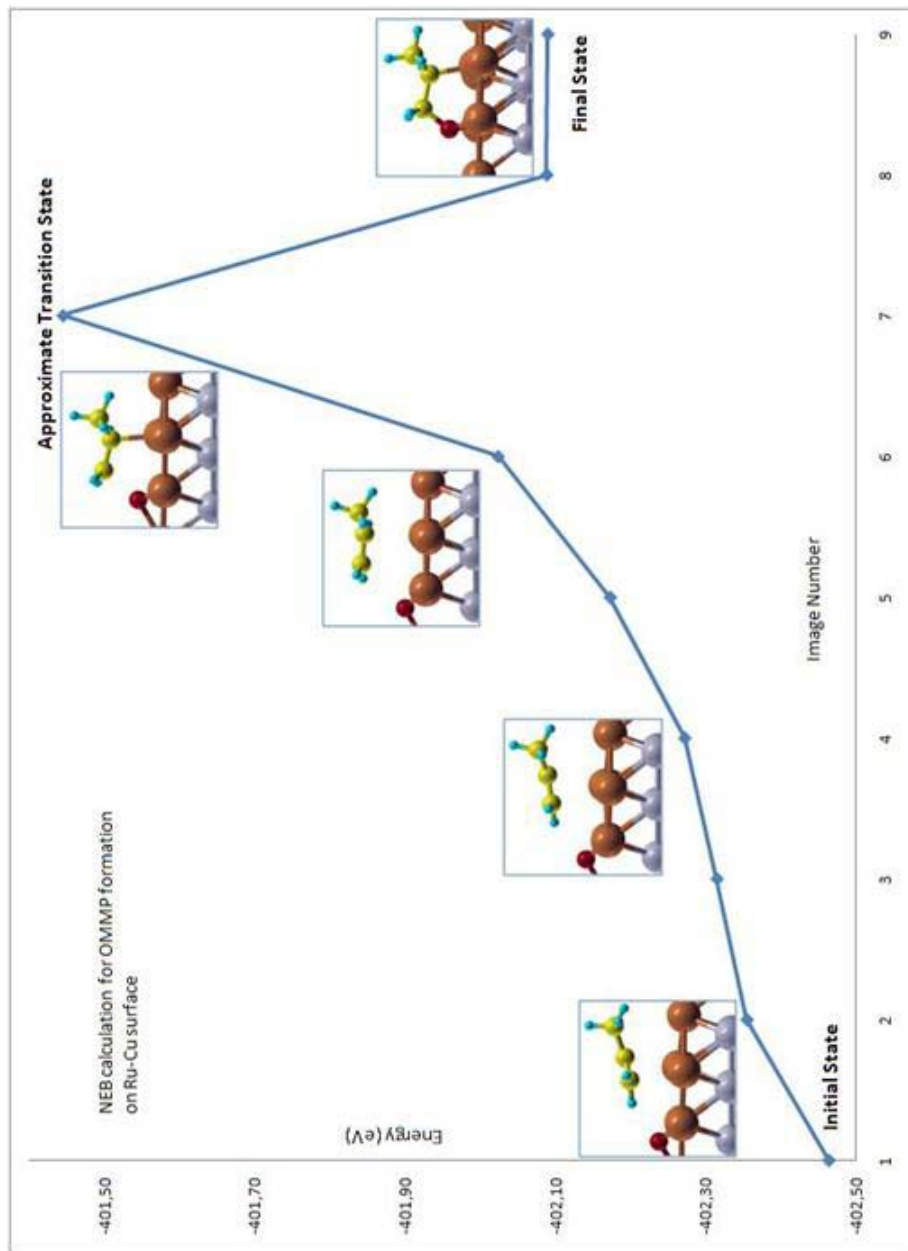


Figure 4.15: Energy profile obtained for OMMP formation reaction on Ru-Cu(111) surface

As seen in Figure 4.15, the image having the highest energy along the minimum energy path is appointed as the approximate TS structure. The structure is ‘approximate’ in the sense that a structure can only be evaluated as the ‘real’ TS after characterization by vibrational frequency analysis. Nevertheless, it is seen that after careful and rigorous CI-NEB calculations, the TS structures obtained are ‘real’ as it is proven by vibrational frequency analysis.

4.7.2 Transition State Structures for Allylic Hydrogen Stripping and OMMP Formation Reactions

The TS structures obtained for allylic hydrogen stripping and OMMP formation reactions on Cu(111) and Ru-Cu(111) are illustrated in Figures 4.16, 4.17, 4.18, 4.19.

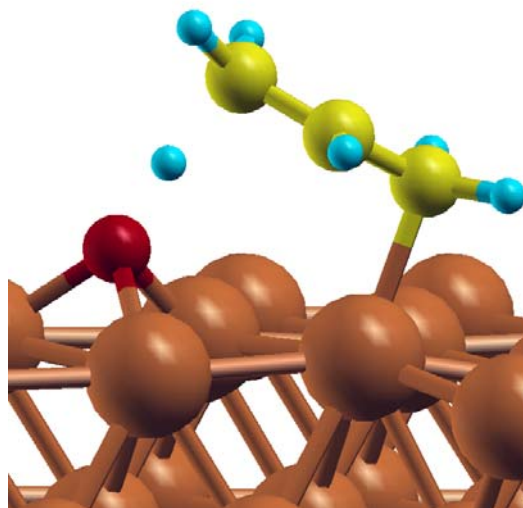


Figure 4.16: Side view of TS structure for allylic hydrogen stripping on Cu(111)

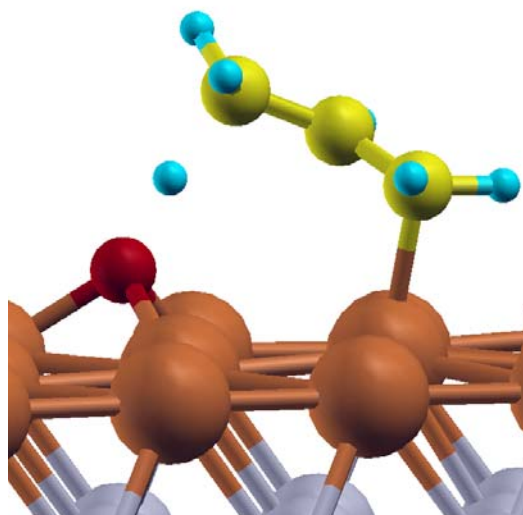


Figure 4.17: Side view of TS structure for allylic hydrogen stripping on Ru-Cu(111)

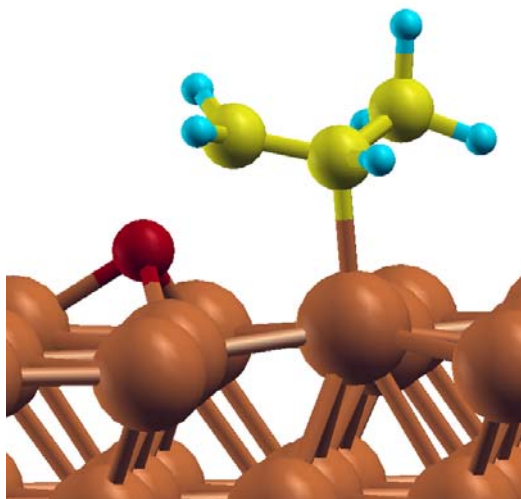


Figure 4.18: Side view of TS structure for OMMP formation on Cu(111)

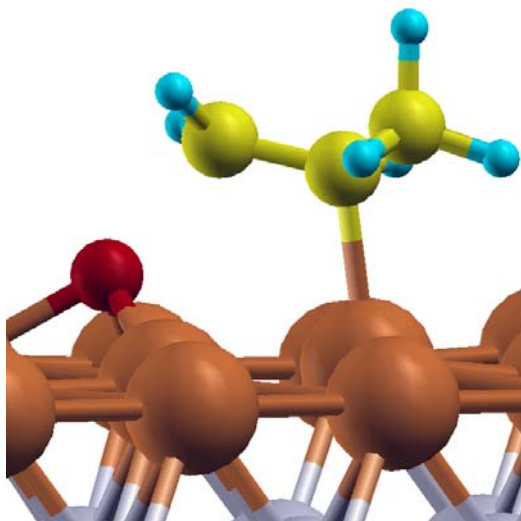


Figure 4.19: Side view of TS structure for OMMP formation on Ru-Cu(111)

In order to investigate the differences in the formation of allyl and OMMP intermediates on these two metal surfaces, it is of importance to compare the structural parameters calculated for TS structures of each reaction. These structural parameters (in general) increase the insight that can be obtained for the specific reactions by pointing out desired parameters that can be correlated with the catalytic properties of the investigated structure.

Calculated bond lengths of TS structures for OMMP formation and allylic hydrogen stripping are given in Table 4.6.

Table 4.6: Relevant bond lengths of TS structures for OMMP formation and allylic hydrogen stripping on Cu(111) and Ru-Cu(111) surfaces (in Å)

Bond lengths	Cu(111)	Ru-Cu(111)
O-H for AHS	1.23	1.26
C3-H for AHS	1.36	1.34
O-C1 for OMMP	1.96	1.99
Cu-C2 for OMMP	2.24	2.22

It can be seen that for allylic hydrogen stripping, the proton transferred from carbon to oxygen is located closer to oxygen on Cu(111) than on Ru-Cu(111) in the TS structure. For OMMP formation, O-C1 distance elongates and Cu-C2 distance shortens going from Cu(111) to Ru-Cu(111). However, the effect of the changes in bond lengths on energetics are not clear from the examination of these two systems and detailed examinations of more systems may be needed in order to arrive to a conclusion.

4.7.3 Transition State Structures for PO and PA formation reactions

The TS structures obtained for AHS and OMMP formation reactions on Cu(111) and Ru-Cu(111) are illustrated in Figures 4.20, 4.21, 4.22, 4.23.

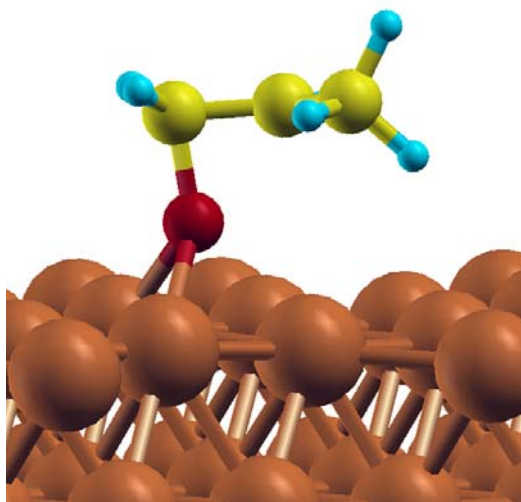


Figure 4.20: Side view of TS structure for PO formation on Cu(111)

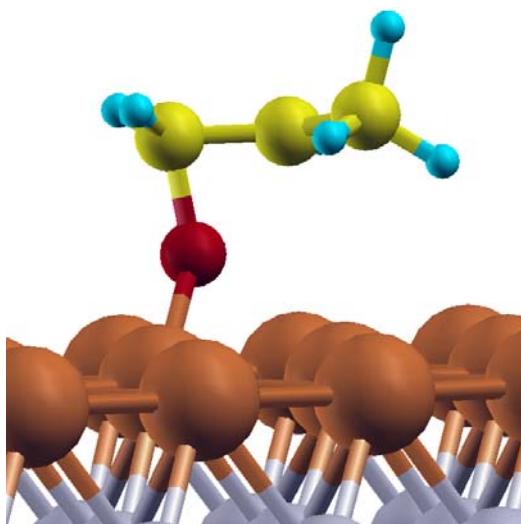


Figure 4.21: Side view of TS structure for PO formation on Ru-Cu(111)

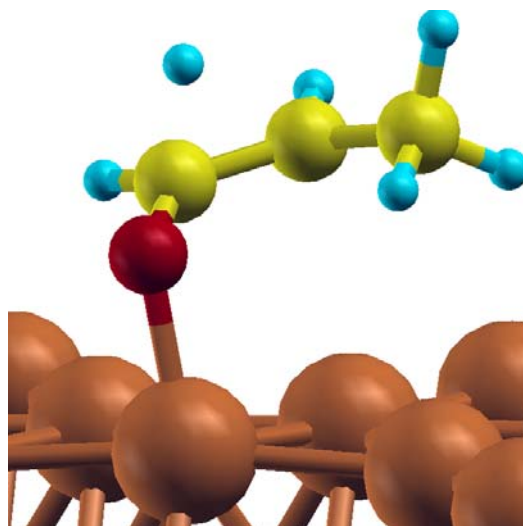


Figure 4.22: Side view of TS structure for PA formation on Cu(111)

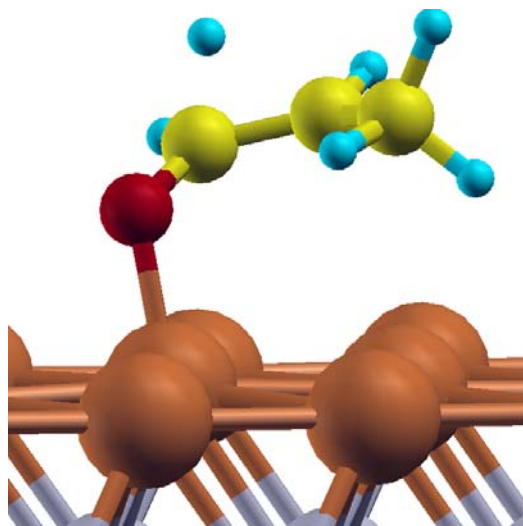


Figure 4.23: Side view of TS structure for PA formation on Ru-Cu(111)

Calculated bond lengths of TS structures for PO and PA formations are given in table 4.7.

Table 4.7: Relevant bond lengths of TS structures for PO and PA formations on Cu(111) and Ru-Cu(111) surfaces (in Å)

Bond lengths	Cu(111)	Ru-Cu(111)
O-C1 for PO	1.47	1.47
O-C2 for PO	1.95	1.90
H-C1 for PA	1.23	1.22
H-C2 for PA	1.61	1.60

As Table 4.7 is examined, it is seen that both the C-O bond length in PO formation and the C-H bond length in PA formation get shorter on Ru-Cu(111) compared to Cu(111) surface. This may be correlated with the increase in the activation barriers for both PO and PA formation on Ru-Cu(111) compared to Cu(111) surface; however, a more detailed analysis is again needed to validate the comment.

4.7.4 Vibrational Frequency Analysis

All calculated TS structures are characterized by vibrational frequency analysis performed within the harmonic oscillator approximation. During the calculations, only the reactive species and the underlying top surface layer were displaced from their equilibrium positions by 0.02 Å while the other metallic layers were kept fixed. The investigated TS structures show a single mode of imaginary frequency along the minimum energy path. The frequencies calculated for each reaction are summarized in Table 4.8.

Table 4.8: Single imaginary frequencies of the TS structures obtained for the investigated reactions (cm^{-1})

	Cu(111)	Ru-Cu(111)	Type of vibration
Allyl	1184	1139	C3-H stretching
OMMP	432	455	C1-O stretching
PO	448	393	O-C1-C2 rocking
PA	903	1012	C1-H-C2 rocking

4.7.5 Energetics of the Investigated Reactions on Cu(111) and Ru-Cu(111) Surfaces

After the TS structures have been determined, activation barriers for the reactions can be calculated. The activation barriers obtained for the investigated reactions are given in Table 4.9.

Table 4.9: Activation barriers of reactions within oxametallacycle mechanism on Cu(111) and Ru-Cu(111) surfaces (in eV)

Formations	Cu(111)	Ru-Cu(111)
Allyl	0.834	0.484
OMMP	0.752	0.915
PO	1.282	1.123
PA	1.368	1.611

The overall energy profile comparing the energetics of each reaction on Cu(111) and Ru-Cu(111) surfaces is given in Figure 4.24.

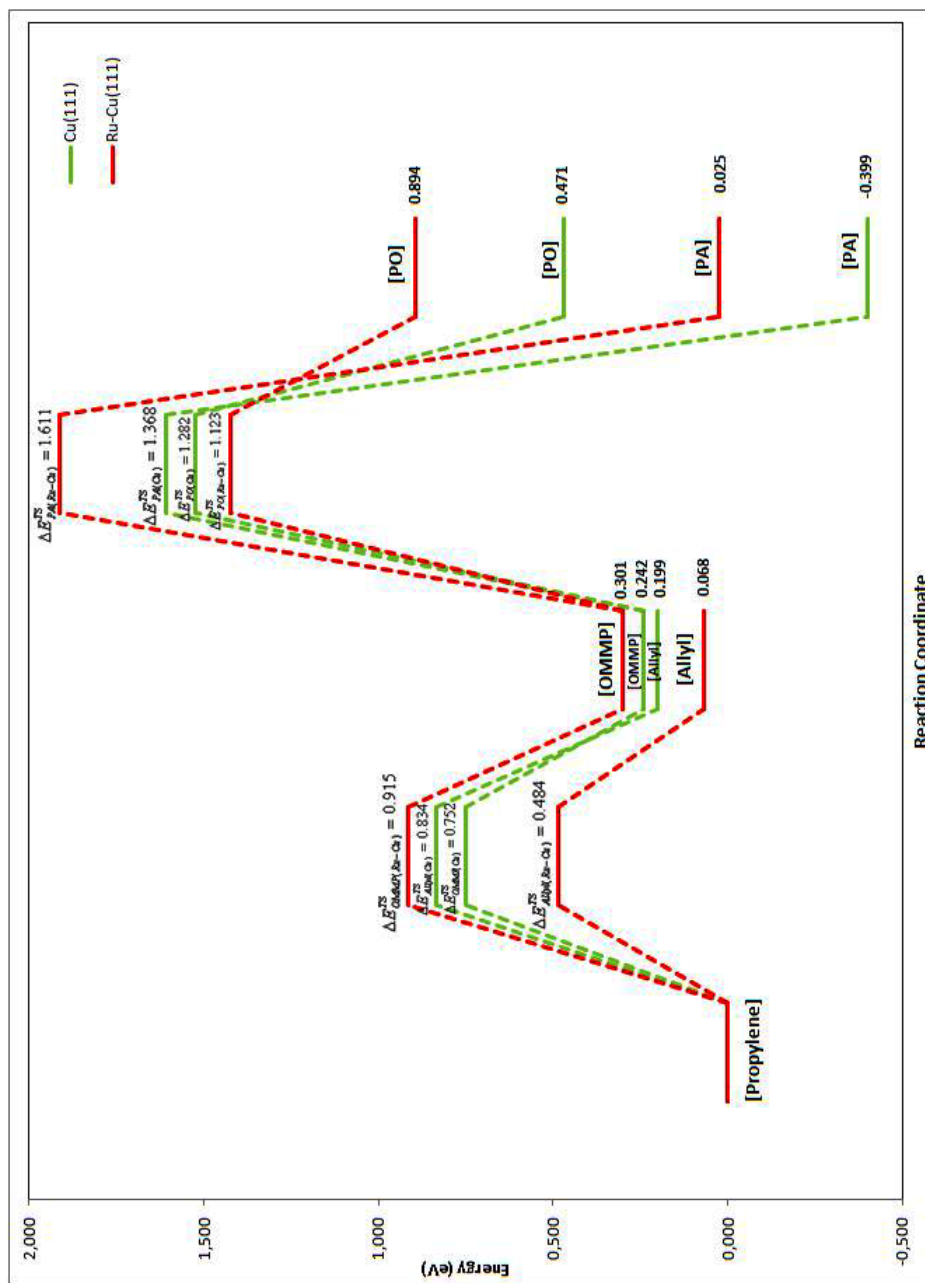


Figure 4.24: Energy profile for propylene epoxidation reactions on Cu(111) and Ru-Cu(111) surfaces

Cu(111) surface was recently theoretically investigated in the literature for propylene epoxidation within the oxametallacycle mechanism utilizing periodic DFT calculations with VASP code. The comparison of results obtained in our study for propylene epoxidation reactions on Cu(111) with the literature values [8] are given in Table 4.10.

Table 4.10: Comparison of the energetics obtained on Cu(111) surface with the literature (in eV)

	Our study	Torres et al.
Allyl	0.834	0.600
OMMP	0.752	0.540
PO	1.123	0.960
PA	1.368	1.100

The results obtained on the Cu(111) surface are consistent in trends with the prior study [8] about propylene epoxidation on Cu(111). In our study, the results are obtained on Cu(111) and Ru-Cu(111) surfaces with the same parameters and methods, thus, energy differences between the two systems lead to cancellation of errors inherent in DFT calculations. Furthermore, since the purpose of this study is not to obtain exact energies but to compare the relative barriers of steps on both Cu(111) and Ru-Cu(111) surfaces, the energetics can provide meaningful insight.

These results are the evidence of a significant electronic effect of the Ru substrate on the Cu monolayer. While the formation of OMMP is favored on Cu(111) surface over the allylic hydrogen stripping reaction, the opposite is true (and to a great extent) over the Ru-Cu(111) surface. It is generally accepted that [8, 43] the high PO selectivity is determined with a low barrier for OMMP formation compared to the barrier of hydrogen stripping. Thus, it is also evident from the results that the Ru-Cu(111) surface would favor combustion instead of PO formation and would be ineffective as a selective PO epoxidation catalyst.

4.8 SO₂ Adsorption on Oxygen Covered Cu(111) and Ru-Cu(111) Surfaces

It is important to evaluate the reason behind this ineffectiveness of the Ru-Cu(111) surface. Recently, it was proposed that the amphoteric character of the oxygen adsorbed on the metallic surface was primarily responsible for the PO selectivity [8, 43]. In essence, it was reported

that the lower the basicity of the oxygen, the higher the PO selectivity. To validate this proposal, the adsorption of SO_2 , a Lewis acid probe, was investigated. SO_2 binding energy is known to scale with the basicity of the oxygen atom [8]. Optimized geometries of SO_2 adsorbed on Cu(111) and Ru-Cu(111) surfaces are given in Figures 4.25 and 4.26.

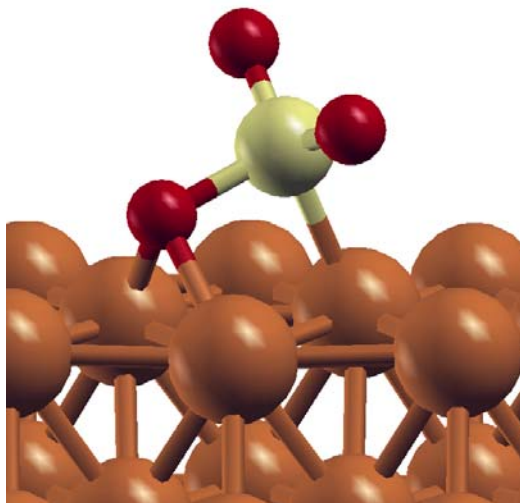


Figure 4.25: Side view of SO_2 binded to oxygen chemisorbed on on Cu(111)

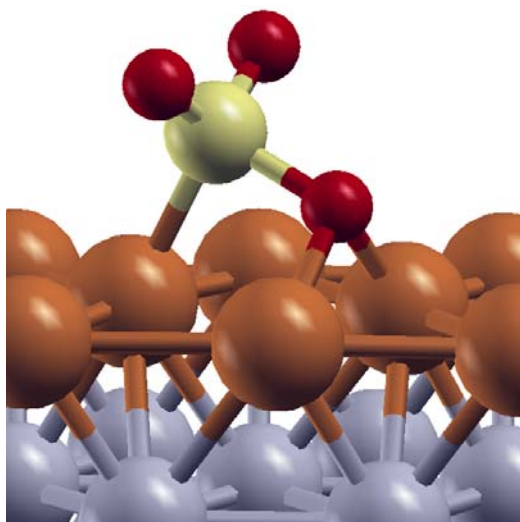


Figure 4.26: Side view of SO_2 binded to oxygen chemisorbed on on Ru-Cu(111)

The results obtained on both systems are given in Table 4.11.

Table 4.11: SO₂ binding energies on oxygenated Cu(111) and Ru-Cu(111) surfaces (in eV)

Cu(111)	0.447
Ru-Cu(111)	0.742

It is immediately seen from the energetics that the Ru-Cu(111) surface has a higher binding energy, and thus a higher affinity to bind SO₂. Thus, it is concluded that the oxygen adsorbed on the Ru-Cu(111) surface has a higher basicity, compared with the one on Cu(111) surface. Combining this with the energetics in Figure 4.24, the conclusion of previous studies about the effect of oxygen basicity on PO selectivity is also confirmed in this study, linking the inefficiency of the Ru-Cu(111) system to the higher basicity of the oxygen atom adsorbed on it.

CHAPTER 5

CONCLUSIONS

The direct, gas phase epoxidation reactions of propylene with oxygen on slab models of the metallic Cu(111) and bimetallic Ru-Cu(111) catalyst surfaces are investigated with periodic Density Functional Theory (DFT) calculations. The level of theory used is PW91 functional within the Generalized Gradient Approximation (GGA).

The generally accepted oxametallacycle mechanism governing heterogeneous alkene epoxidation was followed and reactions within this mechanism are evaluated. Each elementary step is investigated through the calculation of transition state (TS) structures utilizing the Climbing Image-Nudged Elastic Band (CI-NEB) method and rigorous optimizations.

The reactions investigated are allyl radical, propylene oxametallacycle (OMMP), propionaldehyde (PA) and propylene oxide (PO) formation reactions. The desired path for PO formation starts with the adsorption of propylene on oxygenated metal surfaces and follows as the formation of OMMP through the reaction of co-adsorbed propylene and oxygen and finally the transformation of the OMMP intermediate to PO. Formation of allyl radical and PA molecule are the competing reaction pathways for OMMP and PO formation reactions, respectively. Thus, the main desired property of a selective epoxidation catalyst is outlined as having a lower energy barrier for OMMP formation compared to allylic hydrogen stripping, as emphasized in literature.

Adsorption of atomic oxygen to clean, optimized metallic slabs is the starting point of the mechanism. DFT calculations revealed that Ru-Cu(111) surface chemisorbs oxygen more exothermically (4.88 eV) compared to the Cu(111) surface (4.65 eV). Following the oxygenation of the slabs, propylene was adsorbed onto the oxygenated systems. As in the case of oy-

gen chemisorption, propylene was also found to be adsorbed 0.17 eV (average) more exothermically on the oxygenated Ru-Cu(111) than on the oxygenated Cu(111) surface. These results pointed out at a glance that Ru-Cu(111) has an increased electron density compared to Cu(111) surface itself.

As the reaction path is analyzed, it was found that Cu(111) favors oxametallacycle formation over allylic hydrogen stripping, consistent with the literature. On the other hand, the results on Ru-Cu(111) indicate that the activation barrier for the stripping of the hydrogen atom is lowered, while the activation barrier for OMMP formation is increased on the Ru-Cu(111) surface compared to the Cu(111) surface.

Thus, it can be concluded that the Ru-Cu(111) surface would be ineffective for PO formation and rather promote combustion, based on the surface models and the reaction mechanism proposed. The slight decrease in the activation barrier of PO formation over Ru-Cu surface is incomparable with the decrease in the activation barrier of the allylic hydrogen stripping and therefore would not affect the conclusion that Ru-Cu(111) surface would be less selective than Cu(111) surface. Propylene epoxidation is thermodynamically favored but kinetically inhibited over Ru-Cu(111) surface.

This conclusion on the propylene epoxidation effectiveness of the Ru-Cu(111) surface was not totally unexpected through combination of information on the reason of metallic surface ability to epoxidize propylene [8] and the information about the electronic structure of the Ru-Cu catalyst surface [56].

In a previous publication of Christmann et. al [55], it was shown through work function measurements that a (slight) charge transfer would occur from Ru substrate to metallic Cu layer in Ru-Cu bimetallic catalysts. This would increase the electron density around the Cu atoms and consequently around the oxygen atom adsorbed on Cu(111) surface, making them more electronegative. Combining this with the hypothesis of Torres et. al [8], it can be expected that this phenomenon would increase the Lewis basicity of the oxygen adsorbed on Cu(111) and thus decrease the activation barrier of the allylic hydrogen stripping, since the highly basic oxygen atom would have an increased affinity to strip hydrogen atoms.

In fact, this is the result obtained after the presented DFT investigation of SO₂ adsorption on the oxygenated Cu(111) and Ru-Cu(111) surfaces. It is shown that the binding energy of SO₂

to surface oxygen increased for Ru-Cu(111) surface compared to the Cu(111) surface. Thus, it is confirmed, through theoretical calculations, that a charge transfer occurs from Ru(0001) substrate to Cu(111) monolayer which makes the surface more electronegative. This, in turn, makes the adsorbed oxygen more basic due to the increased electronic density around the oxygen atom. Therefore, the selectivity of the Ru-Cu(111) surface decreases for OMMP, and hence PO, formation compared to Cu(111) alone.

To conclude, Ru-Cu(111) bimetallic surface was investigated for the first time as an epoxidation catalyst analyzing the use of this important bimetallic system for PO epoxidation and comparing it to the pure single crystal surface of Cu(111). The results extend the validity of the effect of the oxygen basicity on PO selectivity obtained on metal surfaces to bimetallic systems, making a reference point for further studies on potential bimetallic propylene epoxidation catalysts.

REFERENCES

- [1] Dingerdissen, U., Martin A., Herein, D., Wernicke, H. J., *'The Development of Industrial Heterogeneous Catalysis'* in *Handbook of Heterogeneous Catalysis*, Vol. 1, Wiley, Weinheim, 2008.
- [2] Davis, B. H., *'Development of the Science of Catalysis'* in *Handbook of Heterogeneous Catalysis*, Vol. 1, Wiley, Weinheim, 2008.
- [3] Gates, B. C., *Catalytic Chemistry*, Wiley, Singapore, 1992.
- [4] van Santen, R. A., Neurock, M., *Molecular Heterogeneous Catalysis*, Wiley, Weinheim, 2006.
- [5] Dumesic, J. A., Huber, G. W., Boudart, M., *'Principles of Heterogeneous Catalysis'* in *Handbook of Heterogeneous Catalysis*, Vol. 1, Wiley, Weinheim, 2008.
- [6] Sabatier, P., *La catalyse en chimie organique*, B'éranger, Paris, 1920.
- [7] Murzin, D., Salmi, T., *Catalytic kinetics [electronic resource]*, Elsevier, Amsterdam, 2005.
- [8] Torres, D., Lopez, N., Illas, F., Lambert, R., *Angew. Chem. Int. Ed.*, 46, 2055 (2007).
- [9] Trent, D. L., *'Propylene Oxide'* in *Kirk-Othmer Encyclopedia of Chemical Technology*, Vol. 20, Wiley, New York, 1996.
- [10] Nijhuis, T. A., Makkee, M., Moulijn, J. A., Weckhuysen, B. M., *Ind. Eng. Chem. Res.*, 45, 3447 (2006).
- [11] Cook, D. B., *Handbook of Computational Quantum Chemistry*, Dover Publications Inc, New York, 2005.
- [12] Pople, J. A., Beveridge, D.L., *Approximate Molecular Orbital Theory*, McGraw-Hill, New York 1970.
- [13] Gasiorowicz, S., *Quantum Physics*, Wiley, New Jersey, 2003.
- [14] Soyer, S., MSc. Dissertation, METU, Ankara, 2005.
- [15] Nørskov, J. K., Bligaard, T., Rossmeisl, J., Christensen, C. H., *Nature Chem.*, 01 (2009).
- [16] Kohn, W., Sham, L. J., *Phys. Rev.*, 140 A1133 (1965).
- [17] Slater, J.C., *Phys. Rev.*, 81, 385 (1951).
- [18] Hohenberg, P., Kohn, W., *Phys. Rev.*, 136, B864 (1964).
- [19] Ziegler, T., *Chem. Rev.* 91, 651 (1991).
- [20] Becke, A. D., *Chem. Phys.*, 98, 5648 (1993).

- [21] Parr, R. G., *Density-functional theory of atoms and molecules*, Clarendon Press, Oxford 1989.
- [22] Scuseria, G. E., *J. Phys. Chem.*, A103, 4783 (1999).
- [23] van Santen, R. A., *Theoretical Heterogeneous Catalysis*, World Scientific, Singapore, 1991.
- [24] Levine, R. D., *Molecular Reaction Dynamics*, Cambridge University Press, Cambridge, 2005.
- [25] Rhodin, T. N, Ertl G., *The Nature of the Surface Chemical Bond*, North Holland, Amsterdam, 1981.
- [26] Morrison, S. R., *The Chemical Physics of Surfaces*, Plenum, New York, 1977.
- [27] Illas, F., *Models in Computational Materials Science*, Presentation, Barcelona, 2007.
- [28] Payne, M. C., Teter, M. P., Allan, D. C., Arias, T. A., Joannopoulos, J. D., *Rev. Mod.Phys.*, 64, 1045 (1992).
- [29] Chadi D. J., Cohen M. L., *Phys. Rev. B*, 8, 5747 (1973).
- [30] Monkhorst, H.J., Pack, J.D., *Phys. Rev. B*, 13, 5188 (1976).
- [31] Mimura, N., Song, Z., Akita, T., Yamashita, H., Tsubota, S., Oyama, S. T., *Science And Technology In Catalysis 2006*, p. 389, 2006.
- [32] Akimoto, M., Ichikawa, K., Echigoya, E., *J. Catal.*, 76, 333 (1982).
- [33] Hayashi, T., Tanaka, K., Haruta, M., *J. Catal.*, 178, 566 (1998).
- [34] Sinha, A. K., Seelan, S., Tsubota, S., Haruta, M., *Angew. Chem. Int. Ed.*, 43, 1546 (2004).
- [35] Cowell, J. J., Santra, A. K., Lambert, R. M., *J. Am. Chem. Soc.*, 122, 2381 (2000).
- [36] Vaughan, O. P. H., Kyriakou, G., Macleod, N., Tikhov, M., Lambert, R. M., *J. Catal.*, 236, 401 (2005).
- [37] Lu, J., Luo, M., Lei, H., Bao, X., Li, C., *J. Catal.*, 211, 552 (2002).
- [38] Chu, H., Yang, L., Zhang, Q., Wang, Y., *J. Catal.*, 241, 225 (2006).
- [39] Zhu, W., Zhang, Q., Wang, Y., *J. Phys. Chem. C*, 112, 7731 (2008).
- [40] Yang, S., Zhu, W., Zhang, Q., Wang, Y., *J. Catal.*, 254, 251 (2008).
- [41] Llorca, J., Dominguez, M., Ledesma, C., Chimento, R. J., Medina, F., Sueiras, J., Angurell, I., Seco, M., Rossell, O., *J. Catal.*, 258, 187 (2008).
- [42] Mimura, N., Song, Z., Akita, T., Yamashita, H., Tsubota, S., Oyama, S. T., *Science And Technology In Catalysis 2006*, p. 389, 2006.
- [43] Roldan, A., Torres, D., Ricart, J. M., Illas, F., *J. Mol. Catal. A: Chem.*, 306, 6 (2009).
- [44] Cant, N. W., Hall W. K., *J. Catal.*, 52, 81 (1978).

- [45] Barteau, M. A., Madix, R. J., J. Am. Chem. Soc., 105, 345 (1983).
- [46] Jones, G. S., Mavrikakis, M., Barteau, M. A., Vohs, J. M., J. Am. Chem. Soc., 120, 3196 (1998).
- [47] Medlin, J. W., Barteau, M. A., Vohs, J. M., J. Mol. Catal. A: Chem., 163, 129 (2000).
- [48] Linic, S., Barteau, M. A., J. Am. Chem. Soc., 125, 4034 (2003).
- [49] Torres, D., Lopez, N., Illas, F., Lambert, R., J. Am. Chem. Soc., 127, 10774 (2005).
- [50] Sinfelt, J. H., J. Catal., 29, 308 (1973).
- [51] Chyan, O., Arunagiri, T. N., Ponnuswamy, T., J. Electrochem. Soc., 150, C347 (2003).
- [52] Connor R., Adkins, H., J. Am. Chem. Soc., 54, 4678 (1982).
- [53] Sinfelt, J. H., Lam, J. L., Cusumano, J. A., Barnett, A. E., J. Catal., 42, 227 (1976).
- [54] Sinfelt, J. H., Via, G. H., Lytle, F.W., J. Chem. Phys., 72, 9 (1980).
- [55] Christmann, K., Ertl, G., Shimizu, H., J. Catal., 61, 397 (1980).
- [56] Shimizu, H., Christmann, K., Ertl, G., J. Catal., 61, 412 (1980).
- [57] Potschke, G. O., Behm, R. J., Phys. Rev. B, 44, 1442 (1991).
- [58] Ruebush, S. D., Couch, R. E., Thevuthasan, S., Wang, Z., Fadley, C. S., Surf. Sci., 387, L1041 (1997).
- [59] Kresse, G., Furthmuller, J., Phys. Rev. B, 54, 11169 (1996).
- [60] Perdew, J. P., Chevary, J. A., Vosko, S. H., Jackson, K. A., Pederson, M. R., Mark, R., Singh, D. J., Fiolhais C., Phys. Rev. B, 46, 6671 (1992).
- [61] Perdew, J. P., Wang, Y., Phys. Rev. B, 45, 13244 (1992).
- [62] Blochl, P. E., Phys. Rev. B, 50, 17953 (1994).
- [63] Kresse, G., Furthmuller, J., Comput. Mater. Sci., 6, 15 (1996).
- [64] Henkelman, G., Uberuaga, B. P., Jonsson, H., J. Chem. Phys., 113, 22, 9901 (2000).
- [65] Wyckoff, R. W. G., *Crystal Structures*, Vol. 1, Wiley, New York, 1963.
- [66] Torres, D., Neyman, K., Illas, F., Chem. Phys. Lett., 429, 86 (2006).
- [67] Lambert, R. M., Williams F. J., Cropley R. L., Palermo A., J. Mol. Catal. A: Chem., 228, 27 (2005).

APPENDIX A

VASP FILES

A.1 Sample Input and Output

A VASP input consists of 4 specific files. Because of that reason, instead of an input file, we have to talk about an ‘input folder’ for a VASP calculation. Thus, the name of the job is given to the work directory. 4 specific files, which always have to have the same names, are listed as:

1. INCAR
2. KPOINTS
3. POSCAR
4. POTCAR

As a summary, INCAR is the main input file in the sense that optimization algorithms, convergence criteria, smearing functions and many other calculation parameters are entered in that file. K-POINTS is the file which tells the program how many k-points are used to sample the Brillouin zone. POSCAR is the geometrical input, that is the positions of all atoms in the calculations are entered in POSCAR file. POTCAR is the pseudopotential file, where the choice of pseudopotentials are indicated. Each element has its own POTCAR file. In order to generate a POTCAR file for the system, separate POTCAR files are attenuated.

A sample INCAR file is shown in Figure A.1.

A sample KPOINTS file is shown in Figure A.2.

```
SYSTEM = Ru
!ISTART = 0
!PREC = HIGH
!ISIF = 2
IBRION = 2; NFREE = 20;
NSW = 150
LREAL = AUTO
ISMear = 1; SIGMA = 0.2;
ENCUT = 500
IALGO = 48
NBANDS = 320
!EDIFFG = -0.01
!LDIPOLE = 3
!LDIPOLE = .TRUE.
```

Figure A.1: A sample INCAR file

```
K-Points
0
Monkhorst Pack
4 4 1
0 0 0
```

Figure A.2: A sample KPOINTS file

A sample POSCAR file is shown in Figure A.3.

```

Ru0001-3x3x4
1.000000
7.091189 4.094100 0.000000
0.000000 8.188200 0.000000
0.000000 0.000000 25.45420
36 9 1 3 6
Selective Dynamics
Cartesian
0.787902000 1.364686000 0.000000000 F F F
0.787902000 4.094059000 0.000000000 F F F
0.787902000 6.823514000 0.000000000 F F F
3.151608000 2.729373000 0.000000000 F F F
3.151608000 5.458745000 0.000000000 F F F
3.151608000 8.188200000 0.000000000 F F F
5.515385000 4.094100000 0.000000000 F F F
5.515385000 6.823473000 0.000000000 F F F
5.515385000 9.552927000 0.000000000 F F F
1.575804000 2.729373000 2.151427000 F F F
1.575804000 5.458827000 2.151427000 F F F
1.575804000 8.188200000 2.151427000 F F F
3.939581000 4.094100000 2.151427000 F F F
3.939581000 6.823555000 2.151427000 F F F
3.939581000 9.552927000 2.151427000 F F F
6.303287000 5.458786000 2.151427000 F F F
6.303287000 8.188241000 2.151427000 F F F
6.303287000 10.917614000 2.151427000 F F F
0.787889000 1.364664000 4.299296000 F F F
0.787930000 4.094061000 4.299242000 F F F
0.787876000 6.823476000 4.299275000 F F F
3.151596000 2.729398000 4.299242000 F F F
3.151642000 5.458804000 4.299216000 F F F
3.151641000 8.188227000 4.299219000 F F F
5.515365000 4.094059000 4.299275000 F F F
5.515391000 6.823515000 4.299219000 F F F
5.515374000 9.552908000 4.299229000 F F F
1.575931000 2.729598000 6.377690000 T T T
1.591712000 5.457827000 6.387247000 T T T
1.591682000 8.189249000 6.386857000 T T T
3.930769000 4.107374000 6.387260000 T T T
3.939621000 6.823637000 6.376404000 T T T
3.931143000 9.539840000 6.386611000 T T T
6.296249000 5.473061000 6.386846000 T T T
6.296174000 8.174396000 6.386613000 T T T
6.303464000 10.917925000 6.363024000 T T T
0.787798000 1.364506000 8.494461000 T T T
0.787109000 4.093005000 8.493958000 T T T
0.737760000 6.823897000 8.490363000 T T T
3.151089000 2.728161000 8.493964000 T T T
3.128035000 5.417919000 8.617714000 T T T
3.129284000 8.227470000 8.618755000 T T T
5.540791000 4.050868000 8.490371000 T T T
5.560558000 6.823776000 8.618752000 T T T
5.540855000 9.597036000 8.490217000 T T T
3.939587000 6.823577000 9.637414000 T T T
6.509682190 8.760258950 10.903655720 T T T
5.076231800 8.930115580 10.417761610 T T T
4.167852280 7.758564650 10.735272400 T T T
4.647614910 9.868227700 10.781808020 T T T
3.171400600 8.100045950 11.043990010 T T T
4.589332290 7.145388340 11.545461130 T T T
7.111416790 9.651471000 10.700277420 T T T
6.544969330 8.573462540 11.987543900 T T T
7.009688950 7.911927360 10.418761820 T T T

```

Figure A.3: A sample POSCAR file

The first lines of a sample POTCAR file is shown in Figure A.4.

```

PAW_GGA Ru 03Mar1998
8.0000000000000000
parameters from PSCTR are:
URHFIL =Ru: s1 d7
LEXCH = 91
EATOM = 455.6262 eU. 33.4876 Ry

TITEL = PAW_GGA Ru 03Mar1998
LULTRA = F use ultrasoft PP ?
IUNSCR = 1 unscreen: 0-lin 1-nonlin 2-no
RPACOR = 2.170 partial core radius
POMASS = 101.070; ZVAL = 8.000 mass and valenz
RCORE = 2.600 outmost cutoff radius
RWIGS = 2.650; RWIGS = 1.402 wigner-seitz radius (au A)
ENMAX = 213.271; ENMIN = 159.953 eU
RCLOC = 1.830 cutoff for local pot
LCOR = T correct aug charges
LPAW = T paw PP
EAUG = 333.494
DEXC = -.025
RMAX = 3.157 core radius for proj-oper
RAUG = 1.300 factor for augmentation sphere
RDEP = 2.687 core radius for depl-charge
QCUT = -3.959; QGAM = 7.918 optimization parameters

Description
 1 E TYP RCUT TYP RCUT
 2 .000 23 2.600
 2 .000 23 2.600
 0 .000 23 2.600
 0 .000 23 2.600
 1 -.200 23 2.600
 1 2.000 23 2.600
 3 .000 7 .000

Error from kinetic energy argument (eU)
NDATA = 100
STEP = 20.000 1.050
123. 121. 119. 117. 115. 112. 109. 107.
104. 101. 99.0 95.4 91.7 88.0 84.3 80.5
76.7 72.9 69.1 63.5 59.8 56.2 51.0 47.6
44.3 39.6 35.1 32.3 28.3 24.7 21.3 18.3
15.6 13.1 11.0 9.07 6.94 5.60 4.13 3.24
2.29 1.58 1.06 .682 .426 .257 .151 .788E-01
.511E-01 .372E-01 .340E-01 .338E-01 .331E-01 .307E-01 .254E-01 .201E-01
.149E-01 .975E-02 .623E-02 .428E-02 .349E-02 .331E-02 .328E-02 .311E-02
.274E-02 .214E-02 .153E-02 .105E-02 .753E-03 .661E-03 .646E-03 .624E-03
.548E-03 .430E-03 .300E-03 .224E-03 .189E-03 .183E-03 .174E-03 .150E-03
.111E-03 .811E-04 .678E-04 .654E-04 .615E-04 .503E-04 .373E-04 .293E-04
.276E-04 .263E-04 .214E-04 .162E-04 .134E-04 .130E-04 .115E-04 .884E-05
.707E-05 .679E-05 .606E-05 .470E-05

END of PSCTR-controll parameters
local part
71.8095875659990810
.10549876E+03 .10548468E+03 .10544240E+03 .10537197E+03 .10527341E+03
.10514678E+03 .10499215E+03 .10480959E+03 .10459920E+03 .10436111E+03
.10409544E+03 .10380235E+03 .10348200E+03 .10313459E+03 .10276033E+03
.10235945E+03 .10193218E+03 .10147882E+03 .10099963E+03 .10049493E+03
.99965060E+02 .99410354E+02 .98031185E+02 .98227943E+02 .97601034E+02
.96950807E+02 .96277951E+02 .95582692E+02 .94865601E+02 .94127185E+02
.93367974E+02 .92588515E+02 .91789379E+02 .90971154E+02 .90134448E+02
.89279886E+02 .88408115E+02 .87519796E+02 .86615607E+02 .85696244E+02
.84762414E+02 .83814840E+02 .82854257E+02 .81881411E+02 .80897058E+02
.79901963E+02 .78896900E+02 .77882649E+02 .76859996E+02 .75829730E+02
.74792645E+02 .73749537E+02 .72701203E+02 .71648437E+02 .70592035E+02
.69532788E+02 .68471483E+02 .67408901E+02 .66345817E+02 .65282996E+02
.64221195E+02 .63161158E+02 .62103619E+02 .61049297E+02 .59998896E+02
.58953105E+02 .57912597E+02 .56878025E+02 .55850026E+02 .54829215E+02
.53816190E+02 .52811525E+02 .51815774E+02 .50829468E+02 .49853117E+02
.48887205E+02 .47932195E+02 .46988523E+02 .46056604E+02 .45136826E+02
.44229553E+02 .43335122E+02 .42453847E+02 .41586015E+02 .40731891E+02
.39891711E+02 .39065688E+02 .38254010E+02 .37456842E+02 .36674324E+02

```

Figure A.4: A sample POTCAR file (first lines)

The last lines of a sample POTCAR file is shown in Figure A.5.

```

-164767678471E-03 -175428646997E-03 -186779978997E-03 -198866197715E-03 -211734670193E-03
-225435785832E-03 -240023145829E-03 -255553764136E-03 -272088280619E-03 -289691187004E-03
-300431066949E-03 -320380049280E-03 -349618078069E-03 -372225197539E-03 -396289854432E-03
-421905218165E-03 -449170319875E-03 -478190411366E-03 -509077345019E-03 -54194975832E-03
-576934586707E-03 -614165338258E-03 -653784744387E-03 -695944174972E-03 -740804387034E-03
-788536085837E-03 -839320517385E-03 -893350093891E-03 -950829053768E-03 -101197415784E-02
-107701542341E-02 -114619689802E-02 -121977747457E-02 -129803174974E-02 -138125092760E-02
-146974377018E-02 -156383759712E-02 -166387933628E-02 -177023662726E-02 -188329897977E-02
-200347899007E-02 -213121361339E-02 -226696550130E-02 -241122439889E-02 -256450860785E-02
-272736651597E-02 -290037819486E-02 -308415706753E-02 -327935164737E-02 -348664734981E-02
-370676837775E-02 -394047968180E-02 -418858899577E-02 -445194894796E-02 -473145924816E-02
-502806894995E-02 -534277878754E-02 -567664358588E-02 -603077474184E-02 -640634277454E-02
-680457994093E-02 -722678291324E-02 -767431551306E-02 -814861149651E-02 -865117738348E-02
-918359532310E-02 -974752598620E-02 -103447114740E-01 -109769782313E-01 -116462399496E-01
-123545004459E-01 -131038564988E-01 -138965006224E-01 -147347237568E-01 -156209178508E-01
-165575783101E-01 -175479628133E-01 -185928107396E-01 -196969103445E-01 -208625350239E-01
-220927222456E-01 -233906429277E-01 -24759519401E-01 -262020381397E-01 -27723998831E-01
-293266439515E-01 -310144938195E-01 -327913771952E-01 -346612277510E-01 -366280799639E-01
-386960639714E-01 -408693993520E-01 -431523872247E-01 -455494840638E-01 -480648866124E-01
-507033252791E-01 -534692483885E-01 -563672076590E-01 -594017612679E-01 -625774548640E-01
-658980003812E-01 -693702525007E-01 -729961826092E-01 -767808500938E-01 -807283700150E-01
-848426825967E-01 -891275075741E-01 -935863112397E-01 -982222580348E-01 -103038163335E+00
-108036441692E+00 -113219051193E+00 -118587433826E+00 -124142451743E+00 -129884319334E+00
-135812531043E+00 -141925784889E+00 -148221901660E+00 -154697739807E+00 -161349106054E+00
-168170661812E+00 -175155825470E+00 -182296670714E+00 -189583821013E+00 -197006340475E+00
-204551621276E+00 -212205267942E+00 -219950978787E+00 -227770424921E+00 -235643127340E+00
-243546332853E+00 -251454889870E+00 -259341125468E+00 -267174725804E+00 -274922622387E+00
-282548887376E+00 -290014641201E+00 -297277975165E+00 -304293889676E+00 -311014244858E+00
-317387714215E+00 -323359724613E+00 -328872358786E+00 -333864192871E+00 -338270045283E+00
-342020629273E+00 -345042134989E+00 -347255814880E+00 -348577687842E+00 -348918471859E+00
-348183779824E+00 -346274504764E+00 -343087262689E+00 -338514791091E+00 -332446265956E+00
-324767543516E+00 -315361358620E+00 -304107519178E+00 -290883121618E+00 -275562791544E+00
-258018942022E+00 -238122042527E+00 -215740095668E+00 -190742723144E+00 -162994464622E+00
-132361094614E+00 -907079642700E-01 -619001764969E-01 -210032045569E-01 -217166337583E-01
-687916327629E-01 -19550706585E-01 -174125427035E-01 -232635780325E-01 -29520232654E-01
-361938674740E+00 -432951287182E+00 -50037092705E+00 -580105630292E+00 -672569024734E+00
-761547526601E+00 -855162882729E+00 -953436046218E+00 -105636377717E+01 -116391486118E+01
127602595393E+01
End of Dataset

```

Figure A.5: A sample POTCAR file (last lines)

VASP produces a large number of output files although not all of them are necessary in the calculation of standard parameters. The output files that is of interest in this study can be summarized as:

1. out
2. OUTCAR
3. CONTCAR
4. XDATCAR
5. WAVECAR

“out” is the standard output generated by the program. The first lines of a sample output file for a VASP optimization calculation is shown in Figure A.6.

```

GNU nano 1.3.12 File: out
running on 16 nodes
distr: one band on 1 nodes, 16 groups
vasp.4.6.31 08Feb07 complex
POSCAR found: 5 types and 55 ions
LDA part: xc-table for Ceperly-Alder, standard interpolation
found WAUECAR, reading the header
POSCAR, INCAR and KPOINTS ok, starting setup
WARNING: wrap around errors must be expected
FFT: planning ... 2
reading WAUECAR
the WAUECAR file was read successfully
initial charge from wavefunction
entering main loop

```

	N	E	dE	d eps	ncg	rms	rms(c)
RMM:	1	-0.402278211594E+03	-0.40228E+03	-0.23602E+00	15405	0.208E+00	0.149E+00
RMM:	2	-0.404908161303E+03	-0.26299E+01	-0.45737E-01	15363	0.118E+00	0.114E+01
RMM:	3	-0.402230718690E+03	0.26774E+01	-0.21880E-01	15392	0.779E-01	0.130E+00
RMM:	4	-0.402199602252E+03	0.31116E-01	-0.57195E-02	15361	0.537E-01	0.921E-01
RMM:	5	-0.402190238840E+03	0.93634E-02	-0.32861E-02	15386	0.344E-01	0.796E-01
RMM:	6	-0.402179000148E+03	0.11239E-01	-0.16544E-02	15376	0.273E-01	0.326E-01
RMM:	7	-0.402170106340E+03	0.89381E-03	-0.31850E-03	15369	0.112E-01	0.269E-01
RMM:	8	-0.402177082112E+03	0.10242E-02	-0.10447E-03	15311	0.652E-02	0.132E-01
RMM:	9	-0.402176957583E+03	0.12453E-03	-0.44472E-04	14001	0.464E-02	0.912E-02
RMM:	10	-0.402177050380E+03	-0.92797E-04	-0.26455E-04	10686	0.371E-02	

```

1 F= -.40217705E+03 E0= -.40216033E+03 d E =-.402177E+03
BRION: g(F)= 0.290E-03 g(S)= 0.000E+00
bond charge predicted

```

	N	E	dE	d eps	ncg	rms	rms(c)
RMM:	1	-0.402172157203E+03	-0.40218E+03	-0.39334E-02	15370	0.303E-01	0.557E-02
RMM:	2	-0.402172767766E+03	-0.61056E-03	-0.11499E-03	15219	0.760E-02	0.179E-01
RMM:	3	-0.402172407236E+03	0.36053E-03	-0.19100E-04	10613	0.302E-02	0.907E-02
RMM:	4	-0.402172293411E+03	0.11382E-03	-0.52990E-05	8960	0.157E-02	0.353E-02
RMM:	5	-0.402172352541E+03	-0.59130E-04	-0.34219E-05	9057	0.135E-02	

```

2 F= -.40217225E+03 E0= -.40216070E+03 d E =-.302161E-03
BRION: g(F)= 0.583E-03 g(S)= 0.000E+00 retain N= 1 mean eig= 0.41
eig: 0.412
bond charge predicted

```

	N	E	dE	d eps	ncg	rms	rms(c)
RMM:	1	-0.402177558847E+03	-0.40218E+03	-0.11632E-02	15323	0.150E-01	0.207E-02
RMM:	2	-0.402177704754E+03	-0.14591E-03	-0.26143E-04	9907	0.318E-02	0.724E-02
RMM:	3	-0.402177650506E+03	0.54249E-04	-0.45261E-05	8966	0.179E-02	

```

3 F= -.40217765E+03 E0= -.40216097E+03 d E =-.297964E-03
BRION: g(F)= 0.102E-03 g(S)= 0.000E+00 retain N= 2 mean eig= 3.57
eig: 0.348 6.792
bond charge predicted

```

	N	E	dE	d eps	ncg	rms	rms(c)
RMM:	1	-0.402177701455E+03	-0.40218E+03	-0.29294E-03	15265	0.867E-02	0.279E-02
RMM:	2	-0.402170955790E+03	-0.12543E-02	-0.17000E-04	10210	0.232E-02	0.243E-01
RMM:	3	-0.402172759563E+03	0.11962E-02	-0.10801E-04	9322	0.266E-02	0.250E-02
RMM:	4	-0.402172750851E+03	0.71200E-06	-0.18827E-05	8095	0.879E-03	

```

4 F= -.40217776E+03 E0= -.40216109E+03 d E =-.108346E-03
BRION: g(F)= 0.693E-04 g(S)= 0.000E+00 retain N= 3 mean eig= 4.29
eig: 12.351 0.360 0.172
bond charge predicted

```

	N	E	dE	d eps	ncg	rms	rms(c)
RMM:	1	-0.402177827800E+03	-0.40218E+03	-0.20600E-03	15022	0.725E-02	0.140E-02
RMM:	2	-0.402177879953E+03	-0.52073E-04	-0.30707E-05	9040	0.136E-02	

```

5 F= -.40217780E+03 E0= -.40216121E+03 d E =-.121101E-03
BRION: g(F)= 0.650E-04 g(S)= 0.000E+00 retain N= 4 mean eig= 4.70
eig: 17.052 0.455 0.127 0.383
bond charge predicted

```

	N	E	dE	d eps	ncg	rms	rms(c)
RMM:	1	-0.402177884067E+03	-0.40218E+03	-0.12466E-03	14545	0.567E-02	0.218E-02
RMM:	2	-0.402170652264E+03	-0.76820E-03	-0.10078E-04	9534	0.219E-02	0.194E-01
RMM:	3	-0.402172902331E+03	0.74993E-03	-0.60613E-05	8942	0.200E-02	0.148E-02
RMM:	4	-0.402172901336E+03	0.99518E-06	-0.91615E-06	8722	0.601E-03	

```

6 F= -.40217790E+03 E0= -.40216124E+03 d E =-.213832E-04
BRION: g(F)= 0.625E-04 g(S)= 0.000E+00 retain N= 5 mean eig= 4.55
eig: 17.520 0.448 0.534 0.534 3.695

```

Figure A.6: A sample “out” file (first lines)

The “out” file keeps track of the general running information of the code like iteration number etc. The columns that are seen in Figure A.6 are explained as:

- N, iteration count
- dE, change of total energy
- d eps, change of the eigenvalues (fixed potential)
- ncg, number of optimisation steps
- rms, total residual vector
- rms(c), charge density residual vector

At the end of the calculation, the reason of the stopping of the code is illustrated in “out” file, like convergence, exceeding of the specified number of iterations etc. The end of the “out” file is shown in Figure A.7.

```

11 F= -.35302941E+03 E0= -.35301003E+03 d E =-.354371E-01
curvature: -3.89 expect dE=-0.736E-02 dE for cont linesearch -0.907E-03
trial: gam= 0.02917 g(F)= 0.189E-02 g(S)= 0.000E+00 ort = 0.307E-02 (trialstep = 0.178E+01)
search vector abs. value= 0.211E-02
bond charge predicted
  N      E              dE              d eps              ncg              rms              rms(c)
RMM: 1    -0.353039313745E+03  -0.35304E+03  -0.17438E+00  8981  0.202E+00  0.164E-01
RMM: 2    -0.353032677463E+03  0.66363E-02  -0.30622E-02  8998  0.378E-01  0.419E-01
RMM: 3    -0.353030971064E+03  0.17064E-02  -0.17779E-03  9012  0.880E-02  0.253E-01
RMM: 4    -0.353029957762E+03  0.10133E-02  -0.40525E-04  7653  0.407E-02  0.941E-02
RMM: 5    -0.353029894020E+03  0.63742E-04  -0.24398E-04  5921  0.338E-02
12 F= -.35302989E+03 E0= -.35301159E+03 d E =-.403726E-03
trial-energy change: -0.000484 1.order -0.001891 -0.003530 -0.000252
step: 1.9182(charm= 1.9182) dis= 0.00430 next Energy= -353.031311 (dE=-0.190E-02)
bond charge predicted
  N      E              dE              d eps              ncg              rms              rms(c)
RMM: 1    -0.353029831611E+03  -0.35303E+03  -0.98844E-03  8954  0.155E-01  0.742E-02
RMM: 2    -0.353031212770E+03  -0.13812E-02  -0.88448E-04  8913  0.551E-02  0.295E-01
RMM: 3    -0.353029690721E+03  0.15220E-02  -0.40746E-04  7864  0.392E-02  0.379E-02
RMM: 4    -0.353029697033E+03  -0.63117E-05  -0.36528E-05  5069  0.143E-02
13 F= -.35302970E+03 E0= -.35301134E+03 d E =-.286739E-03
curvature: -1.02 expect dE=-0.125E-02 dE for cont linesearch -0.141E-04
trial: gam= 0.75319 g(F)= 0.123E-02 g(S)= 0.000E+00 ort =-0.171E-03 (trialstep = 0.176E+01)
search vector abs. value= 0.216E-02
reached required accuracy - stopping structural energy minimisation
writing wavefunctions
dft@dft10:~/work/ali/vasp_hesap/4_RuCu/4_0ads$

```

Figure A.7: A sample “out” file (last lines)

OUTCAR is the main OUTPUT file that contains most of the information on the calculation.

Individual parts are separated by dashed lines. These parts include:

- first part: reading INCAR, POTCAR, POSCAR
- nearest neighbor distances and analysis of symmetry
- information on what was parsed from INCAR
- verbose job information
- information on lattice, k-points and positions
- information on the basis set (number of plane waves)
- non local pseudopotential information
- information for each electronic step

The first lines of a sample OUTCAR file is shown in Figure A.8.

```

vasp.4.6.31 08Feb07 complex
executed on LinuxIFC date 2009.07.28 15:41:54
running on 8 nodes
distr: one band on 1 nodes, 8 groups
-----
INCAR:
POTCAR: PAW_GGA Ru 03Mar1998
POTCAR: PAW_GGA Cu 05Jan2001
POTCAR: PAW_GGA O 05Jan2001
POTCAR: PAW_GGA Ru 03Mar1998
URHFIM =Ru: s1 d7
LERCH = 91
EATOM = 455.6262 eV, 33.4876 Ry

TITEL = PAW_GGA Ru 03Mar1998
LULTRA = F use ultrasoft PP ?
IUNSCR = 1 unscreen: 0-lin 1-nonlin 2-no
RPAOR = 2.170 partial core radius
POMASS = 101.070; ZVAL = 8.000 mass and valenz
RCORE = 2.600 outmost cutoff radius
RWIGS = 2.650; RWIGS = 1.402 wigner-seitz radius (au)
ENMAX = 213.271; ENMIN = 159.953 eV
RCLOC = 1.830 cutoff for local pot
LCOR = T correct aug charges
LPAM = T paw PP
EAUG = 333.494
DEXC = -.025
RMAX = 3.157 core radius for proj-oper
RAUG = 1.300 factor for augmentation sphere
RDEF = 2.687 core radius for depl-charge
QCUT = -3.959; QGAM = 7.918 optimization parameters

Description
1 E TYP RCUT TYP RCUT
2 .000 23 2.600
2 .000 23 2.600
0 .000 23 2.600
0 .000 23 2.600
1 -.200 23 2.600
1 2.000 23 2.600
3 .000 7 .000
local pseudopotential read in
partial core-charges read in
atomic valenz-charges read in
non local Contribution for L= 2 read in
real space projection operators read in
non local Contribution for L= 2 read in
real space projection operators read in
non local Contribution for L= 0 read in
real space projection operators read in
non local Contribution for L= 0 read in
real space projection operators read in
non local Contribution for L= 1 read in
real space projection operators read in
non local Contribution for L= 1 read in
real space projection operators read in
PAW grid and wavefunctions read in

number of l-projection operators is LMAX = 6
number of lm-projection operators is LMMAX = 18

POTCAR: PAW_GGA Cu 05Jan2001
URHFIM =Cu: d10 p1
LERCH = 91
EATOM = 1393.0707 eV, 102.3878 Ry

TITEL = PAW_GGA Cu 05Jan2001
LULTRA = F use ultrasoft PP ?

```

Figure A.8: A sample OUTCAR file (first lines)

The last lines of a sample OUTCAR file is shown in Figure A.9.

```

3.15109    2.72816    8.49396    0.002473   -0.000011   -0.005198
3.12803    5.41792    8.61771   -0.019314   -0.033453   -0.051962
3.12928    8.22747    8.61876   -0.025711   -0.033806   -0.061856
5.54079    4.05007    8.49037   -0.002295   -0.002810   -0.002222
5.56056    6.02370    8.61875    0.042132   -0.005363   -0.061856
5.54085    9.59704    8.49022    0.002474    0.004205   -0.011042
3.93959    6.82358    9.63741   -0.005251   -0.009095    0.004474
-----
total drift:                                -0.003334   -0.022133    1.117986
-----

reached required accuracy - stopping structural energy minimisation
writing wavefunctions
  LOOP+:  UPU time 2083.46: CPU time 2104.94

General timing and accounting informations for this job:
=====
Total CPU time used (sec):    70296.049
  User time (sec):           68114.169
  System time (sec):         2181.880
  Elapsed time (sec):        70070.916

Maximum memory used (kb):      0.
Average memory used (kb):      0.

Minor page faults:            1862728
Major page faults:             0
Voluntary context switches:    4536614

```

Figure A.9: A sample OUTCAR file (last lines)

CONTCAR files is updated after every converged ionic step. Thus, at the end of the calculation, final geometry is written to CONTCAR file. It has the same format as the POSCAR file. This is helpful especially to run a calculation from a desired step or to continue a erroneously halted calculation. In those cases, it is just sufficient to copy CONTCAR as the POSCAR file and re-run the calculation.

Like CONTCAR, XDATCAR file also stores geometric information of converged ionic steps. However, the file is not overwritten with the new geometry as in the case of CONTCAR, but instead each geometry obtained after each ionic step are written consecutively in the same file. This helps the researcher to investigate the evolution of the chemical system in terms of chemical parameters. For example, if the input geometry is not chosen well and the results of the calculations are diverging from the desired geometry, this can be easily traced by the visualization of the XDATCAR file.

Finally, the massive WAVECAR file (in the order of several gigabytes) stores the wavefunctions of the investigated system. In order for the WAVECAR file to be written by VASP, either the calculations should converge and come to an end, or the calculation should stop at the end of the specified number of steps. If a calculation is started without the WAVECAR, the code

will first create the wavefunctions to be used by a trial and error procedure. It helps to shorten computational time to set the CODE to write the WAVECAR file and stop after a specified number of steps. Afterwards, the new calculation starts from the existing wavefunctions read from the pre-written WAVECAR, reducing the computational time.